Luminescent Cyclometalated Platinum and Palladium Complexes with Novel Photophysical Properties

by

Eric Turner

A Dissertation Presented in Partial Fulfillment
of the Requirements for the Degree
Doctor of Philosophy

Approved May 2014 by the
Graduate Supervisory Committee:

Jian Li, Chair
James Adams
Terry Alford

ARIZONA STATE UNIVERSITY

August 2014

ABSTRACT

Organic light emitting diodes (OLEDs) is a rapidly emerging technology based on organic thin film semiconductors. Recently, there has been substantial investment in their use in displays. In less than a decade, OLEDs have grown from a promising academic curiosity into a multi-billion dollar global industry.

At the heart of an OLED are emissive molecules that generate light in response to electrical stimulation. Ideal emitters are efficient, compatible with existing materials, long lived, and produce light predominantly at useful wavelengths. Developing an understanding of the photophysical processes that dictate the luminescent properties of emissive materials is vital to their continued development.

Chapter 1 and Chapter 2 provide an introduction to the topics presented and the laboratory methods used to explore them. Chapter 3 discusses a series of tridentate platinum complexes. A synthetic method utilizing microwave irradiation was explored, as well as a study of the effects ligand structure had on the excited state properties. Results and techniques developed in this endeavor were used as a foundation for the work undertaken in later chapters.

Chapter 4 introduces a series of tetradentate platinum complexes that share a phenoxy-pyridyl (popy) motif. The new molecular design improved efficiency through increased rigidity and modification of the excited state properties. This class of platinum complexes were markedly more efficient than those presented in Chapter 3, and devices employing a green emitting complex of the series achieved nearly 100% electron-to-photon conversion efficiency in an OLED device.

Chapter 5 adapts the ligand structure developed in Chapter 4 to palladium. The resulting complexes exceed reported efficiencies of palladium complexes by an order of magnitude. This chapter also provides the first report of a palladium complex as an emitter in an OLED device. Chapter 6 discusses the continuation of development efforts to include carbazolyl components in the ligand. These complexes possess interesting luminescent properties including ultra-narrow emission and metal assisted delayed fluorescence (MADF) emission.

For Penelope

ACKNOWLEDGMENTS

I would like to offer my sincere thanks to my advisor, Dr. Jian Li for extending me the opportunity to explore such an interesting series of topics. The challenging lab environment allowed me to grow as a scientist and conveyer of complex ideas. I would also like to acknowledge the hard work and time invested by Dr. James Adams and Dr. Terry Alford in preparing for my comprehensive exam and dissertation defense.

I would like to extend similar appreciation to my colleagues, past and present, for the open exchanging of ideas. Specifically, I would like to thank the chemists: Dr. Zixing Wang, Brian Guthrie, Sijesh Madakuni, Aritra Dhar Liang Huang, Dr. Guijie Li, Dr., Zhiqiang Zhu, Alicia Wolf, and Dr. Xiaochun Hang for their insight into processes as well as help preparing materials. Similarly, I would like to thank the device engineers: Nathan Bakken, Tyler Fleetham, Jeremy Ecton, Barry O'Brien, and Greg Norby for their assistance in fabricating OLEDs and helpful discussions on device physics. In addition, I would like to give a big thank you to Nathan Bakken for the opportunity to work at Intel for the past year and develop an entirely new and complimentary set of skills.

Finally, I would like to thank my family for their love and support over the years. Specifically, I would like to thank my wife, Tiffany, for her amazing perseverance in seeing me though this long, and at time arduous process.

TABLE OF CONTENTS

CHAPTER Page

LIST OF TABLES

LIST OF FIGURES

Figure Page

Figure Page

Figure Page

Figure Page

Figure Page

INTRODUCTION

1.1 Motivation

Organic light emitting devices (OLEDs) have attracted interest from researchers and electronics producers alike in recent years. OLEDs have been incorporated into commercially available smart phones, televisions, monitors, digital cameras, tablet computers, and lighting fixtures[1] (Figure 2.1). Research is ongoing to improve material and device design so that products containing OLEDs can be made more efficient, more affordable, and better performing.

Figure 2.1 (a) Samsung Galaxy S5 phone with 5.1" super AMOLED 1920 x 1080 display[2] and (b) LG 55" curved OLED television[3]

Organic light emitting diodes vary widely in the specifics of their design, but all OLEDs contain one or more thin layers of organic compounds sandwiched between two conductors (Figure 2.2a). When voltage is applied, positive and negative charge carriers migrate into the device from opposing sides. Electron-hole pairs localize and form an exciton on an electroluminescent (EL) material located within the organic layers. When the exciton decays, a photon is emitted at a

wavelength characteristic to the EL material (Figure 2.2b). The device can be constructed on a variety of substrates including materials that are extremely thin, have novel shapes, are transparent, or flexible.[4]

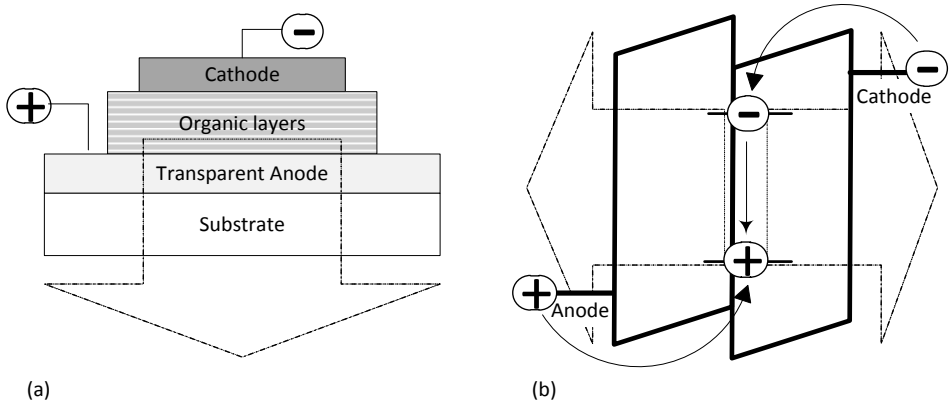

Figure 2.2 (a) simplified organic light emitting diode (OLED) device structure, (b) energy diagram for typical OLED showing charge injection, exciton formation, exciton decay, and light emission.

Organic light emitting diodes are promising candidates to supplant liquid crystal displays (LCDs) as the dominant technology. LCDs operate by selectively filtering a white backlight to produce the requisite red, blue, and green colors to display. This represents an inherent source of inefficiency, and requires additional layers that increase the manufacturing complexity and product thickness. The direct emission process of OLEDs means displays can have lower power consumption, increased contrast, thinner form factors, faster refresh times, and brighter colors. These qualities make OLEDs particularly attractive for mobile devices, where a premium is placed on size, weight, battery life, and durability. The freedom of substrate selection is another major advantage of OLEDs. The ability to build devices on curved substrates provides increased design flexibility. Those based on

transparent substrates could be incorporated into windows or automobile windshields, and those based on flexible ones could be worn or carried with ease.

Issues with production cost, scalability, and device lifetime have been major obstacles to the commercial success of OLEDs, but conditions are improving. There remains a need for stable, efficient luminescent complexes with emission well matched for the products in which they will be incorporated. Subsequent chapters are focused on the design, synthesis, and characterization of emitters to accomplish this goal.

1.2 OLED Development

The market for displays and light based on organic light emitting diodes (OLEDs) has expanded rapidly in recent years. The total value of goods shipped that contained OLEDs has grown from 91 million dollars in 2002, to 3 billion dollars in 2010, and is expected to climb past five billion dollars by 2016.[5] Although products based on OLEDs have seen wide spread commercial success only recently, electroluminescence from organic molecules, the phenomenon on which they are based, has been known for over 50 years (Figure 2.3).

The first reports came from France in the 1950's. Electroluminescence was observed when 1-2 mm thick cellophane films doped with acridine orange or acriflavine were placed between electrodes of aluminum and saline, and then subjected to alternating current operating at potentials up to 2,000 volts.[6] Attempts were made to explain the mechanism in terms relevant to contemporary inorganic phosphors, but the physics behind the emission was not well understood.

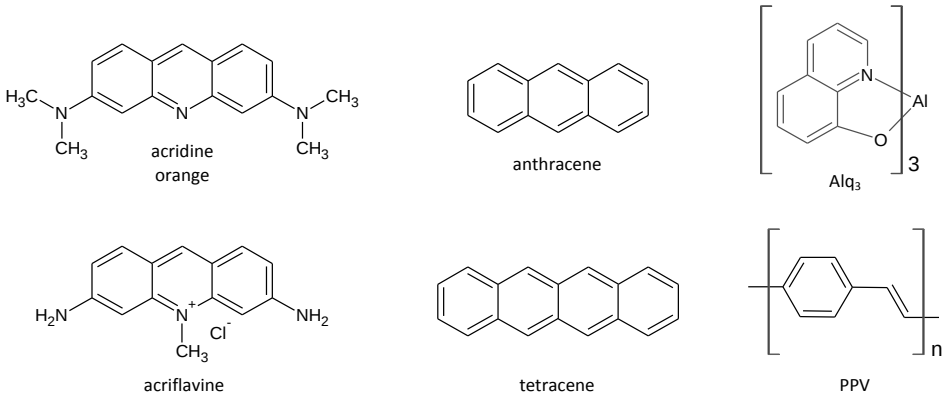

Figure 2.3 Materials used in the early development of OLEDs

In the following decade, more careful study was given to charge injection and recombination mechanisms. Electroluminescence was observed when carefully grown crystals of anthracene measuring 10-20 μm thick were sandwiched between metal or liquid electrodes and potentials of 400-2000 volts were applied. When tetracene was doped into anthracene, the emission occurred exclusively from the lower energy tetracene.[7] The light emission under a variety of voltage conditions was studied. In experiments with pulsed voltages, it was found that appreciable luminescence appeared even after a pulse had ended, suggesting the cause of this delayed luminescence was carrier recombination.[8] Furthermore, the liquid electrodes could be modified to produce hole injection on one side, and electron injection on the other,[9] resulting in greatly increased currents and luminance over devices without injecting electrodes. Experiments were also run aimed at understand the behavior of singlet and triplet excitons within the crystal. It was noted that only emission from the singlet states was observed. The existence of triplets could be discerned, however, by the delayed fluorescence caused by triplet-triplet annihilation, although the bulk of the triplets decayed non-radiatively.[10]

Further refinement of the mechanisms behind electroluminescence in anthracene continued through the 1970's.[11-15] The success of these early forays with single crystals spawned attempts to improve the power efficiency by reducing the turn on voltage through the use of thinner organic films. Vacuum thermal evaporation was used to produce polycrystalline films in the sub-micrometer range. The method was successful in reducing the turn on voltage below 100 volts. However, it was found that the morphology that resulted from vacuum deposition produced unstable carrier injection and transport, and was very susceptible to pinhole defects.[15-17]

In 1982 a series of papers by Partridge et al.[18, 19] focused on the use of fluorescently doped polyvinylcarbazole (PVCz) as a charge carrier transport layer, a high work function hole injection electrode of antimony pentachloride/PVCz, and a low work function electron injection electrode of cesium metal. Films were deposited through a combination of spin coating for PVCz containing layers, and thermal evaporation for the metal electrodes. The process resulted in 500 nm thick conformal films and stable charge injection, which solved many of the problems associated with previous attempts and would serve as an important building block for future devices.

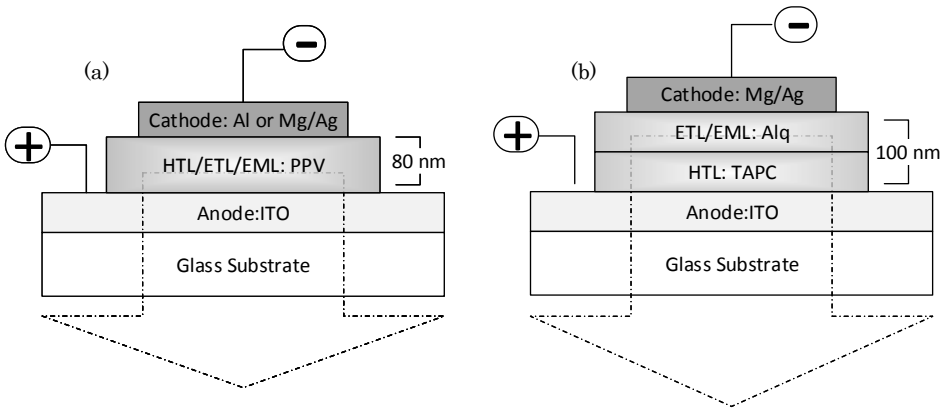

Figure 2.4 Seminal OLED device structures: (a) small molecule OLED by Tang et al. and (b) polymer OLED by Burroughes et al.

In 1987 Tang et al.[20] reported a ground breaking structure which used indium tin oxide (ITO) as the hole injection electrode, 1,1-bis[di(tolyl)aminophenyl] cyclohexane (TAPC) as a hole transport layer (HTL), tris(8-hydroxyquinolinato) aluminium (Alq_3) as the combined electron transport layer (ETL) and emissive layer (EML), and a magnesium/gold electron injection electrode (Figure 2.4a). The work was significant in several respects. The advent of unipolar TPAC as the HTL allowed for efficient hole transport, as well the blocking of electrons from Alq_3. The device was also composed of amorphous films that were 50-100 nm thick, which improved the power efficiency significantly while maintaining conformal coverage. The Au/Mg electrode was significantly more stable that previously reported ones made of more reactive metals. The resulting devices had an EL quantum efficiency of 1%, luminous efficiency of 1 lm/W, and lifetimes around 100 hours. It was the first efficient, modern OLED and its reporting set off a new round of research based on small molecules. Tang's work was followed shortly in 1990 by Burroughes et al. who adapted it for use with poly(p-phenylene vinylene) (PPV), producing devices with EL

quantum efficiencies of 8%, and spawned investigations into polymer based OLEDs (Figure 2.4b).[21]

It was clear to researchers at the time that there were problems with these early devices that needed to be corrected if the higher efficiencies necessary for commercialization were to be realized. The early two layer devices allowed charge carriers to migrate through the device and be quenched by the opposing electrode. New layers were added to block this diffusion and promote exciton recombination in the desired area.[22-25] Also, the neat films that formed early emissive layers showed strong self-absorption which attenuated light output. This could be avoided if lower energy emitters were dispersed in low concentration throughout a host material. Tang found that EL efficiencies were doubled if florescent dye molecules were doped into host Alq_3.[26] Doping also allowed greater flexibility in the choice of emitters, since they did not have to serve a charge transport role. Research also continued into materials and device structures that enhanced charge injection, carrier mobility, and device lifetime through improved morphology and electrochemical stability.

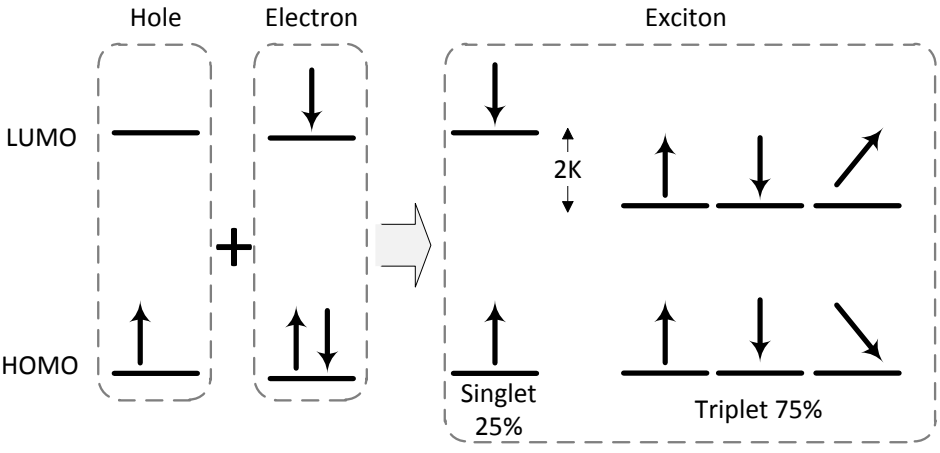

Figure 2.5 Exciton formation scheme showing singlet and triplet states separated in energy by twice the exchange integral (K)[27]

As devices became more efficient at trapping excitons on the emissive molecules, the drawbacks of fluorescent emitters became a more pressing issue. Their inherent limitation lies in the nature of these excitons. The electron and hole both carry a spin of ±1/2, and in combination, form singlet excitons with total spin of 0 or triplet excitons that have a total spin of 1. Based on spin statistics, and confirmed through experiment,[28, 29] the ratio of triplet to singlet exciton formation is 3:1 (Figure 2.5). Singlets localized on florescent emitters decay radiatively with lifetimes of nanoseconds. However, the lifetimes associated with radiative decay from the triplet state can be seconds long, allowing non-radiative processes to dominate (Figure 2.6).

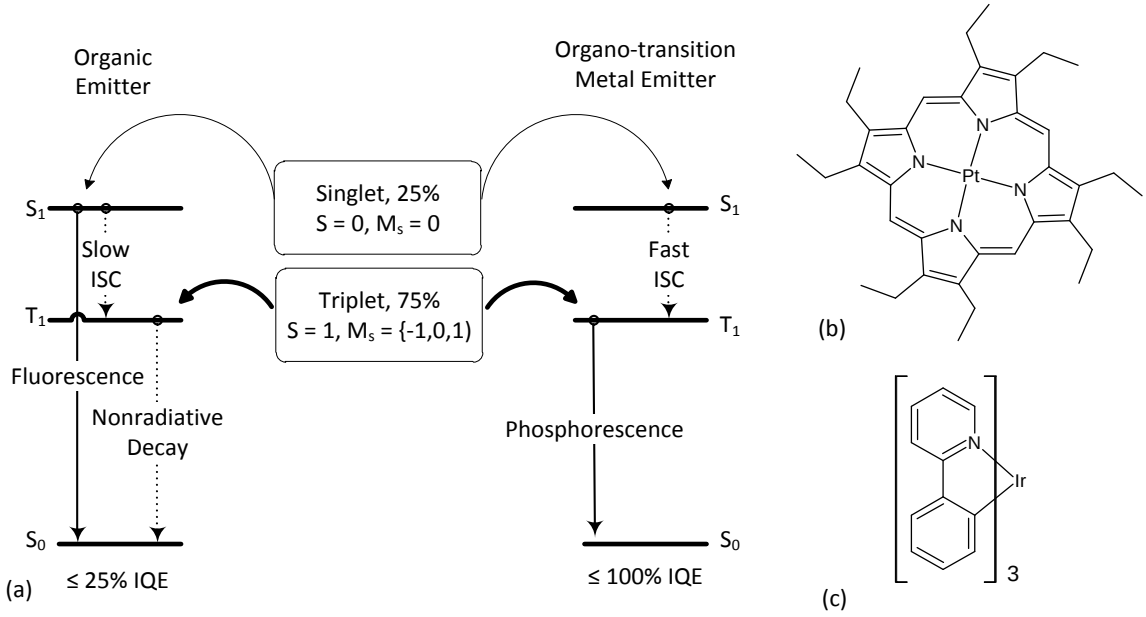

Figure 2.6 Comparison of exciton harvesting mechanics found in organic and organo-transition metal emitters, and phosphorescent emitters (b) PtOEP and (c) $Ir(ppy)_3$

In the late 1990's, attempts were made to harvest these triplet excitons. One method was to cool the devices to cryogenic temperatures to freeze out non-radiative

processes, and allow the slow rate of phosphorescence to compete.[30, 31] This was met with limited success, and was not useful for any practical application. Complexes based on lanthanide cores[32-35] were also studied. They had radiative lifetimes in the millisecond range, which was orders of magnitude slower than the rate of several hundred nanoseconds for exciton generation. As a result, the lanthanide complexes became saturated with excitons, and there was not a significant increase in efficiency over standard fluorescent emitters. Radiative lifetimes of phosphorescent emitters needed to be reduced significantly if they were to harvest triplets effectively and achieve improved device efficiencies. It was found that when platinum octaehtylporpherin (PtOEP) was doped into Alq_3 in a simple two layer device, at low current the efficiency was limited only by the inherent PL efficiency of PtOEP, meaning triplets were being collected in the device with nearly ideal efficiency.[36]

Despite the effectiveness of PtOEP at harvesting triplet excitons at low currents, it still possessed a relatively long lifetime of 90 μs,[37] and was sensitive to triplet-triplet annihilation at higher current densities.[38] Furthermore, it emitted in the deep red region, and no simple structure modification was possible to shift the excited state energy higher while maintaining its emissive properties.

When a cyclometalated compound *fac*-tris(2-phenylpyridinato, N,C2') iridium (*fac*-$Ir(ppy)_3$) was used as the emitter, lifetimes were found to be about two orders of magnitude shorter, and efficiencies were maintained at higher current densities. When devices were optimized for this new emitter, internal quantum efficiencies approached 100%.[39, 40] The high efficiency of $Ir(ppy)_3$, coupled with its inherent modifiability, has made heavy metal based phosphorescent compounds the object of intense research and an integral component in many modern OLEDs.

Modern bottom emitting small molecule OLED designs consist of several layers of vacuum deposited organic layers sandwiched between a metal cathode and transparent anode (Figure 2.7). Each layer is designed to promote efficient charge injection or transport to the emissive layer and/or discourage charge carrier and exciton leakage away from the emissive layer. Within the emissive layer, emitters are doped in low concentration within a higher energy host matrix. Excitons formed in the emissive layer are harvested by the emitter and light is emitted upon decay of the exciton.

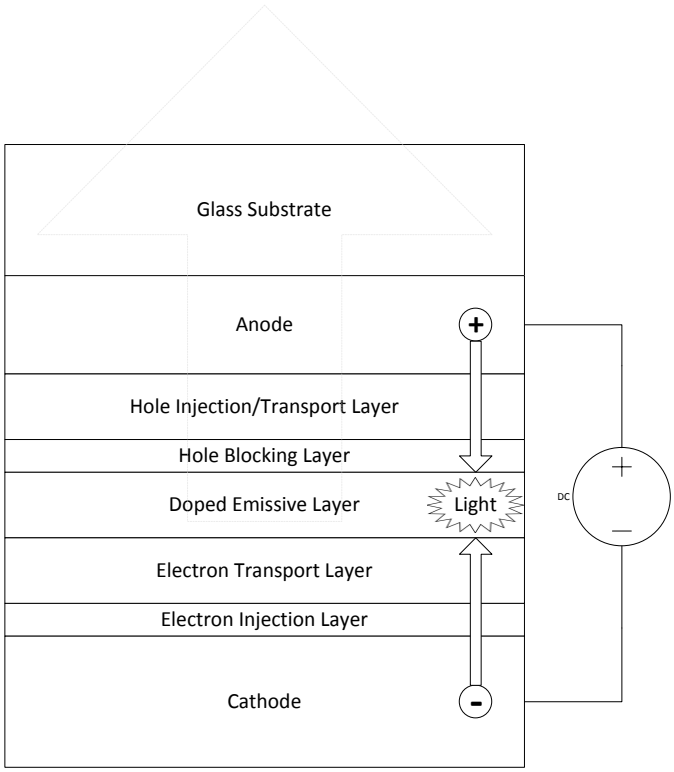

Figure 2.7 Representative device structure of a modern small molecule based bottom emitting OLED.

1.3 Excited State Dynamics

Exploring the mechanism driving the luminescent properties of transition metal based organo-transition metal complexes is vital to their continued development. The general structure of the complexes consists of a metal ion center surrounded by one or more coordinating ligands. Typically, ligands can be categorized as emitting or ancillary. Emitting ligands frequently contain aromatic motifs with band gaps in the optical range. Ancillary ligands, if present, must have excited state energies that are sufficiently high to prevent direct involvement in emission process.[27]

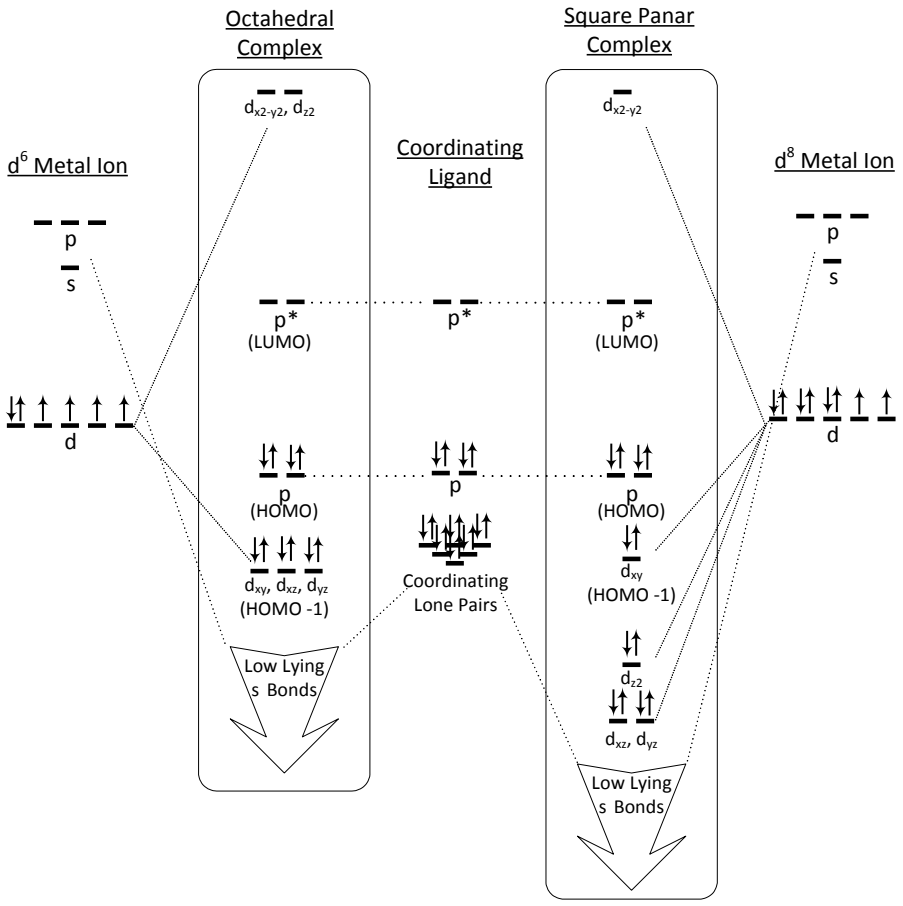

Figure 2.8 Energy levels important in luminescence formed by ligand coordination with d^6 and d^8 metal ions using ligand field theory[27]

Ligand field theory is useful in visualizing the electronic landscape that develops upon coordination (Figure 2.8).[41] The orbitals holding the donated electrons of the ligand mix with unoccupied p and s orbitals of the metal ion and form low lying σ bonding states. The partially filled d orbital of the transition metal ion is split by the ligand field, forming occupied stabilized states and destabilized unoccupied states. The geometry of the resulting complex is determined by the number of electrons present in the d shells and the stabilization/destabilization effects provided by this splitting. The highest occupied molecular orbital (HOMO) and lowest occupied molecular orbital (LUMO) of the emitting ligand are both of π

character and have energies that fall above and below the occupied and unoccupied metal centered d orbitals.

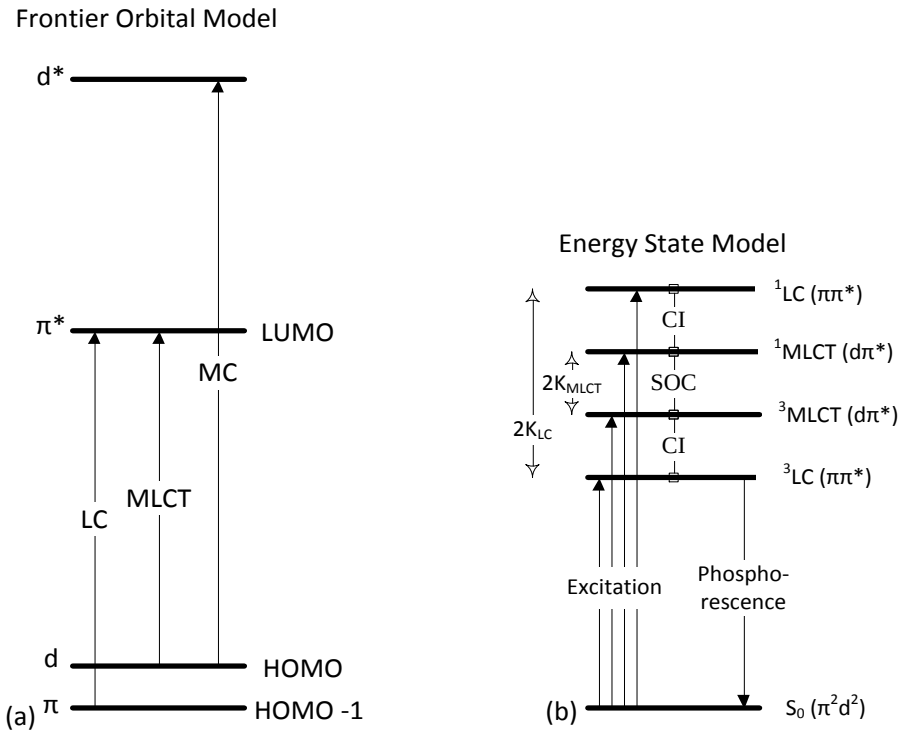

Figure 2.9 (a) Frontier orbital model showing electronic transitions that dominate the emission properties and (b) energy state model that accounts for singlet and triplets as well as configuration ineteraction (CI) and spin orbit coupling (SOC) between states.

From the simplified frontier orbital model (Figure 2.9a), a few important transitions can be identified. Transitions that occur between the occupied π orbitals and the unoccupied π* orbitals of the ligand are called ligand centered (LC) transitions. Transitions that occur between the occupied d orbitals of the metal and the unoccupied π* orbitals of the ligand are called metal-to-ligand charge transfer (MLCT) transitions. Transitions that occur between the occupied d orbitals of the metal and the unoccupied d* orbital of the metal are called metal centered (MC) transitions.

The three states introduced in the frontier orbital model do not take into account singlet and triplet states, which are of great importance in phosphorescent emitters (Figure 2.9b). Pairs of electrons in the triplet state naturally have lower spatial overlap due to Pauli exclusion principle mandate effects. This leads to reduced electron-electron repulsion, and as a consequence, lower excited state energy. This effect is quantified by the exchange integral (K). The value of the exchange integral, and thus the energy difference between singlet and triplet states, becomes larger the more spatially confined the electrons are. As a result, different states can have vastly different exchange integrals. In organo-transition metal emitters like $Ir(ppy)_3$, the energy difference between the HOMO of the metal d orbitals and the HOMO-1 of the ligand orbitals is usually small in comparison to the difference in exchange integrals between MLCT and LC transitions. As a result, the energy of the ^{3}LC and ^{3}MLCT are frequently closely spaced, and lowest excited state is often a mixture of both.

Quantum mechanical mixing driven by configuration interaction and spin orbit coupling occurs between these close lying states, subject to certain selection rules.[27] As a result, none of the states are "pure" singlets or triplets, but are instead admixtures. This has important consequences for the lowest lying triple state. Direct relaxation from this state is formally forbidden, and this is evident by the lack of appreciable triplet emission found in early organic dye based devices. However, when ^{1}MLCT character is mixed in, this transition becomes significantly more allowed. The lowest excited state can be approximated through first order perturbation theory. Equation 2.1 assumes a predominantly ligand centered triplet state.

Equation 2.1 Wave function describing the lowest excited triplet state modeled by first order perturbation theory.

$$\Psi_{T_1} = \sqrt{1-\alpha^2}\,\left|\ {}^3\mathrm{LC}\right\rangle + \alpha\,\left|\ {}^1\mathrm{MLCT}\right\rangle, \alpha = \frac{\left\langle\ {}^3\mathrm{LC}\left|\mathrm{H_{SO}}\right|\ {}^1\mathrm{MLCT}\right\rangle}{\Delta E}$$

The coefficient provides an estimate on the amount of ^{1}MLCT character mixed in to the pure ^{3}LC state. This value becomes larger when the energy difference between the two states is reduced, or the amount of spin orbit coupling is increased. The significant admixture of ^{1}MLCT into ^{3}LC states of organo-transition metal complexes is responsible for their enhanced triplet harvesting and lower emission lifetimes (Figure 2.10).

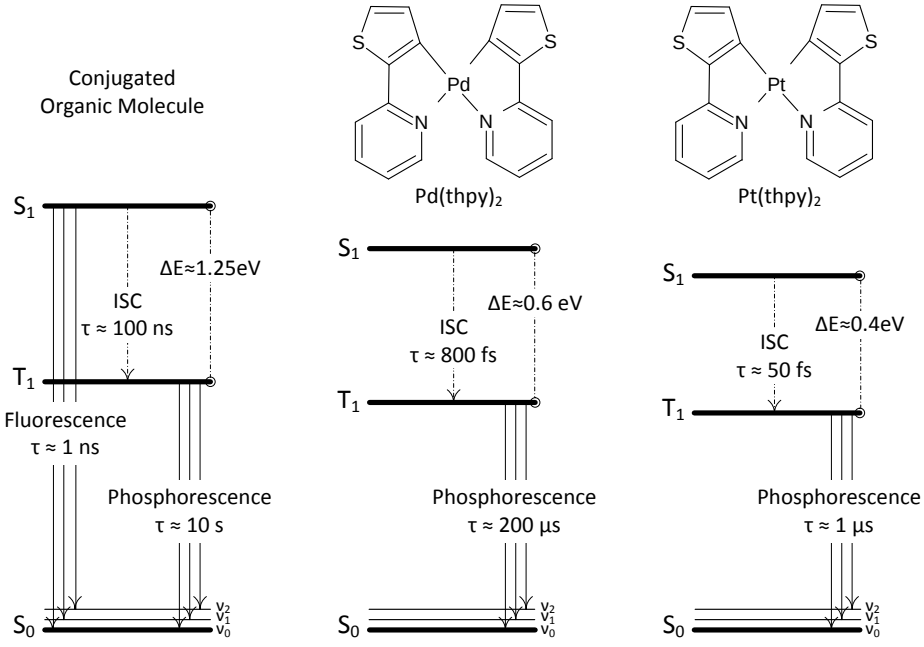

Figure 2.10 Lifetimes associated with electronic transitions. Singlet metal character in the lowest excited state increases from left to right.[42]

The importance of SOC, and the greater amounts of ^{1}MLCT character they induce, is clearly demonstrated when comparing the emission properties of a pure organic compound, cis-bis[2-(2-thienyl)pyridine]palladium ($Pd(thpy)_2$), and cis-Bis[2-

(2-thienyl)pyridine]platinum ($Pt(thpy)_2$). Spin orbit coupling increases with increasing atomic weight, so SOC found in platinum compounds will be larger than that of palladium compounds, which is in turn larger than that of purely organic compounds. Intersystem crossing (ISC) rates are sluggish in purely organic compounds, and are often orders of magnitude slower than fluorescence. However, when even relatively small amounts of ^{1}MLCT is mixed in, ISC lifetimes shorten from nanosecond timescales to femtoseconds. This means that singlet excitons localized on an emitter with significant SOC will decay to a triplet before any significant florescence can occur. Also, increased ^{1}MLCT character delocalizes the excited state, which reduces the exchange integral, which in turn reduces the energy difference between the singlet and triplet states.[27]

Radiative decay rates from the triplet state are similarly enhanced. The decay rates of seconds found in organic molecules fall into the microsecond range when modest amounts of SOC is involved. This reduced radiative lifetime means the emission process can compete with, or even overwhelm non-radiative decay pathways, resulting in efficient phosphorescent emission.

Another important parameter controlled by the excited state properties is the shape of the emission spectra. Emission generally occurs from the lowest vibration mode of the excited state to a series of vibration modes in the ground state, creating a spectrum with vibronic progressions. The strength of the various possible transitions are governed by the Franck-Condon principle,[43, 44] which states electronic transitions are more likely to occur when they do not involve changes in nuclear coordinates. Changes in equilibrium geometry between the ground and excited electronic states determine which vibrational modes in the ground state provide the

most similar nuclear environment to the excited state. Rigid molecules and those with increased MLCT character tend to form excited states with lower distortion with respect to their equilibrium ground state geometry.[27] The room temperature spectra of transition metal complexes frequently lack the definition of distinct transitions. There are often several overlapping vibrational sidebands and significant line broadening as the temperature increases. Increased MLCT character will incorporate metal-ligand vibrations, adding additional modes.

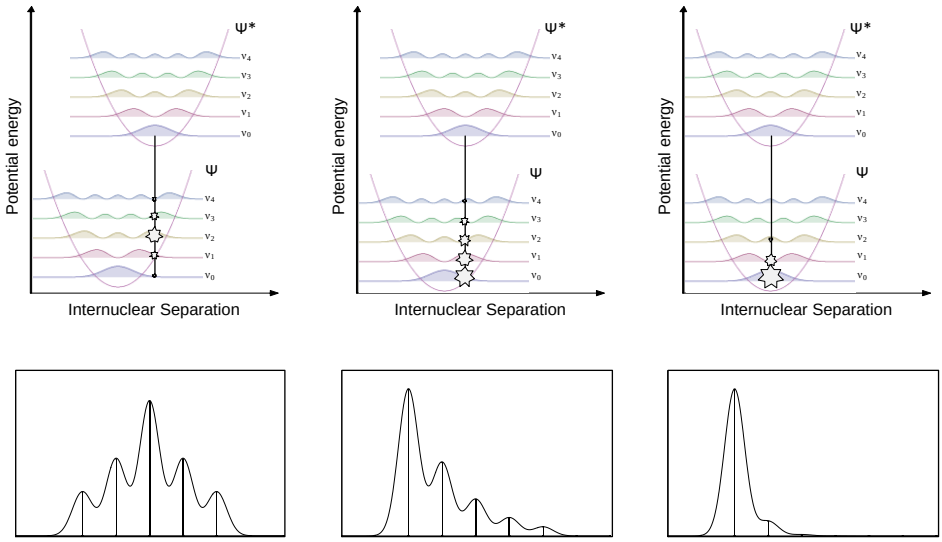

Figure 2.11 The effect of differences in equilibrium geometry between the ground and excited state on the resulting emission spectra.

When there is a small difference in equilibrium (Figure 2.11, right), transitions to the lowest vibrational modes are favored as they share similar nuclear coordinates. The resulting spectra has the largest peak from the transition to the lowest vibrational mode ($v_{0,0}$), and progressively decreasing vibronic side bands representing transitions to higher vibrational modes. However, larger differences in equilibrium geometry (Figure 2.11, left) favor transitions to higher vibrational modes because the displacement provided by the higher vibrational modes provides

better overlap with the distorted geometry of the excited state. Emission spectra resulting from large changes in equilibrium geometry have peaks centered at lower energy than the pure electronic transition ($0 \rightarrow 0$), and decreasing vibronic side bands to both sides.

Complexes can be designed to be narrow or broad emitters, depending on the intended function. Displays require that the light output occur in narrow regions of red, blue, and green for maximum color purity and luminous efficiency. Rigid molecules with significant MLCT contributions are needed to produce these desired emission properties.

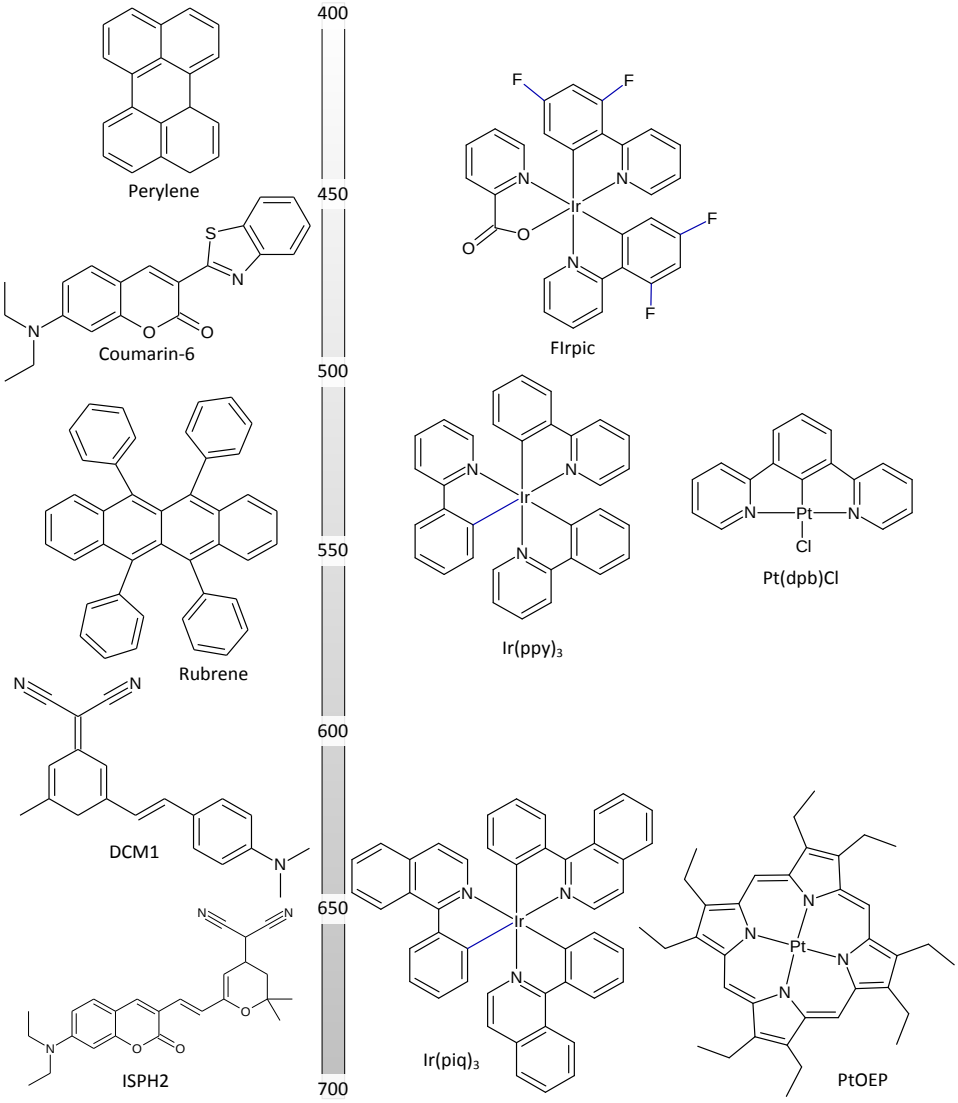

Figure 2.12 Selected florescent (left) and phosphorescent (right) emitters covering the visible spectrum[4]

CHAPTER 2

METHODS

2.1 Instrumentation

Unless otherwise noted, chemicals were purchased from commercial sources and used without further purification. Purification of synthesized complexes was accomplished with column chromatography, slow recrystallization, and/or train sublimation in a vacuum furnace, resulting in over 99% purity. For microwave reactions, a Discover microwave reactor (CEM Corporation) was used.

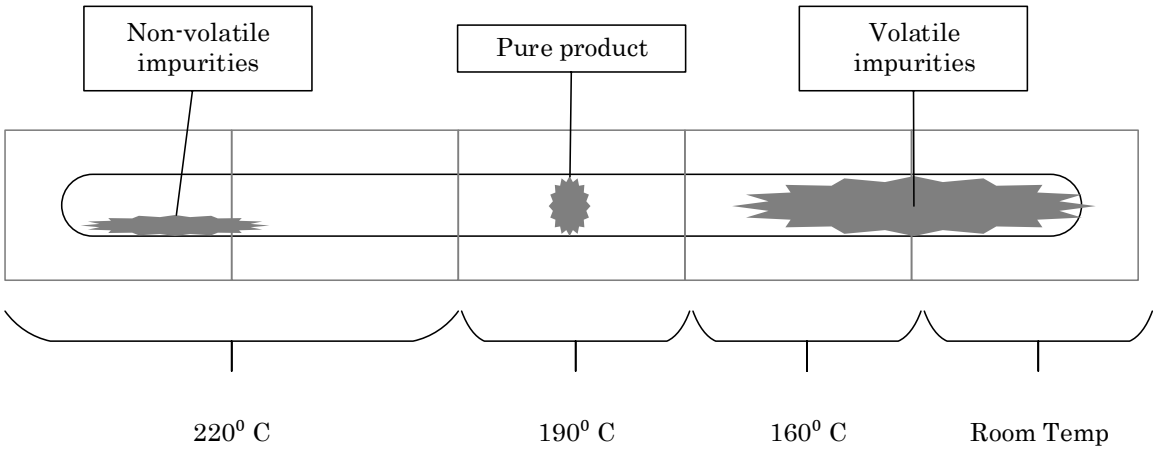

Figure 2.1 Typical train sublimation settings for the complexes synthesized herein. Pressure is on order of 10^{-6} Torr.

NMR spectra were recorded on a Varian Gemini-400 MHz spectrometer with TMS as the internal reference. Chemical shifts were referenced to residual protiated solvent. Mass spectra were recorded on an Applied Biosystems Voyager DESTR MALDI-TOF mass spectrometer. The Microanalysis Laboratory at Zhejiang

University performed all elemental analysis on the Vario EL III Elemental Analyzer.

X-ray diffraction data were collected on a Bruker SMART APEX CCD diffractometer with graphite monochromated Mo KR radiation (λ = 0.71073 Å) at 298(2) K. A sphere of diffraction data was collected and the intensity data were processed using the SAINT program. The cell parameters for complexes were obtained from the least-squares refinement of spots using the SAINT program. Absorption corrections were applied by using SADABS.[45] All calculations for the structure determination were carried out using the SHELXTL package (version 6.14).[46] Initial Pt atomic positions were located by Patterson methods using XS, and the remaining structure was found using difference maps and refined by least-squares methods using SHELXL-97. Calculated hydrogen positions were input and refined in a riding manner along with the attached carbons.

Cyclic voltammetry and differential pulsed voltammetry were performed using a CH Instrument 610B electrochemical analyzer. Anhydrous DMF (Aldrich) was used as the solvent under a nitrogen atmosphere, and 0.1 M tetra(n-butyl)-ammonium hexafluorophosphate was used as the supporting electrolyte. A silver wire was used as the pseudo-reference electrode. A Pt wire was used as the counter electrode, and glassy carbon was used as the working electrode. The redox potentials are based on the values measured from differential pulsed voltammetry and are reported relative to a ferrocenium/ferrocene (Fc^+/Fc) redox couple used as an internal reference (0.45 V vs. SCE).[47] The reversibility of reduction and oxidation was determined using cyclic voltammetry. If peak anodic and peak cathodic currents have an equal magnitude under the conditions of fast scan (100 mV/s or above) and

slow scan (50 mV/s), then the process is defined as reversible; if the magnitudes in peak anodic and peak cathodic currents are the same in fast scan but slightly different in slow scan, the process is defined as quasi-reversible; otherwise, the process is defined as irreversible.[48]

The UV−visible spectra were recorded on a Hewlett-Packard 4853 diode array spectrometer in a solution of dichloromethane. Photoluminescence spectra measurements were collected on a Horiba Jobin Yvon FluoroLog-3 spectrometer. Room temperature solution measurements were obtained in degassed dichloromethane in a sealed quartz cuvette. Low temperature (77 K) measurements were taken in 2-methyl-tetrahydrofuran in a glass NMR tube. Room temperature thin films spectra were acquired in a spin-coated poly(methyl methacrylate) matrix under nitrogen flow. Variable temperature measurements were taken in a spin-coated poly(methyl methacrylate) thin film under vacuum in a liquid nitrogen cooled Janis VPF cryostat.

Luminescent lifetimes (τ) of complexes were obtained with an IBH Datastation Hub FluoroLog-3. Samples exhibiting luminescent lifetimes below 5 μs were excited using NanoLED sources and measured using a time correlated single photon counting method; Samples with lifetimes above 5 μs were excited using SpectraLED sources and measured with a multichannel scaling single photon counting method.

OLED devices were fabricated in a Travato physical vapor deposition system on glass substrates with a patterned transparent indium tin oxide (ITO) anode. Prior to organic depositions, the ITO substrates were cleaned by subsequent sonication in water, acetone, and isopropanol followed by a 15 min UV−ozone

treatment. Individual devices have areas of 0.04 cm^2. I–V–L characteristics were taken with a Keithley 2400 Source-Meter and a Newport 818 Si photodiode inside a nitrogen-filled glovebox. Electroluminescence (EL) spectra were taken using the FluoroLog-3. Agreement between luminance, optical power, and EL spectra was verified with a calibrated Photo Research PR-670 spectroradiometer. All devices are assumed to be Lambertian emitters.

Density functional theory (DFT) calculations were performed using the Titan software package (Wave Function, Inc.) at the B3LYP/LACVP** level.[49-51] The HOMO and LUMO energies were determined using a minimized singlet geometry to approximate the ground state.

Solution quantum efficiency measurements were carried out at room temperature in a solution of dichloromethane. Before emission spectra were measured, the solutions were thoroughly bubbled with nitrogen inside of a glovebox. Oxygen content was less than 1 ppm. Solutions of coumarin 47[52] (coumarin 1, Φ = 0.73, excited at 360 nm), coumarin 6[53] (Φ = 0.78, excited at 420 nm), and rhodamine B[54] (Φ = 0.70 excited at 510 nm) in ethanol were used as a reference. The equation $\Phi_s = \Phi_r \frac{\eta_s^2 A_r I_s}{\eta_r^2 A_s I_r}$ was used to calculate the quantum yields. The subscript 's' denotes the sample, subscript 'r' the coumarin reference, Φ the quantum yield, η the refractive index, A the absorbance, and I the integrated area of the emission band.[55] Absolute PL quantum efficiency measurements of doped thin film were carried out on a Hamamatsu C9920 system equipped with a xenon lamp, integrating sphere, and a model C10027 photonic multichannel analyzer. Luminescent decay rates were calculated by manipulating the equations $k_r = \frac{\Phi}{\tau}$ and $\tau = \frac{1}{k_r + k_{nr}}$.

2.2 Outline of Research Presented

Chapter 3 discusses a series of tridentate platinum complexes. Novel synthetic techniques including microwave irradiation were used, a metallization reaction mechanism was proposed, and the effects of ligand structure on the excited state properties was explored. Two methods were developed for color tuning. One involved adding electron withdrawing and electron or electron donating groups to the central phenyl ring. The second involved altering the size of the accepting N-aryl groups. The second technique was used to tune the complexes presented in subsequent chapters.

Chapter 4 introduces a series of tetradentate platinum complexes that share a phenoxy-pyridyl (popy) ligand fragment. The new molecular design improved efficiency through increased rigidity and modification of the excited state properties. This class of platinum complexes were markedly more efficient than those presented in Chapter 3, and devices employing a green emitting complex of the series achieved nearly 100% electron-to-photon conversion efficiency in an OLED device. The success of this class of tetradentate shifted future molecular designs toward tetradentate complexes.

Chapter 5 applies the ligand structure developed in Chapter 4 to palladium. Palladium produced some synthetic challenges that were overcome with a low temperature metallization step. The photophysical properties of this class were carefully studied. The complexes span the visible spectrum and exceed reported quantum efficiencies of palladium complexes by an order of magnitude. This chapter

also provides the first report of a palladium complex as an emitter in an OLED device.

Chapter 6 introduces complexes with carbazolyl components in the ligand and discusses their design and characterization. Platinum complexes with a bis-carbazolyl structure were synthesized and exhibited ultra-narrow emission. Likewise a series of palladium complexes were synthesized that emitted through a metal assisted delayed fluorescence (MADF) process. The lifetimes of the palladium complexes were studied across a range of temperatures and higher lying metal centered quenching states and emissive singlet states were resolved. These new classes of platinum and palladium complexes represent the foundation on which a significant portion of the current development within the lab is built.

CHAPTER 3

TRIDENTATE PLATINUM COMPLEXES

3.1 Introduction

Cyclometalated complexes incorporating iridium and platinum have been the focus of considerable research which began in earnest in the early 2000's. While potential applications are numerous, including sensitizers,[56-58] photocatalysts,[59, 60] and chemosensors,[61-63] the bulk of work to date has been focused on developing the complexes for use as emissive materials for organic light emitting diode (OLED) based display and lighting applications.[64-70]

Both octahedral iridium and square planar platinum complexes have rich histories in photophysics. However, iridium complexes[71-73] have largely overshadowed those based on platinum as the former quickly achieved nearly 100% quantum efficiency and short luminescent lifetimes.

Despite the relative dominance of iridium, platinum remains an exciting field to explore. Square planar platinum complexes possess excellent structural flexibility, with the ability to employ a wide variety of cyclometalating ligands. Bidentate complexes[49, 74] with C^C and C^N coordination and tridentate[75-80] variations with N^C^N, C^N^N, and C^N^C have been particularly well explored.

Across these classes, complexes containing aromatic chelates of the type N^C^N (e.g. *m*-di(2-pyridinyl)benzene, Pt(dpb)Cl),[75, 81] have demonstrated quantum efficiencies and lifetimes that are competitive with many iridium based complexes. Efficient blue, green, and white OLEDs have been fabricated using platinum emitters of this type.

It has been well documented[82-87] that luminescence from Pt(II) complexes originates from the admixture of ligand-centered (^{3}LC) states and metal- to-ligand-charge-transfer (MLCT) states. As such, substitution modifications to the ligand can significantly alter the emission energy.[49, 68, 88, 89]

In spite of the promising work conducted thus far, the extent to which structural modifications affect the photophysical and electrochemical properties of the complex is not fully understood. To investigate this, a series of platinum complexes were synthesized. Changes were made to both the central phenyl ring and the N-heterocycles (Figure 3.1). To enable faster throughput,[89, 90] microwave heating was explored. Additionally, analogs to Pt(dpb)Cl were synthesized to highlight the electrochemical and photophysical differences in an effort to better understand the class of materials as a whole. The knowledge gained in this study was used to develop the new classes of materials that are presented in later chapters.

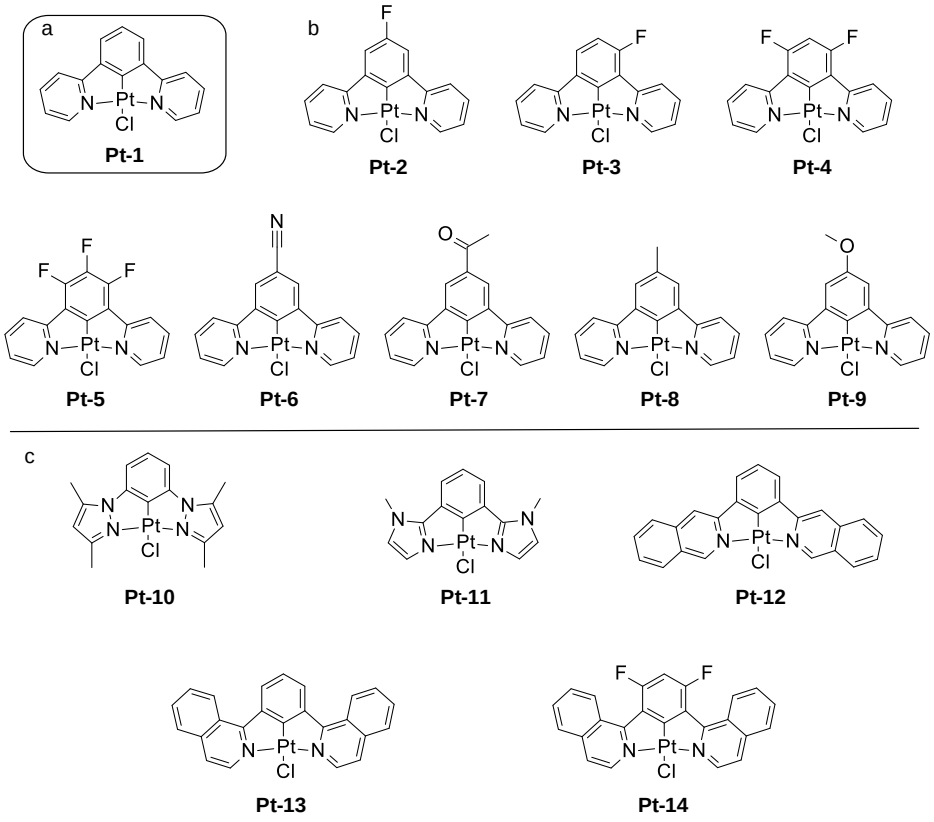

Figure 3.1 Structural formula and abbreviations used for the Pt(N^C^N)Cl complexes

3.2 Synthesis and Structural Characterization

3.2.1 Ligand Synthesis with Traditional Heating

One reliable avenue to synthesize the requisite ligands is via a Stille Reaction[90-92] that couples an organo-stannyl functionalized pyridyl group to a bis-halogenated phenyl substrate in the presence of a base and palladium catalyst. This method was used to synthesize the ligands with pyridyl substituents (Pt-1 – Pt-9) for which the organo-stannyl precursor was commercially available.

The 1,3-dibromobenzyl derivative (10 mmol), 2-(tri-n-butylstannyl)pyridine (11.4 g, 30 mmol), palladium triphenylphosphine dichloride (70 mg, 0.1 mmol), and

lithium chloride (2.55 g, 60 mmol) was added to toluene (70 mL). The mixture was set to reflux under a nitrogen atmosphere for 3 days, whereupon it was cooled to room temperature, filtered, and the filtrate poured into a solution of potassium fluoride. The organic phase was extracted with dichloromethane, and subsequently washed with a brine solution and dried over anhydrous magnesium sulfate. The resulting solution was evaporated to dryness and the crude product was subjected to column chromatography on silica using a mixture of hexanes and ether (4:1) as the eluent. Reaction results were generally good, with pure products isolated in 65 – 85% yields.

Scheme 3.1 Synthesis of m-di(2-pyridinyl)benzene and Pt(N^C^N)Cl complexes.

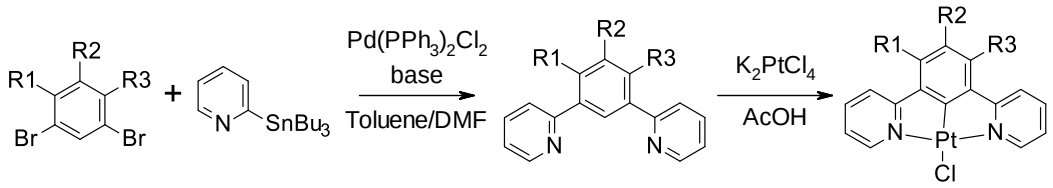

The ligand of Pt-12 was prepared by combining 1,3-diethynylbenzene (1.26 g, 10 mmol), *N*-(2-bromobenylidene)-*tert*-butylamine (5.0 g, 21 mmol), copper(I)iodide (10 mg, 0.05 mmol), and palladium triphenylphosphine dichloride (10 mg, 0.015 mmol) in triethyl amine (40 mL). The mixture was heated to 50^0 C for 6 hours, after which the solvent was removed under reduced pressure. The residue was then dissolved in anhydrous dimethylformamide, copper(I) iodide (50 mg, 0.25 mmol) was added, and the mixture was heated to 100^0 C for an additional 48 hours. The resulting mixture was allowed to cool, poured into water and extracted by dichloromethane. The organic phase was washed with brine, and dried over anhydrous magnesium sulfate. The residue was purified with column

chromatography that employed a silica stationary phase and a mixture of hexanes and ether (4:1) as the eluent.

The ligands of Pt-13 and Pt-14 were prepared by a Suzuki Coupling reaction.[93] The substituted 1,3-phenyldiboronic acid bis(pinacol) ester (1.0 mmol), palladium acetate (11 mg, 0.05 mmol), triphenyl phosphine (52 mg, 0.2 mmol), and 1-chloroquinoline (0.41g, 2.5 mmol) was dissolved in a 1:1 dimethyoxane/2M potassium carbonate aqueous solution (20 mL) and heated to reflux under a nitrogen atmosphere for 24 hours. After cooling, the mixture was diluted with ethyl acetate (100 mL) and washed with brine. The organic phase was separated, dried with anhydrous magnesium sulfate, and filtered. The filtrate was concentrated under reduced pressure and the residue purified by column chromatography on silica gel with a mixture of hexanes and ether (4:1) as the eluent with yields of 53% and 72% for Pt-13 and Pt-14 ligands respectively.

3.2.2 Microwave Accelerated Stille Reaction

The direct adaptation of this recipe with 1,3-di-bromobenzene under to microwave conditions failed to produce the desired product. Temperatures climbed slowly in response to input power, and it was hypothesized that inefficient absorption of microwave radiation by toluene was responsible.[94] To counter this, screening experiments were run with more polar solvent profiles ranging from 9:1 toluene to dimethylformamide to pure dimethylformamide. The heating response improved markedly under these conditions,[95] but the desired product remained elusive.

This set of experiments was run again with copper(II)oxide replacing lithium chloride as the base. Under these conditions, pure dimethylformamide produced excellent yields, while those containing toluene continued to fair poorly. The full battery of compounds was synthesized with pure dimethylfomamide as the solvent to compare the efficacy of microwave radiation to traditional heating.

Under a nirtogen atmosphere, the 1,3-dibromobenzene derivative (1 mmol), 2-(tri-n-butylstannyl)pyridine (1.14 g, 3 mmol), palladium triphenylphosphine dichloride (7 mg, 0.01 mmol), and copper(II)oxide (0.24g, 3 mmol) were added to stirring dimethylformamide (4 mL) in a 10 mL pressure vessel. The reaction mixture was rapidly heated to 160^0 C with 200 watts of power under air cooling. After 15 minutes, the microwave input was stopped and the mixture was allowed to cool to room temperature. The reactor contents were then diluted with dichloromethane (100 mL) and stirred with a solution of potassium fluoride for 30 minutes. The organic phase was washed further with brine, filtered, and the filtrate dried over magnesium sulfate. The solvent was evaporated under reduced pressure, and the crude product purified by column chromatography with silica as the stationary phases and a mixture of hexanes and ether (4:1) as the eluent. Yields were comparable to the traditional heating method, ranging from 60-79%.

3.2.3 Metal Coordination with Traditional Heating

As was the case with ligand synthesis, microwave[96, 97] was compared to traditional heating[90] via comparative reactions. The traditional method involves adding *m*-substituted benzyl ligands (1 mmol) and potassium tetrachloroplatinate(II) (0.41g, 1 mmol) to acetic acid (60 mL). The mixture was set

to reflux under a nitrogen atmosphere for three days. After cooling, the reaction mixture was filtered and the precipitate was washed with water, cold methanol, and ether. The crude product was further purified by recystalization in dimethyl sulfoxide and methanol followed by train sublimation. Reaction yields were largely good, ranging from 20 – 90%.

3.2.4 Metal Coordination with Microwave Heating

Just as in the ligand reaction, the solvent needed to be adjusted to better absorb microwave energy. A mixture of 9:1 acetic acid to water was found to absorb sufficient energy while maintaining the desired solvating abililty of acetic acid. To this solvent (3 mL), the ligand (1 mmol) and potassium tetrachloroplatinate(II) (0.41g, 1 mmol) were added under a nitrogen atmosphere and sealed in a microwave pressure vessel. The mixture was heated to 160^0 C under 200 W of power and air cooling. After 30 minutes, the irradiation was stopped and the solution allowed to cool to room temperature. The crude product was worked up in similar fashion to that of the traditional method. Yields generally exceeded those of the traditional method and ranged from 21 – 90%, and were much higher than those reported for microwave reactions with iridium.[96, 97]

3.2.5 Structure Verification

The structures of the platinum complexes were verified by proton nuclear magnetic resonance spectroscopy, matrix-assisted laser desorption/ionization spectroscopy, and combustion analysis.

1. Platinum[2,6-di(2-pyridinyl-KN)-4-fluorophenyl-KC] chloride (Pt-2). ^{1}H NMR (500 MHz, $CDCl_3$): δ 7.25 (d, J = 10.0 Hz, 2H), 7.34 (ddd, J_1 = 1.5 Hz, J_2 = 5.5

Hz, J_3 = 8.0 Hz, 2H), 7.66 (dd, J_1 = J_2 = 8.0 Hz, 2H), 7.99 (ddd, J_1 = 1.5 Hz,J_2 = J_3 = 8.0 Hz, 2H), 9.39 (dd, J_1 = 5.5 Hz,J_2 = 21.0 Hz, 2H). HRMS (MALDI-TOF), *m/z* calcd for [$C_{16}H_{10}ClFN_2Pt$]: 479.0164. Found: 478.9798. Calcd for [Mþ-Cl]: 444.0476. Found 444.0356. Anal. Calcd. for $C_{16}H_{10}ClFN_2Pt$: C, 40.05; H, 2.10; N, 5.84. Found: C, 39.16; H, 2.20; N, 5.89.

2. Platinum[2,6-di(2-pyridinyl-KN)-3-fluorophenyl-KC] chloride (Pt-3). ^{1}H NMR (500MHz,$CDCl_3$): δ 6.84 (dd, J_1 = 8.5Hz, J_2 = 11.5Hz, 1H), 7.23 (ddd, J_1= 1.0 Hz, J_2 = 5.5Hz, J_3 = 7.5 Hz, 1H), 7.29 (ddd, J_1 = 2.0 Hz, J_2 = 5.5 Hz, J_3 = 7.0 Hz, 1H), 7.40 (dd, J_1 = 4.0 Hz, J_2 = 8.5 Hz, 1H), 7.58 (dd, J_1 = 5.5 Hz, J_2 = 8.0 Hz, 1H), 7.89-7.96 (m, 3H), 9.23 (dd, J_1 = 5.5 Hz, J_2 = 21.0 Hz, 1H), 9.33 (dd, J_1 =5.5 Hz, J_2 = 21.0 Hz, 1H). HRMS (MALDI-TOF), *m/z* calcd for [$C_{16}H_{10}ClFN_2Pt$]: 479.0164. Found: 478.9971. Calcd for[Mþ-Cl]: 444.0476. Found:444.0448. Anal. Calcd. for $C_{16}H_{10}ClFN_2Pt$: C, 40.05; H, 2.10; N, 5.84. Found: C, 39.75; H, 2.25; N, 5.96.

3. Platinum [3,5-difluoro-2,6-di(2-pyridinyl-KN)-phenyl-KC] chloride (Pt-4). ^{1}H NMR (500 MHz, $CDCl_3$): δ 6.67 (t, J = 11.0 Hz, 1H), 7.30 (ddd, J_1 = 1.5 Hz, J_2 = 6.0 Hz, J_3 = 7.5 Hz, 2H), 7.89 (d, J = 7.5 Hz, 2H), 7.96 (ddd, J_1 = 1.5 Hz, J_2 = 7.5 Hz, J_3 = 7.5 Hz, 2H), 9.31 (ddd, J_1 =1.0 Hz, J_2 = 6.0 Hz, J_3 = 21.0 Hz, 2H). HRMS (MALDI-TOF), *m/z* calcd for [$C_{16}H_9ClF_2N_2Pt$]: 497.0070. Found: 496.9369. Calcd for [Mþ-Cl]: 462.0382. Found: 462.0216. Anal. Calcd. for $C_{16}H_9ClF_2N_2Pt$: C, 38.61; H, 1.82; N, 5.63. Found: C, 38.10; H, 1.91; N, 5.74.

4. Platinum [3,4,5-trifluoro-2,6-di(2-pyridinyl-KN)-phenyl-KC] chloride (Pt-5). ^{1}H NMR (500 MHz, $CDCl_3$): δ 7.30 (ddd, J_1 = 1.5 Hz, J_2 = 5.5 Hz, J_3 = 7.5 Hz, 2H), 7.90 (d, J = 8.0 Hz, 2H), 7.96 (ddd, J_1 = 1.5 Hz, J_2 = 7.5 Hz, J_3 = 8.0 Hz,

2H), 9.32 (dd, J_1 = 5.5 Hz, J_2 = 21.5 Hz, 2H). HRMS (MALDI-TOF), *m/z* calcd for [$C_{16}H_8ClF_3N_2Pt$]: 514.9976. Found: 514.9945. Calcd for [Mþ-Cl]: 480.0287. Found: 480.0506. Anal. Calcd. for $C_{16}H_8ClF_3N_2Pt$: C, 37.26; H, 2.66; N, 5.70. Found: C, 40.50; H, 3.10; N, 5.68.

5. Platinum[2,6-di(2-pyridinyl-KN)-4-cyano-phenyl-KC] chloride (Pt-6). ^{1}H NMR (500MHz, CDCl3): δ 7.45 (ddd, J_1 = 1.5Hz, J_2 = 6.0 Hz, J_3 = 7.5 Hz, 2H), 7.73 (s, 2H), 7.79 (d, J = 8.0 Hz), 8.08 (ddd, J_1 = 1.5Hz , J_2 = 7.5Hz, J_3 = 8.0Hz, 2H), 9.45 (dd, J_1 = 6.0 Hz, J_2 = 22.0 Hz, 2H). HRMS (MALDI-TOF), *m/z* calcd for [$C_{17}H_{10}ClN_3Pt$]: 486.0211. Found: 486.0336. Calcd for [Mþ-Cl]: 451.0522. Found: 451.0664. Anal. Calcd. for $C_{17}H_{10}ClN_3Pt$: C, 41.94; H, 2.07; N, 8.63. Found: C, 39.80; H, 1.95; N, 8.40.
6. Platinum [2,6-di(2-pyridinyl-KN)-4-acetylphenyl-KC] Chloride (Pt-7). ^{1}H NMR (500 MHz, $CDCl_3$): δ 2.68 (s, 3H), 7.36 (ddd, J_1 = 1.5 Hz, J_2 = 5.5 Hz, J_3 = 7.5Hz, 2H), 7.83 (d, J = 8.0 Hz, 2H), 8.03, (ddd, J_1 = 1.5 Hz, J_2 = 7.5 Hz, J_3 = 8.0Hz, 2H), 8.07 (s, 2H), 9.40 (ddd, J_1 =1.0 Hz, J_2 =5.5 Hz, J_3 = 22.0 Hz, 2H). HRMS (MALDI-TOF), *m/z* calcd for [$C_{18}H_{13}ClN_2OPt$]: 503.0364. Found: 503.0198. Calcd for [Mþ-Cl]: 468.0676. Found: 468.0892. Anal. Calcd. for $C_{18}H_{13}ClN_2OPt$: C, 42.91; H, 2.60; N, 5.56. Found: C, 42.06; H, 2.76; N, 5.60.
7. Platinum [2,6-di(2-pyridinyl-KN)-4-methylphenyl-KC] Chloride (Pt-8). ^{1}H NMR (500 MHz, $CDCl_3$): δ 2.37 (s, 3H), 7.28 (dd, J_1 = 2.0Hz, J_2 = 7.5Hz, 2H), 7.29 (s, 2H), 7.66 (d, J=8.0 Hz, 2H), 7.93 (ddd, J_1 = 2.0 Hz, J_2 = 7.5 Hz, J_3 = 8.0 Hz, 2H), 9.34 (ddd, J_1 = 1.0 Hz, J_2 = 6.0 Hz, J_3 = 22.0 Hz, 2H). HRMS (MALDI- TOF), *m/z* calcd for [$C_{17}H_{13}ClN_2Pt$]: 475.0415. Found: 475.0691.

Calcd for [Mþ-Cl]: 440.0726. Found: 440.1626. Anal. Calcd. for $C_{17}H_{13}ClN_2Pt$: C, 42.91; H, 2.75; N, 5.89. Found: C, 42.79; H, 2.71; N, 5.47.

8. Platinum [2,6-di(2-pyridinyl-KN)-4-methoxyphenyl-KC] Chloride (Pt-9). ^{1}H NMR (500MHz, $CDCl_3$): δ 3.90(s ,3H), 7.10 (s, 2H), 7.28 (ddd, J_1= 1.5 Hz, J_2 = 6.0 Hz, J_3 = 8.0 Hz, 2H), 7.65 (d, J = 8.0 Hz, 2H), 7.94 (ddd, J_1 = 1.5 Hz, J_2 = J_3 = 8.0 Hz, 2H), 9.34 (ddd, J_1 =1.0Hz, J_2 = 6.0Hz, J_3 = 21.0 Hz, 2H). HRMS (MALDI-TOF), *m/z* calcd for [$C_{17}H_{13}ClN_2OPt$]: 491.0364. Found: 491.0523. Calcd for [Mþ-Cl]: 456.0676. Found: 456.0828. Anal. Calcd. for $C_{17}H_{13}ClN_2OPt$: C, 41.50; H, 2.66; N, 5.70. Found: C, 40.80; H, 2.79; N, 5.68.
9. Platinum [2,6-di(3-isoquinolyl-KN)-phenyl-KC] chloride (Pt-12). ^{1}H NMR (500 MHz, $CDCl_3$): δ 7.27 (t, J = 7.5 Hz, 1H), 7.49 (d, J = 7.5 Hz, 2H), 7.63 (ddd, J_1 = 8.0 Hz, J_2 = 7.0 Hz, J_3 =1.5Hz, 2H), 7.79 (ddd, J_1 =8.0 Hz, J_2 = 7.0Hz, J_3 = 1.5 Hz, 2H), 7.87 (d, J = 8.0 Hz, 2H), 7.97 (dd, J_1 = 4.0, J_2 = 7.0 Hz, 2H), 8.07 (d, J=8.0 Hz, 2H), 10.07 (dd, J = 23 Hz, 2H). Anal. Calcd. for $C_{24}H_{15}ClN_2Pt$: C, 51.31; H, 2.69; N, 4.99. Found: C, 50.73; H, 2.31; N, 5.27.
10. Platinum [2,6-Di(1-isoquinolyl-KN)-phenyl-KC] Chloride (Pt-13). ^{1}H NMR (500MHz, $CDCl_3$): δ 7.44 (t, J = 8.0Hz,1H), 7.68 (d, J = 6.5 Hz, 2H), 7.74 (ddd, J_1 = 1.5 Hz, J_2 = 8.5 Hz, J_3 = 8.0 Hz, 2H), 7.80 (ddd, J_1 = 1.5 Hz, J_2 = 8.5 Hz, J_3 = 6.5 Hz, 2H), 7.95 (d, J = 8.0Hz, 2H), 8.29 (d, J = 8.0 Hz, 2H), 8.99 (d, J = 8.5 Hz, 2H), 9.52 (dd, J_1 = 6.5 Hz, J_2 = 18.5 Hz, 2H). Anal. Calcd. for $C_{24}H_{15}ClN_2Pt$: C, 51.31; H, 2.69; N, 4.99. Found: C, 50.23; H, 2.93; N, 5.04.
11. Platinum [3,5-Difluoro-2,6-di(1-isoquinolyl-KN)-phenyl- KC] Chloride (Pt-14). ^{1}H NMR (500 MHz, $CDCl_3$): δ 6.91 (t, J = 12Hz, 1H), 7.69-7.74 (m, 4H), 7.84 (ddd, J_1 =1.0 Hz, J_2 = 8.0 Hz, J_3 = 8.0 Hz, 2H), 7.92 (d, J = 8.0 Hz, 2H), 8.51

(d, J = 8.5 Hz, 2H), 9.43 (dd, J_1 = 6.5 Hz, J_2 = 18.5 Hz, 2H). HRMS (MALDI-TOF), *m/z* calcd for [$C_{24}H_{13}ClF_2N_2Pt$]: 597.0383. Found: 597.0388. Calcd for [Mþ-Cl]: 562.0695. Found: 562.0765. Anal. Calcd. for $C_{24}H_{13}ClF_2N_2Pt$: C, 48.21; H, 2.19; N, 4.69. Found: C, 47.97; H, 2.41; N, 4.82.

Table 3.1 The Stille cross-coupling reaction and metal coordination yields under two conditions.

	Ligand Yield (%)		Metalization Yield (%)	
	Microwave	Traditional	Microwave	Traditional
Pt-1	67	65	80	70
Pt-2	70	65	84	75
Pt-3	65	60	64	60
Pt-4	74	75	84	80
Pt-5	66	66	86	90
Pt-6	81	76	90	62
Pt-7	69	60	72	66
Pt-8	72	79	42	31
Pt-9	69	60	21	20

Substituent effects were not detected in the formation of ligands for either synthesis method employed. However, substituent effects were present in the metallization reaction under both conditions (Table 3.1). When electron withdrawing groups were present (Pt-2 – Pt-7), yields trended markedly higher than when electron donating groups were present (Pt-8 – Pt-9). The steric hindrance found in

the quinolyl based complexes (Pt-12 – Pt-14) was not sufficient to affect reaction yields.

Scheme 3.2 Proposed Mechanism for the Metal Coordination Reaction

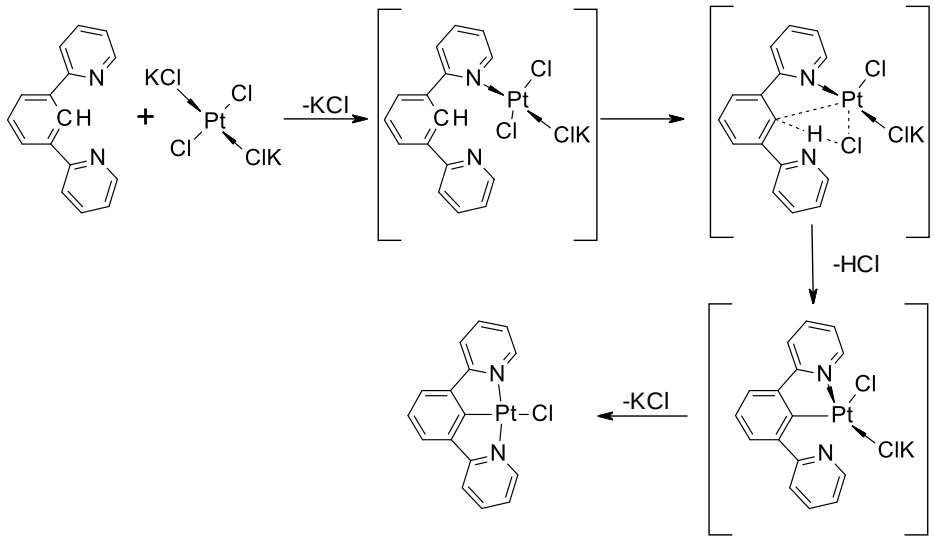

A proposed reaction mechanism (Scheme 3.2) that accounts for the observed substitution effects is a multi-centered pathway that is initiated by nucleophilic attack by the nitrogen in the N-heterocycle on the platinum ion. This is followed by an electrophilic attack by the platinum ion on the C-H bond at the coordination site on the phenyl ring.[98, 99] When electron withdrawing groups are present on the phenyl ring, electron density at the C-H bond decreases, making the site more acidic and the bond is more easily cleaved. Electron donating groups have the opposite effect.

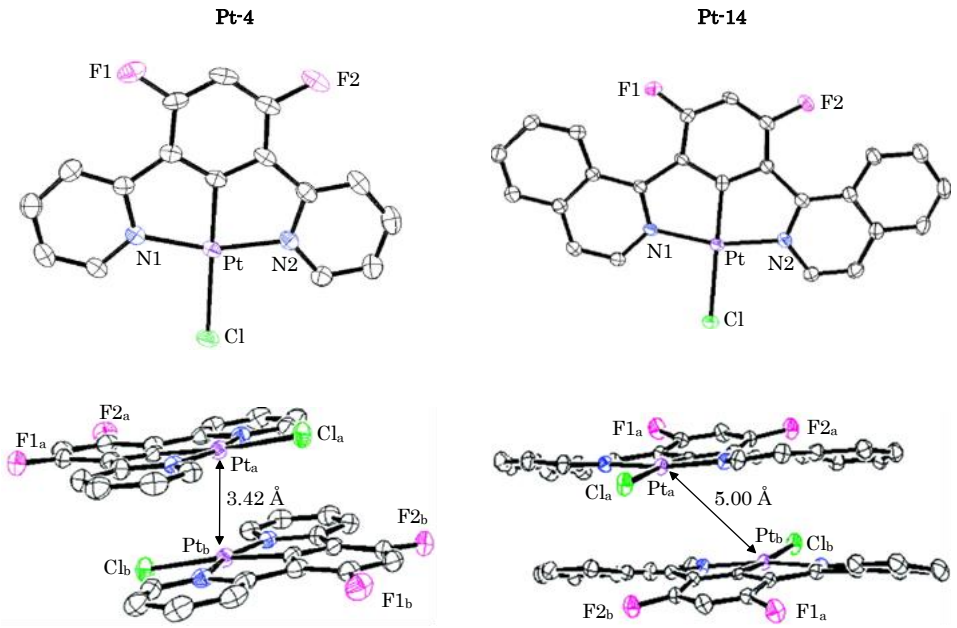

Figure 3.2 ORTEP drawings of Pt-4 (left) and Pt-14 (right) in the monomeric (top) and dimeric (bottom) form. The thermal ellipsoids for the image represent a 25% probability limit. Hydrogen atoms are omitted for clarity. The solid line indicates the shortest distance between two Pt atoms.

Single crystals of Pt-4 and Pt-14 were prepared for x-ray crystallography by sublimation under vacuum in a zoned furnace. Molecular plots are shown in Figure 3.2, the crystallographic data is summarized in Table 3.3, and selected atomic distances are given in Table 3.2. Both Pt-4 and Pt-14 have distorted square planar geometries.

Table 3.2 Selected bond distances and plane-to-plane distance (Å) for Pt complexes discussed in this chapter

	Pt-C	Pt-N_1	Pt-N_2	Pt-Cl	$Pt_a \cdots Pt_b$	$Pt_a \cdots plane_b$
Pt-1[90]	1.907(8)	2.033(6)	2.041(6)	2.417(2)	4.85	3.40
Pt-4	1.910(6)	2.028(5)	2.043(15)	2.412(2)	3.42	3.38
Pt-14	1.918(8)	2.009(7)	2.021(7)	2.412(2)	5.00	3.47

The platinum coordination bonds lengths in the complexes are similar, despite significant differences in the ligand as a whole. The plane-to-plane separation of Pt-4 and Pt-14 dimers is 3.38 Å and 3.47 Å respectively, indicating moderate π – π interactions. The Pt – Pt distance in Pt-14 (5.00 Å) is significantly longer than Pt-4 (3.42 Å), which can be attributed to increased out of plane distortion of the isoquinolinyl groups found in Pt-14 when compared to the pyridyl groups found in Pt-4.

Table 3.3 Crystal data and summary of intensity, data collection, and structure refinement for Pt-4 and Pt-14

	Pt-4	Pt-14
Empirical formula	C16H9ClF2N2Pt	C24H13ClF2N2Pt
Formula weight (g/mol)	497.79	597.90
Temperature (K)	298(2)	298(2)
Wavelength (nm)	0.71073	0.71073
Crystal system	monoclinic	triclinic
Space group	P 21/n	P $\bar{1}$
Unit cell dimentions		
a (Å)	8.3088(12)	7.7675(12)
b (Å)	9.5462(14)	10.9813(17)
c (Å)	17.574(3)	11.7112(18)
α (Å)	90.00	83.038(2)
ß (Å)	94.747(3)	71.078(2)
γ (Å)	90.00	75.310(2)
Volume (Å3)	1389.2(4)	913.1(2)
Z	4	2
dcalc kg/m3	2.380	2.175
Absorption coefficicent (mm^{-1})	10.311	7.864
F(000)	928	568
θ data collection range (deg)	2.430 – 25.096	2.602 – 27.563
Reflections collected	10867	7174
Indepentant reflections	2463	3204
Refinment method	full matrix, least squares on F2	
Data/restraints/parameters	2451/0/199	3204/0/271
Goodness-of-fit on F2	1.120	1.131
Final R indices [I > 2σI]	0.0288	0.397
R indeces (all data)	0.0323	0.0435

3.3 Electrochemical Properties

The electrochemical properties of the platinum complexes were examined using cyclic voltammetry. The redox potentials were determined with differential pulse voltammetry and are referenced to ferrocenium/ferrocene. All variants tested exhibit irreversible oxidation from 0.3-0.6 V and a first reduction that is either quasi-reversible or irreversible occurring between -1.74 and -2.72 V.

Table 3.4 Redox properties of Pt(N^C^N)Cl complexes. All complexes exhibit irreversible oxidation and irreversible or quasi-reversible reduction. Values reported are relative to Fc^+/Fc

Complex	$E_{1/2}^{Ox}$ (V)	$E_{1/2}^{Red}$ (V)	$\Delta E_{1/2}$ (V)
Pt-1	0.41	-2.18	2.59
Pt-2	0.47	-2.08	2.55
Pt-3	0.44	-2.09	2.53
Pt-4	0.50	-2.07	2.60
Pt-5	0.51	-2.07	2.58
Pt-6	0.59	-1.99	2.58
Pt-7	0.44	-2.07	2.53
Pt-8	0.40	-2.18	2.58
Pt-9	0.41	-2.16	2.57
Pt-10	0.57	-2.72	3.29
Pt-11	0.31	-2.73	3.04
Pt-12	0.31	-2.08	2.39
Pt-13	0.34	-1.84	2.18
Pt-14	0.56	-1.74	2.28

The redox properties are strongly affected by structural modifications to the ligand (Table 3.4). Species with electron withdrawing substitutions located on the

phenyl ring such as fluorine, cyano, or acetyl groups (Pt-2 – Pt-6) show an increased oxidation potential and decreased reduction potential when compared to those with electron donating substitutions such as methyl or methoxy groups (Pt-8 – Pt-9).[100] When the aromatic rings are bonded through an electron donating nitrogen (Pt-10), a marked increased oxidation potential occurs when compared to a similar system (Pt-11) sharing a carbon-carbon bonds. Changes to the N-heterocycle also affect changes in the redox behavior that correspond to differences in conjugation. Pyridyl based complexes (Pt-1 – Pt-9) have their first reduction between -1.99 and -2.18 V; five-membered aromatic rings (Pt-10 – Pt-11) near -2.72 V; and quinoline based complexes (Pt-12 – Pt-14) between -1.74 and -2.08 V.

The electrochemical data supports the premise that the reduction occurs mainly on the N-heterocycle region of the ligands, while oxidation is localized largely on the platinum center. This is consistent with most literature reports.[49] Additionally, the irreversible oxidation is expected due to solvent effects acting on the oxidized platinum ion.[101] When compared to similar bidentate complexes, the tridentate versions tend to have markedly lower reduction potentials. For example, the reduction of Pt-1 occurs 0.2 V lower than its bidentate analog (ppy)Pt(acac) (-2.41 V). This can be attributed to the greater conjugation found in the tridentate system.

3.4 Photophysical Properties

The absorption spectra were recorded at room temperature for all complexes. A selection appears in Figure 3.3 and peak values for the full set appear in Table 3.5. Emission spectra at room temperature and 77 K were also recorded and notable

features are shown in Table 3.6. The low temperature emission spectra of Pt-1, Pt-4, Pt-9, and Pt-13 are presented in Figure 3.4 and the room temperature spectra is presented in Figure 3.5.

Table 3.5 Absorption properties of Pt(N^C^N)Cl complexes at room temperature

	absorotion λ_{max} (nm); [ε (10^3 cm^2 mol^{-1})]
Pt-1	255 [25.2], 289 [21.1], 319 [6.1], 379 [8.6], 402 [7.0], 452 [0.15], 485 [0.14]
Pt-2	257 [33.0], 278 [26.3], 290 [28.2], 377 [8.8], 421 [9.9], 496 [0.12]
Pt-3	256 [31.3], 286 [23.3], 322 [7.7], 335 [8.6], 380 [10.4], 477 [0.13]
Pt-4	261 [30.9], 287 [21.8], 322 [8.2], 335 [11.1], 375 [10.4], 439 [0.15], 468 [0.14]
Pt-5	260 [27.0], 289 [19.9], 320 [6.1], 334 [6.8], 380 [8.3], 405 [4.6], 480 [0.08]
Pt-6	268 [43.2], 322 [4.9], 380 [8.1], 403 [6.7], 478 [0.13]
Pt-7	279 [60.1], 330 [9.7], 382 [12.6], 398 [10.5], 482 [0.09]
Pt-8	260 [25.0], 282 [19.9], 293 [21.9], 334 [5.7], 382 [6.8], 413 [6.9], 496 [0.09]
Pt-9	282 [25.0], 293 [27.6], 363 [4.3], 379 [6.3], 440 [8.6], 510 [0.08]
Pt-12	278 [90.1], 362 [28.8], 410 [17.0], 490 [0.03]
Pt-13	285 [19.4], 334 [5.7], 364 [5.0], 422 [5.1], 445 [4.5], 580 [0.06]
Pt-14	284 [66.6], 329 [15.2], 354 [14.4], 369 [15.1], 407 [18.5], 565 [0.04]

The absorption spectra were measured in a solution of dichloromethane.

All platinum complexes studied exhibit strong absorption bands below 300 nm ($\varepsilon > 1 \times 10^4$ L mol^{-1} cm^{-1}), indicative of intra ligand $^1\pi \rightarrow \pi^*$ transitions (LC). A region of lower intensity ($\varepsilon < 2 \times 10^3$ L mol^{-1} cm^{-1}) bands is present between 320 – 460 nm, which can be attributed to metal-to-ligand charge transfer (MLCT) transitions. A much weaker region of absorption exists from 440 – 600 nm ($\varepsilon < 2 \times 10^2$ L mol^{-1} cm^{-1}), which is similar to the respective emission energy of the complexes. This is consistent with $S_0 \rightarrow T_1$ transitions.

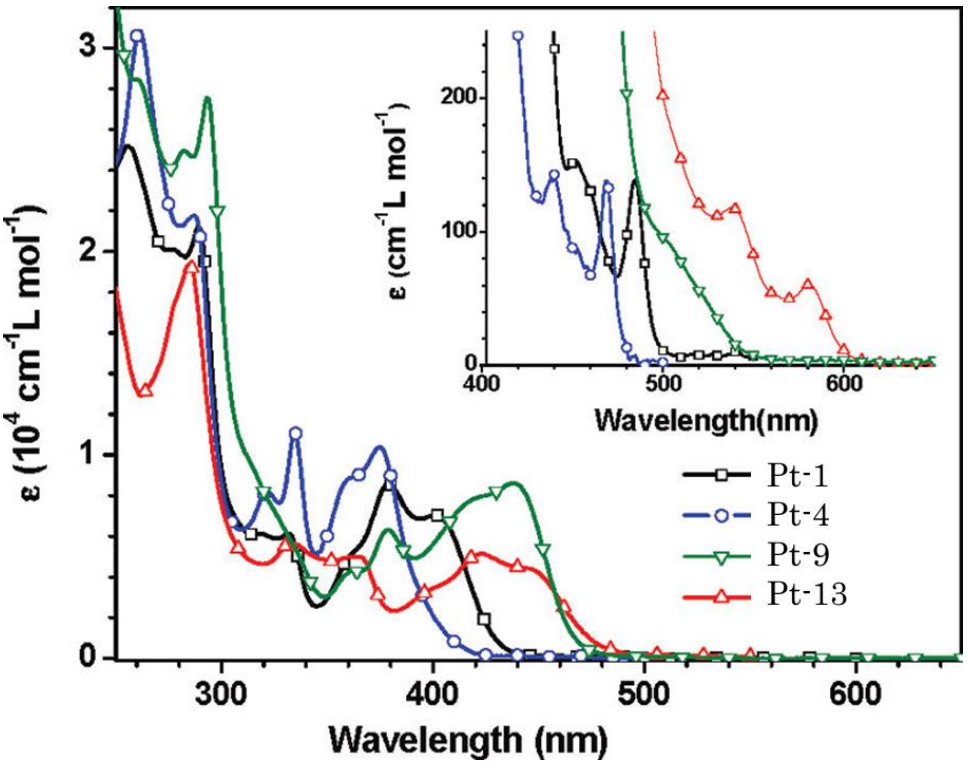

Figure 3.3 The comparison of absorption spectra of Pt-1, Pt-4, Pt-9, and Pt-13 in dichloromethane at room temperature. The T_1 absorption transitions are shown in the inset.

Structural differences between platinum complexes drive changes in their absorption properties. The addition of electron withdrawing groups to the phenyl ring (e.g., Pt-4) results in ^{1}MLCT and $S_0 \rightarrow T_1$ transitions that are higher energy than the unsubstituted Pt-1, which in turn has transition energies that are higher than complexes where electron donating groups (e.g., Pt-9) are present. Similarly, when compared to Pt-1 complexes containing five membered N-heterocycles have larger ^{1}MLCT and $S_0 \rightarrow T_1$ transitions while those based on more conjugated quinolyl groups possess transitions of lower energy. These effects are consistent with what has been reported in literature.[102, 103]

Table 3.6 Luminescent properties of Pt(N^C^N)Cl complexes at room temperature and cryogenic temperature (77 K)

	room temperature					77 K	
	λ_{max} (nm)	τ (μs)	Φ_{PL}	k_r (10^5 s^{-1})	k_{nr} (10^5 s^{-1})	λmax (nm)	τ (μs)
Pt-1	490	7.2	0.60	0.83	0.55	486	5.8
Pt-2	504	7.0	0.39	0.56	0.87	498	7.1
Pt-3	481	6.5	0.52	0.80	0.74	477	5.6
Pt-4	471	5.8	0.60	1.0	0.68	467	5.6
Pt-5	490(sh), 517	7.8	0.46	0.59	0.69	481	5.7
Pt-6	481	4.8	0.58	1.2	0.88	477	5.5
Pt-7	485	6.5	0.63	0.97	0.57	482	6.1
Pt-8	503	7.0	0.46	0.66	0.77	498	7.1
Pt-9	547	13	0.30	0.23	0.54	534	12
Pt-10	432	< 0.01	< 0.01	-	> 100	426	14
Pt-11	470	11	0.56	0.51	0.4	465	12
Pt-12	520(sh), 558	40	0.20	0.05	0.2	514	109
Pt-13	592	3.5	0.07	0.21	2.7	586	5.9
Pt-14	471	3.0	0.34	1.1	2.2	467	6.0

The room temperature emission spectra were measured in a solution of dichloromethane. The emission spectra at 77 K were measured in a solution of 2-methyl-tetrahydrofuran. Coumarin 47 was used as a reference for quantum efficiency measurements except: Coumarin 6, Pt-9; Rhodamine B, Pt-13.

Structural changes that affect ^{1}MLCT and $S_0 \rightarrow T_1$ absorption transitions produce changes in emission energy as well. Electron withdrawing groups on the phenyl ring and lower amounts of conjugation in the N-heterocycle push emission energies higher, while electron donating groups and larger amounts of conjugation have the opposite effect. Complexes based phenyl/pyridyl ligands are strongly luminescent with quantum efficiencies (Φ) ranging from 0.32 – 0.63 and lifetimes

ranging from 4 – 7 μs at room temperature. This is similar to values reported for Pt-1. Quinolyl based complexes are markedly less efficient, with values ranging from 0.07 – 0.2. Mixed results were obtained with the five membered N-heterocycle complexes synthesized. *Bis*-methylimidazole based Pt-11 is highly luminescent (Φ = 0.56) at room temperature, while *bis*-dimethlypyrazole based Pt-10 has almost no detectable emission.

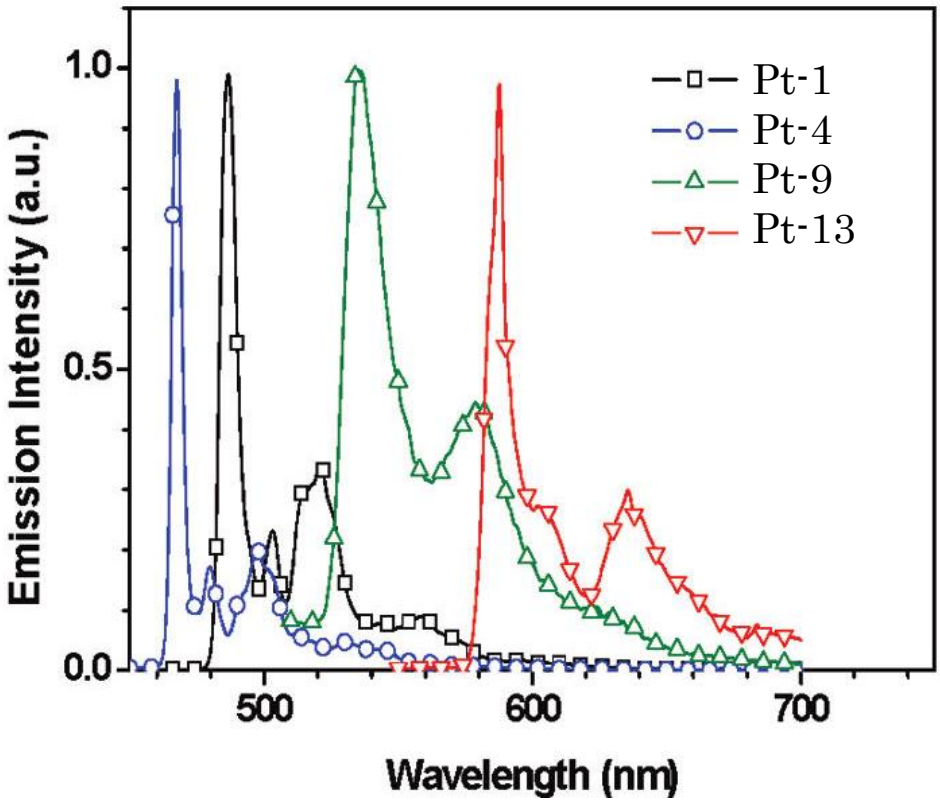

Figure 3.4 The 77K emission spectra of Pt-1, Pt-4, Pt-9 and Pt-13 in 2-methyltetrahydofuran.

Radiative decay rates on the studied complexes spans a wide range ($1.2x10^5$ s^{-1} to $5x10^3$ s^{-1}) and is highly structure dependent. Rates are highest in pyridyl based complexes, although a nearly two fold decrease is seen when electron donating groups are present. Quinolyl based complex show a further 3 – 5 fold decrease in

radiative rates. Pt-11 has rates similar to pyridyl complexes, while those of Pt-10 could not be calculated due to low emission driven by a much higher non-radiative rate decay (>$1x10^7$ s^{-1}). With exception of the aforementioned Pt-10, non-radiative decay rates of the complexes vary to a lesser extent ($2.9x10^5$ – $2x10^4$ s^{-1}). Rates tend to track higher with larger emission energies, suggesting energy gap law effects[104, 105] are present in the emission dynamics. At 77 K (Figure 3.4, Table 3.6), all complexes emit intensely with relatively short lifetimes (5 – 14 μs). An exception is the much longer lifetime (109 μs) measured for Pt-12, which is a result of slow rates of both radiative and non-radiative decay.

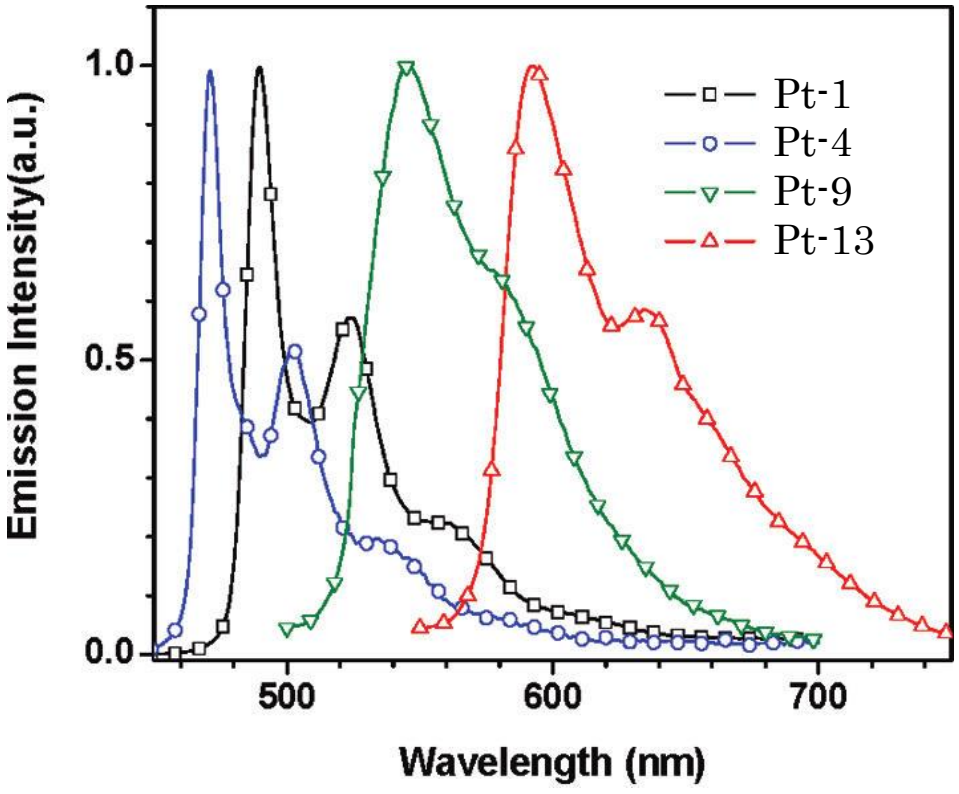

Figure 3.5 The room temperature emission spectra of Pt-1, Pt-4, Pt-9 and Pt-13 measured in dichloromethane.

At room temperature, the complexes all have a structured luminescence spectra with prominent vibronic progressions (Figure 3.5). For all complexes, the dominant vibrational mode (measured at 77 K) occurs near 1300 cm^{-1}. Within a given class, (e.g. pyridyl), the Huang-Rhys factors increase monotonically with decreasing energy of emission.[104, 106, 107]

3.5 Exploration of Ground and Excited State Properties

The lowest excited state of square planar d^8 molecules has been well studied over the past two decades. However, the bulk of the research[108-113] has focused on the characterization of the metal centered d-d excited state, which is an important non-radiative decay mechanism for this class of complexes. At the time of this work, there were few systematic studies that attempted to correlate that excited state of platinum complexes with their luminescent properties.

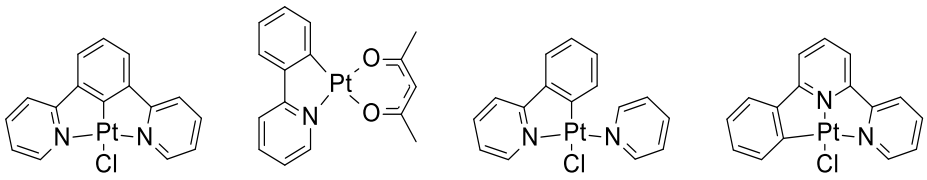

Figure 3.6 Structure of Pt-1 and its analogs.

Previous work[87] has found that the excited states of these complexes tend to be primarily composed of ligand centered triplet transitions (^{3}LC) mixed with lesser amounts of metal-to-ligand charge transfer (^{1}MLCT/^{3}MLCT) character. Obtaining a better understanding of the nature of the excited state would help explain why Pt-1

is more emissive than most platinum complexes reported thus far, and would enable future designs to have further improved luminescent properties.

Table 3.7 Emission properties of Pt-1 its analogs at room temperature

	λmax (nm)	τ (μs)	Φ_{PL}	k_r (10^5 s^{-1})	k_{nr} (10^5 s^{-1})
Pt-1	490	7.2	0.6	0.83	0.55
(ppy)Pt(acac)	484	2.6	0.15	0.57	3.2
(ppy)Pt(py)Cl	485	1.8	0.002	0.011	5.5
Pt(phbpy)Cl	563	0.5	0.025	0.5	19.5

The emission spectra were measured in a solution of dichloromethane. Coumarin 47 was used as a reference for quantum efficiency measurements.

In pursuit of this, the photophysical properties of Pt-1 has been compared with analogs: (ppy)Pt(acac),[49] ppyPt(py)Cl,[114] and Pt(phbpy)Cl.[110] The room temperature absorption (Figure 3.7) and emission spectra (Figure 3.8) of the four complexes is shown as well as a summary of photophysical data (Table 3.7).

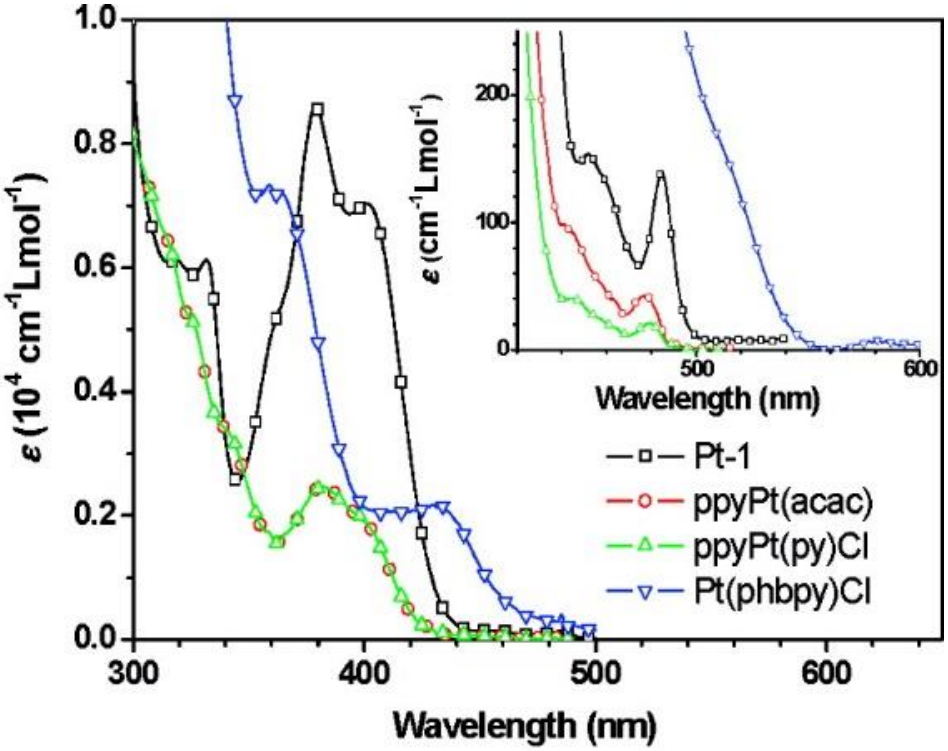

Figure 3.7 The comparison of the absorption spectra of Pt-1, ppyPt(acac), ppyPt(py)Cl, and Pt(pbpy)Cl in dichloromethane at room temperature. The T_1 absorption transitions are shown in the inset.

Pt-1, (ppy)Pt(acac), and (ppy)Pt(py)Cl have similar emission energy, vibronic structures, and triplet absorption energies. However, the quantum efficiency of Pt-1 is significantly higher, which can be attributed to comparably faster rates of radiative decay, and slower rates of non-radiative decay. The ^{1}MLCT absorption transitions in Pt-1 are lower in energy than its analogs, which likely results in better mixing between the more closely spaced ^{1}MLCT and ^{3}LC states.

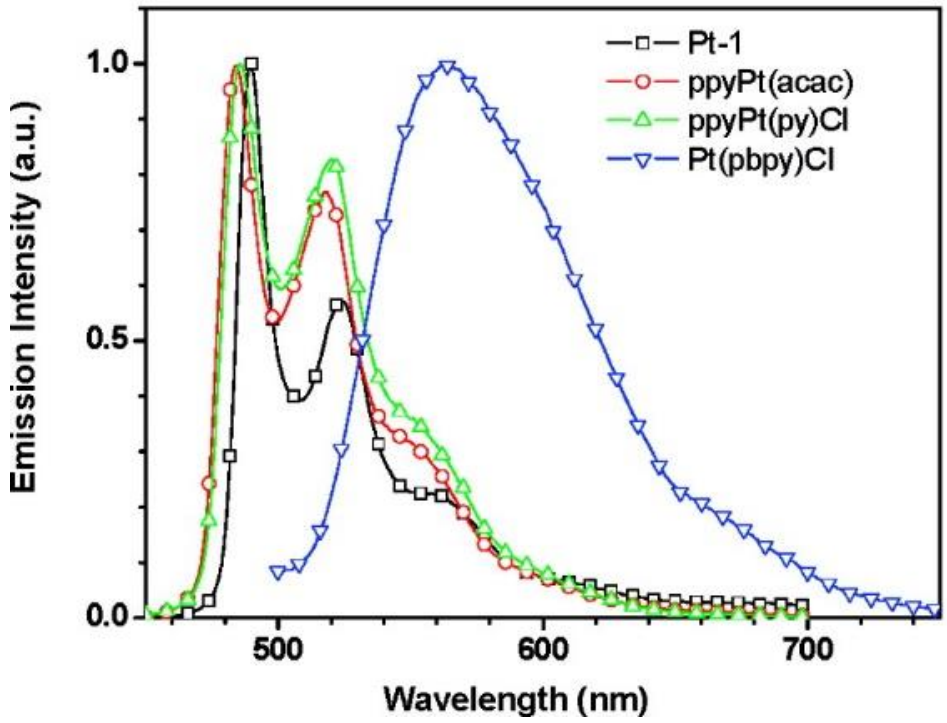

Figure 3.8 The room temperature emission spectra of Pt-1, and its analogs in dichloromethane.

Increased involvement of the ^{1}MLCT state is known to produce faster radiative decay rates as seen in Pt-1. This analysis is further supported by larger extinction coefficient of triplet absorption and smaller Huang-Rhys factor found in the complex. A rigid framework is known to be an important factor in reducing non-radiative decay rates.[115, 116] The 10 fold increase in the non-radiative decay rate of the less constrained (ppy)Pt(py)Cl is clear evidence of this effect.

Also of interest, Pt(phbpy)Cl is unique among the comparative complexes studied, exhibiting vastly different emissive properties despite having a phenyl/pyradyl based tridentate like Pt-1. The altered MLCT absorption, low-featured, red-shifted emission spectra,[110-112] and faster non-radiative decay rate of

Pt(phbpy)Cl suggest the structural difference present greatly affect the excited state properties.

3.6 Conclusion

Microwave heating was used to synthesize several members of a class of tridentate complexes of the type Pt(N^C^N)Cl. This method enabled much shorter reaction times along with modestly improved yield in most cases. Based on the relationship between reaction yield and substituent effects, a multi-centered, nucleophile-assisted electrophilic reaction was proposed as a possible mechanism.

Electrochemical analysis carried out on the complexes suggest that the oxidation process occurs on the platinum ion, while the reduction process occurs largely on the N-heterocycles. The photophysical study undertaken suggests the lowest excited state of the Pt(N^C^N)Cl complexes is primarily ligand centered (^{3}LC), with greater amounts of metal-to-ligand charge transfer when compared to the analogs studied. This configuration allows for a favorable radiative decay rate that can compete with the reduced non-radiative decay processes, resulting in a high quantum yield.

It was also shown that structural modifications could be used to tune the emissive properties of the complexes. Adding electron withdrawing groups to the phenyl ring or substituting smaller, less conjugated N-heterocycles shifted the emission to higher energy, while electron donating groups and larger N-heterocycles had the opposite effect.

This work has illuminated a clear path for further development of emissive materials. Future complexes should be designed in a way that maximizes MLCT

character in the excited state, minimizes non-radiative decay pathways through rigid molecules, and allows for quasi-independent color tuning through ligand modification.

CHAPTER 4

TETRADENTATE PLATINUM COMPLEXES

4.1 Introduction

The work of the previous chapter produced several efficient complexes while providing two methods in which to tune emission color. In the first, functional groups were added to the phenyl ring, altering the HOMO energy. The major drawback of this approach is that halogen abstraction is a well-known degradation mechanism for OLED emitters,[117] and halogen or pseudo-halogen groups are typically needed to increase the emission energy. The second method involved modifying the N-aryl groups to alter the LUMO energy. This method has the inherent advantage of being halogen free. However, both methods in the previous chapter relied on a chloride ancillary ligand. Creating a completely halogen-free complex was a major goal in future designs.

Square planar platinum complexes possess excellent structural flexibility, with the ability to employ a wide variety of cyclometalating ligands.[118-120] Those based on bidentate[49, 74] and tridentate[75-77] ligands have been the most studied, but tetradentate complexes have seen expanded interest in recent years, with many highly efficient examples being reported. Tetradentate platinum complexes are attractive candidates for emitters due to their rigid framework which can aid in thermal stability, as well as reduce non-radiative decay pathways.[116]

A series of complexes have been developed by Che and coworkers that incorporate O^N^C^N type ligands[121] such as 5,5- dibutyl-2-(3-(pyridine-2-yl)-phenyl)-5H-indeno[1,2-b]pyridin- 9-olate31 and O^N^N^O type ligands[122] from

Schiff bases such as N,N-bis(5-bromosalicylidene)-1,2-ethylenediamine and bis(phenoxy)diimine based ligands[123] such as 2,9-bis(2′-hydroxyphenyl)-4,7-diphenyl-1,10-phenanthroline. Other notable examples include bis-cyclometalated complexes of the type N^C*C^N using ligands such as N,N-di(6-phenylpyridin-2- yl)aniline, those of the type C^N*N^C using ligands such as N,N-di(3-(pyridine-2-yl)-phenyl)aniline[124] and 1,1-bis(6-(2,4- difluorophenyl)-2-pyridyl)-1-methoxyethane,[125] and those of the type C^C*N^N[126] using ligands such as N,N-di((1,1”3′,1″terphenyl)-50-yl)-(2,20-bipyridin)-6-amine. Several of these complexes have been incorporated into OLEDs, and while performance has been promising, it is still well below that of comparable iridium based emitters.

To improve over previous platinum emitters, careful ligand design is needed to increase radiative decay rates while simultaneously restricting non-radiative decay mechanisms. In this chapter, the design, synthesis, and characterization of a series of highly emissive tetradentate, bis-cyclometalated platinum complexes that emit light in the blue to green region is detailed.

4.2 Complex Design

The bulk of tetradentate complexes that have been reported recently fall into two main classes. Those reported by the Huo[124, 126] and Marder[125] groups utilize symmetric ligands that incorporate a single six membered chelate ring containing a linking group such as nitrogen or carbon and an identical pair of five membered chelating rings built from units such as phenyl- pyridine or phenyl-pyrazole. In contrast, Che and co-workers have recently reported a diverse set of complexes that use aryl- phenolate groups, in both symmetric[123] and asymmetric[121] configurations,

which incorporate varying numbers of five and six membered chelate rings. Given the design flexibility inherent in square planar systems, it is clear that the complexes that have been reported thus far represent only a small fraction of the set of possible designs. When considering design criteria for new luminescent materials, the resulting complexes should remain rigid for the purposes of thermal stability and reduced non-radiative decay rates, be easily tunable to various emission energies, and have sufficiently fast radiative decay rates.

A class of complexes was envisioned in which a portion of the ligand could be freely modified with widely reported cyclometalating motifs (N^C)[127] and coupled to a shared ancillary portion (LL′)[128] that would not be directly involved in the radiative decay process. This ancillary portion should be relatively easy to reduce and form an additional platinum–carbon bond to destabilize the well- known metal centered quenching states[129] found in platinum complexes. Phenoxyl pyridine (popy) was chosen to fill this role. The addition of the bridging oxygen between the (N^C) and popy portions enables facile metal coordination, whereas (N^C)Pt(popy) still remains as a synthetic challenge.

This design strategy results in a set of asymmetric tetradentate complexes of the type Pt[N^C–O–LL′]. To explore this class, three N^C motifs were selected: phenyl-pyrazole (ppz), phenyl-methylimidazole (pmi), and phenyl-pyridine (ppy).

4.3 Synthesis and Structural Characterization

The tetradentate ligands presented here (Scheme 4.1) were synthesized by two successive Williams ether couplings[130] followed by a suitable coupling reaction to attach the relevant N-heterocycle.

Scheme 4.1 Synthesis of Tetradentate Platinum Complexes PtOO1, PtOO2, and PtOO3

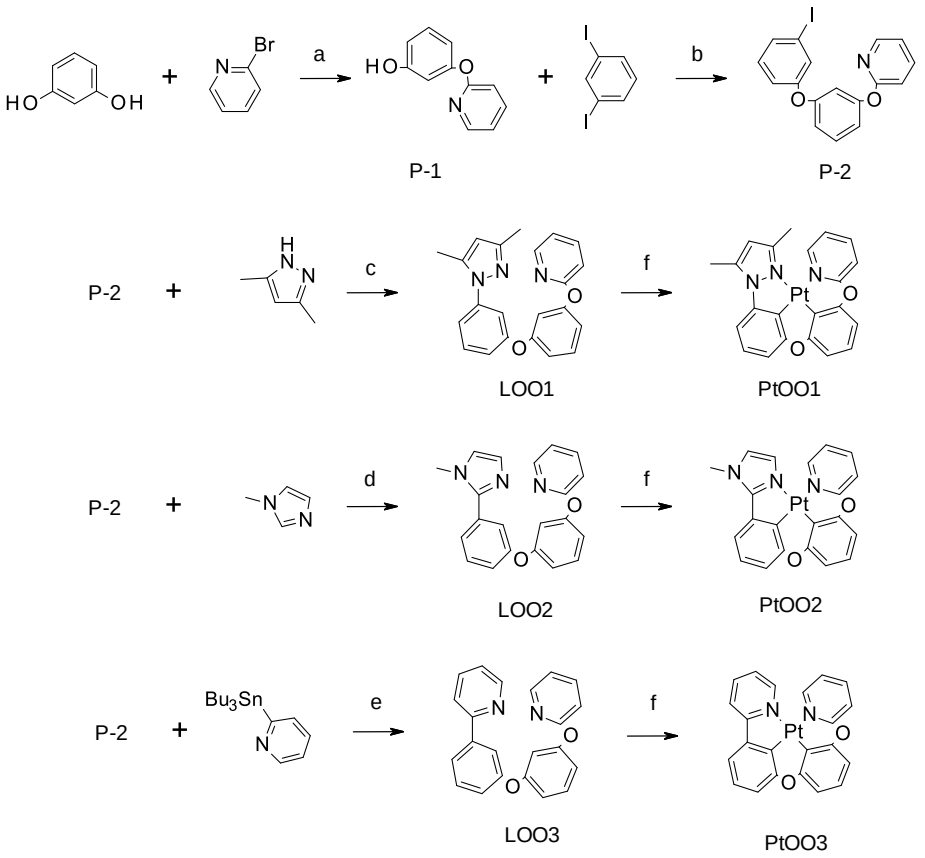

Reagents and conditions: (a) 1-methylimidazole (0.5 equiv), potassium carbonate (2 equiv), copper iodide (10%), pyridine/toluene (1:1), 120 °C. (b) 1-methylimidazole (0.5 equiv), potassium carbonate (2 equiv), copper iodide (10%), toluene, reflux. (c) copper(I) oxide (10%), syn-2-pyridinealdoxime (20%), cesium carbonate (2.5 equiv), acetonitrile, reflux. (d) copper(I) iodide (2 equiv), palladium acetate (10%), 1-methylimidazole (1.5 equiv), dimethylformamide, microwave, 150 W, 160 °C. (e) tetrakis(triphenylphosphine)palladium(0) (5%), potassium fluoride (1.2 equiv), toluene, reflux. (f) Potassium tetrachloroplatinate(II) (1 equiv), acetic acid, reflux

The first ligand precursor, 3-(pyridin-2-yloxy)phenol (P-1) proved to be a synthetic challenge. Resorcinol did not dissolve well in the solvent used in literature (toluene),[130] resulting in poor yield. Additionally, the prescribed workup procedure degraded the intended product through an attack on the remaining hydroxyl group.

To cope with this, the polarity of the solvent was increased, and acetic acid was added to the workup to protect the vulnerable hydroxyl group.

To an oven dried pressure vessel, 2-bromopyridine (15.80 g, 0.10 mol), resorcinol (16.51 g, 0.15 mol), 1-methylimidazole (4.11g, 0.05 mol), potassium carbonate (27.64g, 0.2 mol), and a 1:1 mixture of pyridine and toluene (200mL) were added. The solution was degassed with bubbling nitrogen for 10 minutes, after which copper(I) iodide (1.90 g, 0.01 mol) was added and the solution bubbled 10 minutes further. The vessel was sealed under a nitrogen atmosphere, brought to 120˚ C, and reacted for two days. The mixture was allowed to cool, diluted with toluene (200 mL), and poured into a stirring aqueous solution containing 5% acetic acid. The organic phase and undissolved solids were collected and washed three times with a brine solution. Ethanol was slowly added to the stirring organic phase until the solid matter had dissolved and subsequently dried over anhydrous magnesium sulfate. The mixture was filtered and the solvent removed under reduced pressure and dissolved in hot toluene. Slow cooling of the solution gave an off white product in 35% yield. ^{1}H NMR (400 MHz, $CDCl_3$): δ, 5.98 (s, 1H), 6.59 (s, 1H), 6.64 (d, 1H, J 8.9 Hz), 6.67 (d, 1H, J 7.4 Hz), 6.94 (d, 1H, J 8.2 Hz), 7.02 (vt, 1H, J 5.7 Hz), 7.23 (vt, 1H, J 8.2 Hz), 7.70 (vt, 1H, J 6.9 Hz), 8.23 (b, 1H).

The difficulties present in the synthesis of P-1 (poor solubility, hydroxyl decomposition) were not an issue in the synthesis of 2-(3-(3-iodophenoxy)phenoxy)pyridine (P-2), so the literature reaction conditions and workup were used. To an oven dried pressure vessel, 3-(pyridin-2-yloxy)phenol (P-1, 9.36 g, 0.05 mol), 2,6-diiodobenzene (16.5 g, 0.05 mol), 1-methylimidazole (2.1 g, 0.025 mol), potassium carbonate (13.8 g, 0.1 mol) and toluene (200mL) were added.

The solution was bubbled with nitrogen for 10 minutes. Copper(I) iodide (1.90 g, 0.01 mol) was added, and the solution bubbled 10 minutes further. The vessel was sealed under a nitrogen atmosphere and brought to reflux. The mixture was stirred for two days, cooled, and filtered. The filtrate was washed with water. The aqueous wash was then extracted with dichloromethane. The organic phases were combined, dried with anhydrous magnesium sulfate and filtered. The filtrate was evaporated to a thick oil which was flash chromatographed with silica and dichloromethane. The product was isolated in 60% yield. ^{1}H NMR (400 MHz, $CDCl_3$): δ, 6.80-6.86 (m, 2H), 6.90-6.95 (m, 2H), 6.97-7.04 (m, 2H), 7.19 (vt, 1H, J 7.8 Hz), 7.20-7.25 (m, 2H), 7.34 (vt, 1H, J 8.1 Hz), 7.70 (ddd, 1H, J 8.4, 6.8, 2.0 Hz), 8.22 (dd, 1H, J 5.0, 2.0 Hz).

The ligand of PtOO1, 2-(3-(3-(3,5-dimethyl-1H-pyrazol-1-yl)phenoxy)phenoxy)pyridine (LOO1)[131], was prepared by charging an oven dried flask with copper(I) oxide (0.14 g, 0.001 mol), syn-2-pyridinealdoxime (0.49 g, 0.004 mol), 3,5-dimethylpyrazole (1.15 g, 0.012 mol), cesium carbonate (8.1g, 0.025 mol), 2-(3-(3-iodophenoxy)phenoxy)pyridine (P-2, 3.9 g, 0.01 mol) and anhydrous acetonitrile (100 mL). The mixture was set to reflux for two days, cooled to room temperature, diluted with dichloromethane, and filtered through a plug of Celite. The filtrate was concentrated under reduced pressure and flash chromatographed using silica and dichloromethane. The desired product was isolated in 45% yield. ^{1}H NMR (400 MHz, $CDCl_3$): δ, 2.28 (s, 3H), 2.29 (s, 3H), 5.98 (s, 1H), 6.83 (vt, 1H, J 2.7 Hz), 6.85-6.93 (m, 3H), 6.98-7.04 (m, 2H), 7.13 (vt, 1H, J 2.2 Hz), 7.19 (dd, 1H, J 8.0, 1.8, 0.9 Hz), 7.34 (vt, 1H, J 8.2 Hz), 7.39 (vt, 1H, J 8.1 Hz), 7.69 (dd, 1H, J 7.2, 2.1 Hz), 8.19 (ddd, 1H, J 5.0, 2.0, 0.7 Hz).

The ligand of PtOO2, 2-(3-(3-(1-methyl-1H-imidazol-2-yl)phenoxy)phenoxy)pyridine (LOO2)[132] was prepared via microwave reaction. 2-(3-(3-iodophenoxy)phenoxy)pyridine (P-2, 3.9 g, 0.01 mol), copper(I) iodide (0.38 g, 0.002 mol), 1-methylimidazole (1.2 g, 0.015 mol), and anhydrous dimethylformamide (15 mL) were added to a 35 mL pressure vessel. The mixture was bubbled for 20 minutes. Palladium acetate (0.22 g, 0.001 mol) was added and allowed to bubble from 10 minutes further. The vial was then sealed and loaded into the microwave reactor. The contents of the vessel were irradiated with 150 watts of power and held at a temperature of 160˚ C with air cooling for two hours. The reaction mixture was allowed to cool and poured into a rapidly stirring mixture of dichloromethane and a 15% aqueous solution of ammonium hydroxide. After 30 minutes the organic phase was separated and the aqueous phase extracted with dichloromethane. The organic layers were combined, washed with brine, and dried with anhydrous magnesium sulfate. The mixture was filtered, and the filtrate reduced by evaporation under reduced pressure. The resulting oil was purified by column chromatography with silica as the stationary phase and dichloromethane and methanol (99:1) as the eluent to give the product in 80% yield.

The ligand of PtOO3, 2-(3-(3-(pyridin-2-yl)phenoxy)phenoxy)pyridine (LOO3)[133] was prepared by adding 2-(3-(3-iodophenoxy)phenoxy)pyridine (P-2, 3.9 g, 0.01 mol), potassium fluoride (0.70 g, 0.012 mol), 2-(tripropylstannyl)pyridine (3.7 g, 0.01 mol), and toluene (100 mL) to an oven dried three neck flask. The mixture was bubbled with nitrogen for 20 minutes and tetrakis(triphenylphosphine)palladium(0) (0.58 g, 0.5 mmol) was then added before being bubbled an additional 10 minutes. The contents of the flask were heated to reflux for two days, cooled, and filtered. The

filtrate was poured into a stirring aqueous potassium fluoride solution and after 20 minutes the organic phase separated and dried with anhydrous magnesium sulfate. The mixture was filtered, the filtrate evaporated under reduced pressure, and the oily raw product flash chromaographed with silica and dichloromethane. The desired product was isolated in 65% yield. ^{1}H NMR (400 MHz, $CDCl_3$): δ, 6.82-6.90 (m, 4H), 6.99 (ddd, 1H, J 7.5, 5.0, 0.7 Hz), 7.11 (ddd, 1H, J 8.0, 2.3, 0.7 Hz), 7.24 (ddd, 1H, J 7.3, 4.8, 1.4 Hz), 7.34 (vt, 1H, J 8.1 Hz), 7.44 (vt, 1H, J 7.9 Hz), 7.64-7.78 (m, 5H), 8.19 (dd, 1H, J 5.0, 2.0 Hz), 8.68 (d, 1H, J 5.0 Hz).

The tetradentate platinum complexes were synthesized by direct metallization. The respective ligand (1 mmol), potassium tetrachloroplatinate(II) (0.41g, 1 mmol), and acetic acid (60 mL) were set to reflux under a nitrogen atmosphere for three days. After cooling, the bulk of the solvent was removed under reduced pressure, diluted with dichloromethane, and added slowly to a stirring aqueous solution of sodium bicarbonate. The organic phase was collected, washed with brine, and dried over anhydrous magnesium sulfate. The solution was filtered and the filtrate removed under reduced pressure. The resulting solid was purified by column chromatography with aluminum oxide as the stationary phase and dichloromethane as the eluent. The product was further purified by slow diffusion of ether into dichloromethane, and finally by train sublimation. Complexes were characterized by ^{1}H and ^{13}C NMR and CHN elemental analysis.

PtOO1, 45% yield. Anal. Calcd. for $C_{22}H_{17}N_3O_2Pt$: C, 48.00%; H, 3.11%; N, 7.63%. Found: C, 48.06%; H, 3.21%; N, 7.62%. ^{1}H NMR (400 MHz, $CDCl_3$): δ 2.17 (s, 3H), 2.66 (s, 3H), 6.03 (s, 1H), 6.88−7.01 (m, 3H), 7.04−7.12 (m, 3H), 7.17 (vt, 1H, J 7.8 Hz), 7.32 (d, 1H, J 8.3 Hz), 7.83 (ddd, 1H, J 8.5, 7.1, 1.7 Hz), 8.78 (dd, 1H, J 5.9,

1.7 Hz). ^{13}C NMR (d_6-DMSO): 14.45 (1C), 14.58 (1C), 105.89 (1C), 107.90 (1C), 110.49 (1C), 110.66 (1C), 112.24 (1C), 112.59 (1C), 112.70 (1C), 116.09 (1C), 120.54, (1C), 124.57 (1C), 125.24 (1C), 142.00 (1C), 142.53 (1C), 147.57 (1C),150.33 (1C), 152.31 (1C), 152.43 (1C), 153.45 (1C), 155.81 (1C), 159.80 (1C).

PtOO2, 50% yield. Anal. Calcd. for $C_{21}H_{15}N_3O_2Pt$: C, 47.02%; H, 2.82%; N, 7.83%. Found: C, 47.00%; H, 2.94%; N, 7.77%. ^{1}H NMR (400 MHz, $CDCl_3$): δ 4.02 (s, 3H), 6.91 (dd, 1H, J 7.2, 1.7 Hz), 6.93 (d, 1H, J 1.2 Hz), 7.01 (d, 1H, J 1.4 Hz), 7.04−7.13 (m, 4H), 7.17 (vt, 1H, J 8.1 Hz), 7.27 (dd, 1H, J 7.1, 1.0 Hz), 7.32 (d, 1H, J 8.2 Hz), 7.90 (ddd, 1H, J 8.4, 7.1, 1.8 Hz), 8.81 (dd, 1H, J 5.9, 1.6 Hz). ^{13}C NMR (d_6-DMSO): 35.87 (1C), 104.00 (1C), 109.85(1C), 112.83 (1C), 116.26 (1C), 117.22 (1C), 117.37 (1C), 119.16 (1C), 122.16 (1C), 122.64 (1C), 124.23 (1C), 124.44 (1C), 124.50 (1C), 137.85 (1C), 139.82 (1C), 149.00 (1C), 152.84 (1C), 154.54 (1C), 155.07 (1C), 159.55 (1C).

PtOO3, 70% yield. Anal. Calcd. for $C_{22}H_{14}N_2O_2Pt$: C, 49.53%; H, 2.65%; N, 5.25%. Found: C, 49.57%; H, 2.78%; N, 5.19%. ^{1}H NMR (400 MHz, $CDCl_3$): δ 6.95 (dd, 1H, J 7.2, 1.8 Hz), 7.12−7.27 (m, 6H), 7.33 (d, 1H, J 8.3 Hz), 7.50 (dd, 1H, J 7.2, 1.4 Hz), 7.82 (ddd, 1H, J 8.6, 7.2, 1.6 Hz), 7.88 (ddd, 1H, J 8.7, 7.1, 1.9 Hz), 7.92 (d, 1H, J 8.1 Hz), 8.30 (d, 1H, J 5.5 Hz), 8.48 (dd, 1H, J 5.7, 1.9 Hz). ^{13}C NMR (d_6-DMSO): 106.24 (1C), 110.25 (1C), 112.69 (1C), 116.11 (1C), 117.38 (1C), 119.31 (1C), 120.46 (1C), 122.00 (1C), 124.23 (1C), 124.82 (1C), 124.89, (1C), 125.72 (1C), 139.44 (1C), 142.20 (1C), 147.66 (1C), 148.69 (1C), 149.46 (1C), 152.06 (1C), 154.01 (1C), 155.99 (1C), 159.82 (1C), 164.44 (1C).

4.3.1 X-ray Crystallography

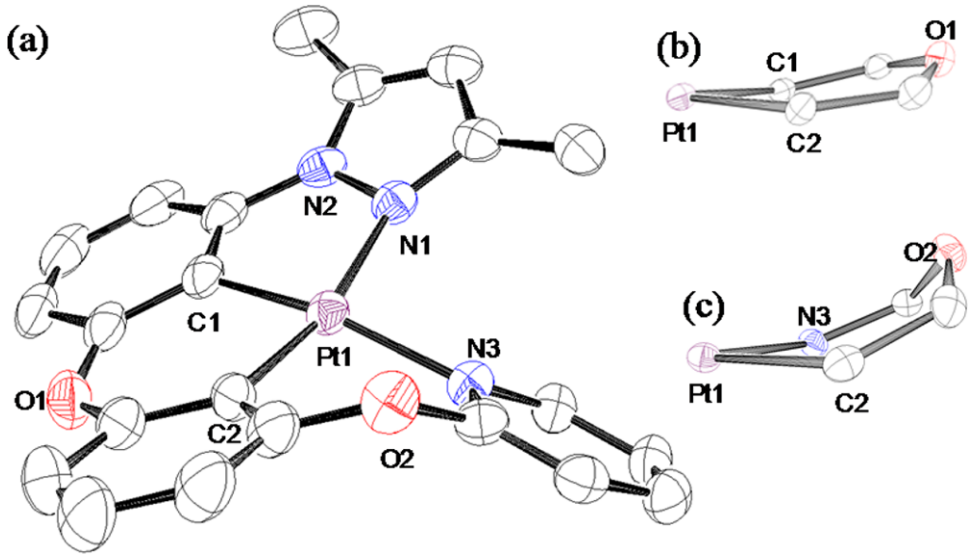

Figure 4.1 Perspective views of (a) PtOO1 with thermal ellipsoids representing the 25% probability limit, (b) the ring joining the two oxygen bridged phenyl rings, and (c) the ring joining the oxygen bridged phenyl and pyridyl rings. Hydrogen atoms were omitted for clarity.

Single crystals of PtOO1 were prepared for x-ray crystal structure determination by slow sublimation in a tube furnace under high vacuum (10^{-6} Torr). In contrast to the tridentate platinum prepared in the previous chapter, the structure of Pt-OO1 was significantly distorted out of plane (Figure 4.1). The boat-like configuration of the oxygen containing six membered rings, $\widehat{Pt-C1-C-O1-C-C2}$ and $\widehat{Pt-C1-C-O1-C-C2}$, are largely responsible for the deviation. The latter shows a larger degree of distortion. Additionally, metal-ligand bond lengths are longer in Pt-001 (Pt–N1pz = 2.097(3) Å, Pt–C1 = 1.970(4) Å, Pt–C2 =1.980(4) Å, and Pt–N3py = 2.093(3) Å) than in a similar tridentate complex[134], Pt(pzpyt)Cl, where pzpyt = 1-(1-pyrazolyl)-3-(2-pyridinyl)-toluene ($Pt–N_{pz}$ = 2.023(6) Å, Pt–C = 1.917(7) Å, and $Pt–N_{py}$ = 2.040(6) Å).

Table 4.1 Crystal data and summary of intensity, data collection, and structure refinement for PtOO1

	PtOO1
Empirical formula	$C_{22}H_{17}N_3O_2Pt$
Formula weight (g/mol)	550.48
Temperature (K)	296(2)
Wavelength (nm)	0.71073
Crystal system	monoclinic
Space group	$P\,2_1/n$
Unit cell dimentions	
a (Å)	15.130(2)
b (Å)	14.199(2)
c (Å)	18.764(3)
α (Å)	90.00
β (Å)	11.922(2)
γ (Å)	90.00
Volume (Å^3)	3739.6(9)
Z	8
d_{calc} kg/m^3	1.956
Absorption coefficicent (mm^{-1})	7.528
F(000)	2112
θ data collection range (deg)	2.608 – 24.924
Refinment method	full matrix, least squares on F^2
Data/restraints/parameters	6572/0/509
Goodness-of-fit on F^2	1.031
Final R indices [I > 2σI]	0.0225
R indeces (all data)	0.0303

4.3.2 Density Functional Theory

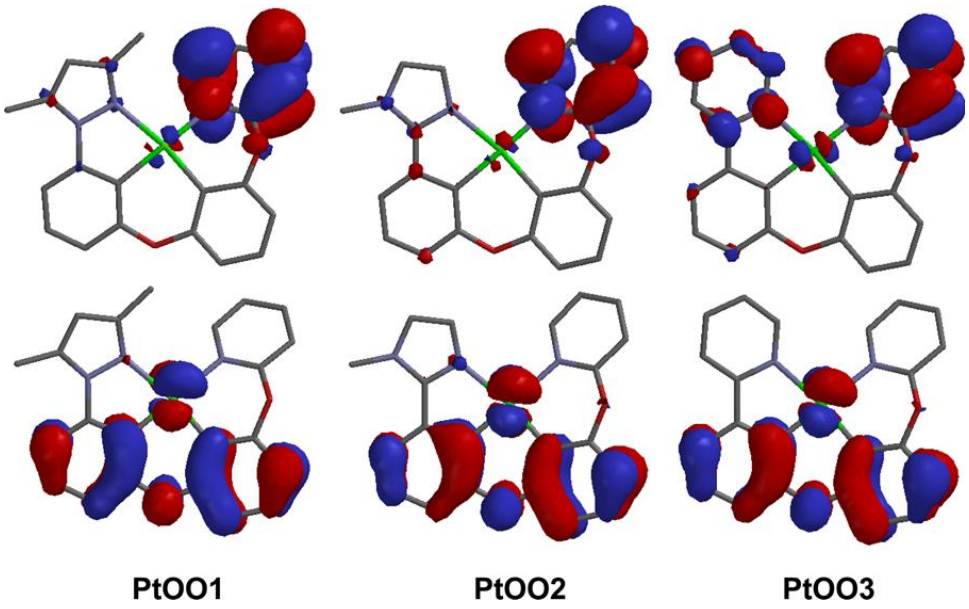

Figure 4.2 Highest occupied molecular orbital (HOMO) (bottom) and lowest unoccupied molecular orbital (LUMO) (top) of Pt[N^C–O–popy] complexes determined through density functional theory (DFT) calculations.

The geometry calculated with density functional theory agrees well with those of x-ray crystallography. DFT calculations show a similar deviation from planarity. With the exception of one carbon-platinum bond, the calculated metal-ligand bond lengths (Pt–$N1_{pz}$ (2.17 Å), Pt–C1 (2.00 Å), Pt–C2 (1.98 Å), and Pt–$N3_{py}$ (2.16 Å)) are longer than those found in the single crystal. The highest occupied molecular orbital (HOMO) and lowest unoccupied molecular orbital (LUMO) of the three tetradentate complexes are shown in Figure 4.2. The platinum metal, the two phenyl rings, and the oxygen atom bridging the rings constitute the bulk of the HOMO density. This is comparable to calculations done on Pt[N^C–N–C^N] complexes using the ligands N,N-di(3-(3-methyl-1H-pyrazol-1-yl)phenyl)aniline and N,N-di(3-(pyridin-2-yl)-phenyl)aniline.[124] Of note, the oxygen bridge of the

Pt[N^C-O-popy] complexes provides significantly less contribution to the HOMO than the triaryl amine in the comparable Pt[N^C–N–C^N] complexes. The LUMO density of PtOO1 and PtOO2 is dominated by the pyridyl ring, with minor contributions from the metal and N-heterocycle. PtOO3 shows additional contributions from its second pyridyl ring.

4.4 Electrochemical Properties

Table 4.2 Redox properties of tetradentate platinum complexes and analogs.

	$E_{1/2}^{Ox}$ (V)	$E_{1/2}^{Red}$ (V)	$\Delta E_{1/2}$ (V)
PtOO1	0.62	-2.59	3.21
Pt(dpzb)Cl[80]	0.57	-2.72	3.29
PtOO2	0.33	-2.62	2.95
Pt(dmib)Cl[80]	0.31	-2.73	3.04
PtOO3	0.38	-2.50	2.88
Pt(dpyb)Cl[75]	0.41	-2.18	2.59
(ppy)Pt(acac)	0.42	-2.41	2.83

All complexes exhibit irreversible oxidation and irreversible or quasi-reversible reduction. Values reported are relative to Fc+/Fc.

The electrochemical properties of the platinum complexes and analogs were examined using cyclic voltammetry (Figure 4.3) and differential pulsed voltammetry. Results are summarized in Table 4.2. The tetradentate complexes exhibit irreversible oxidation processes typical of platinum(II) complexes,[101] with potentials between 0.33 and 0.62 V. Reduction occurs between -2.62 and -2.50 V. The return waves of PtOO1 and PtOO2 are detectable only at scan speeds on order of

volts per second, and are thus considered irreversible. In contrast, Pt-OO3 shows two well defined return peaks at 100 mV/sec, making the process *quasi*-reversible.

The range of reduction values present in the comparable tridentate complexes (−2.73 to −2.18 V) is significantly larger. The narrower range found in the tetradentate complexes suggests reduction occurs on the common pyridyl group. This is supported by the pyridyl-dominated LUMO assignment calculated with density functional theory.

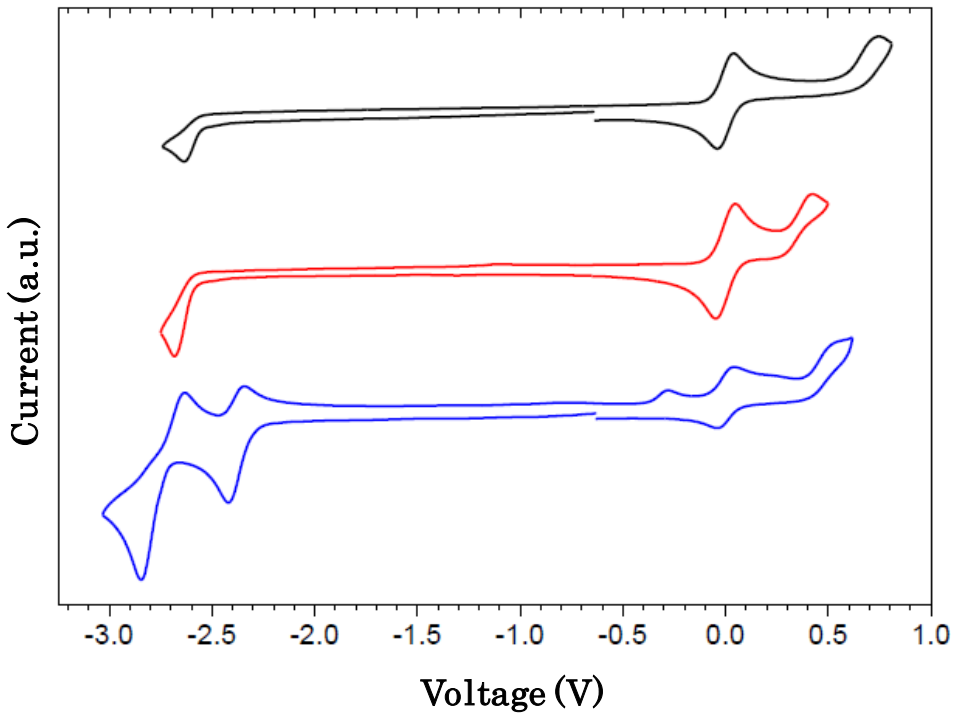

Figure 4.3 Vertically offset cyclic voltammetry scans at 100 mV/s of PtOO1 (top), PtOO2 (middle), and PtOO3 (bottom) in dimethylformamide with ferrocene used as an internal reference. Voltages are referenced to the ferrocene/ferrocenium peak.

4.5 Photophysical Properties

The emission spectra were recorded at room temperature and at cryogenic temperatures (77K) for the tetradentate complexes and their analogs (Table 4.3).

Table 4.3 Photophysical properties of Pt[N^C-O-popy] complexes and their analogs.

	room temperature									77 K	
	λ_{max} (nm)	τ (μs)		Φ_{PL}		k_r (10^5 s^{-1})		k_{nr} (10^5 s^{-1})		λ_{max} (nm)	τ (μs)
		sln	tf	sln	tf	sln	tf	sln	tf		
PtOO1	456	3.0	7.5	0.39	0.83	1.3	1.1	2.0	0.2	420	13
Pt(dpzb)Cl	432	~0	0.7	~0	0.02	-	0.3	-	15	426	15
PtOO2	468	9.0	10	0.64	0.81	0.7	0.8	0.4	0.2	462	12
Pt(dmib)Cl	470	11	-	0.56	-	0.5	-	0.4	-	465	12
PtOO3	512	2.0	4.5	0.63	0.97	3.2	2.2	1.8	0.1	487	5
Pt(dpyb)Cl	490	3.8	5.7	0.60	0.73	1.6	1.3	1.1	0.5	487	7
(ppy)Pt(acac)	484	2.6	6.0	0.15	0.53	0.6	0.9	3.3	0.8	480	9

Room temperature emission spectra were measured in a solution of dichloromethane and in a doped PMMA film. 77 K emission spectra were measured in a solution of 2-MeTHF. Coumarin 47 was used as a reference for quantum efficiency measurement in a dilute solution.

The absorption features of PtOO1, PtOO2, and PtOO3 are strikingly similar (Figure 4.4). Ligand centered (LC) transition dominate below 300 nm, while metal-to-ligand charge transfer (MLCT) transitions occur between 300-420 nm. Weaker, broad triplet transitions occur near the energy of maximum emission.

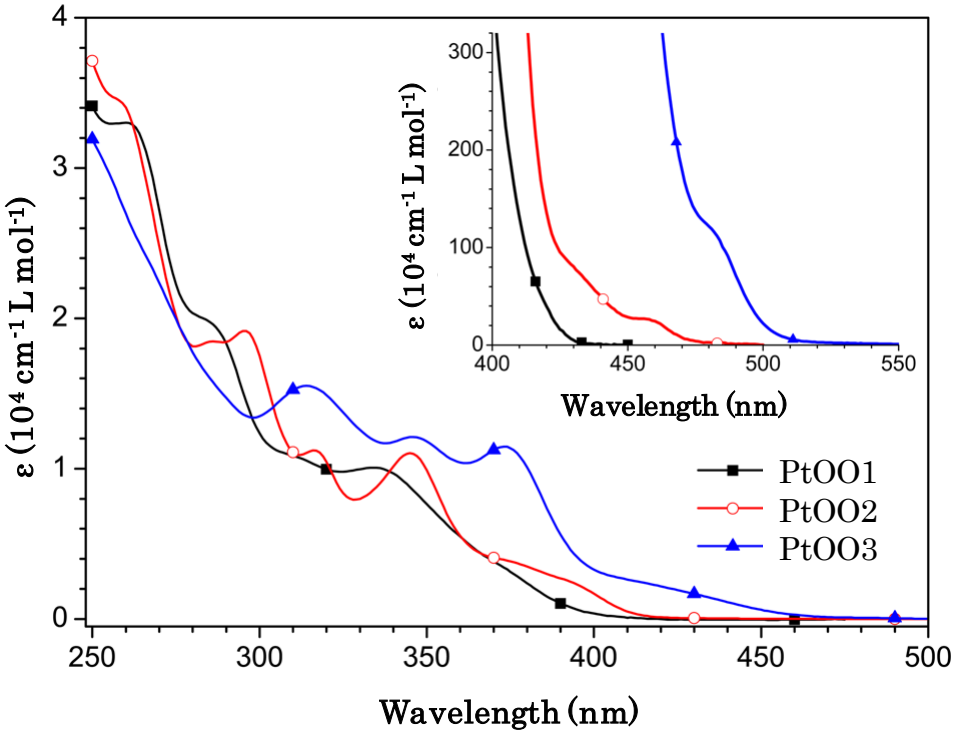

Figure 4.4 The comparison of the absorption spectra of PtOO1, PtOO2, and PtOO3 in dichloromethane at room temperature. The T_1 absorption transitions are shown in the inset.

At 77 K (Figure 4.5), PtOO1, PtOO2, and PtOO3 have sharp vibronic progressions of 1380 cm^{-1}, 1440 cm^{-1}, and 1380 cm^{-1} respectively. This is typical of complexes that emit from an excited state that is primarily ligand centered. Emission maxima ranges from 420 to 487 nm. The energy of emission is dependent on the reducibility of the N-heterocycle that is unique to each complex.

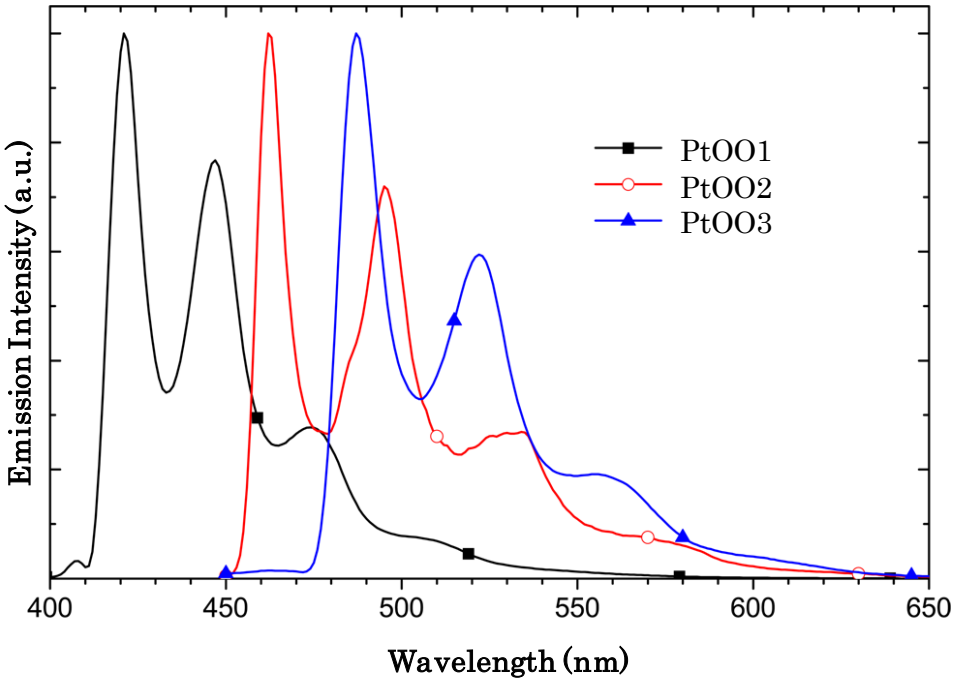

Figure 4.5 77K emission spectra of PtOO1, PtOO2, and PtOO3 in 2-methyltatrahydrofuran.

All tetradentate complexes are highly luminescent in degassed solution, emitting light ranging from green to blue (Figure 4.6). The vibronic progressions found at cryogenic temperatures in PtOO1 and PtOO3 become much less resolved at room temperature, while those of PtOO2 remain intact. Quantum efficiencies of the complexes range from 0.39 to 0.64 in solution and from 0.81 to 0.97 in thin film. These values are among the highest reported for platinum complexes. PtOO1 far exceeds the comparable iridium complex, *fac*-Ir(ppz)3 ($\Phi < 0.01$),[73] as well as the analogous tridentate Pt(dpzb)Cl ($\Phi < 0.01$ Table 4.3). In addition, it emits at much higher energy that the efficient complex based on N,N-di(3-(1H-pyrazol-1-yl)phenyl)aniline ligands.[124] None of the synthesized complexes exhibited eximer emission, regardless of concentration, unlike many other tetradentate complexes.[124]

This may be due to the distortion induced by the bridging oxygen, which disrupts the necessary intermolecular interactions.

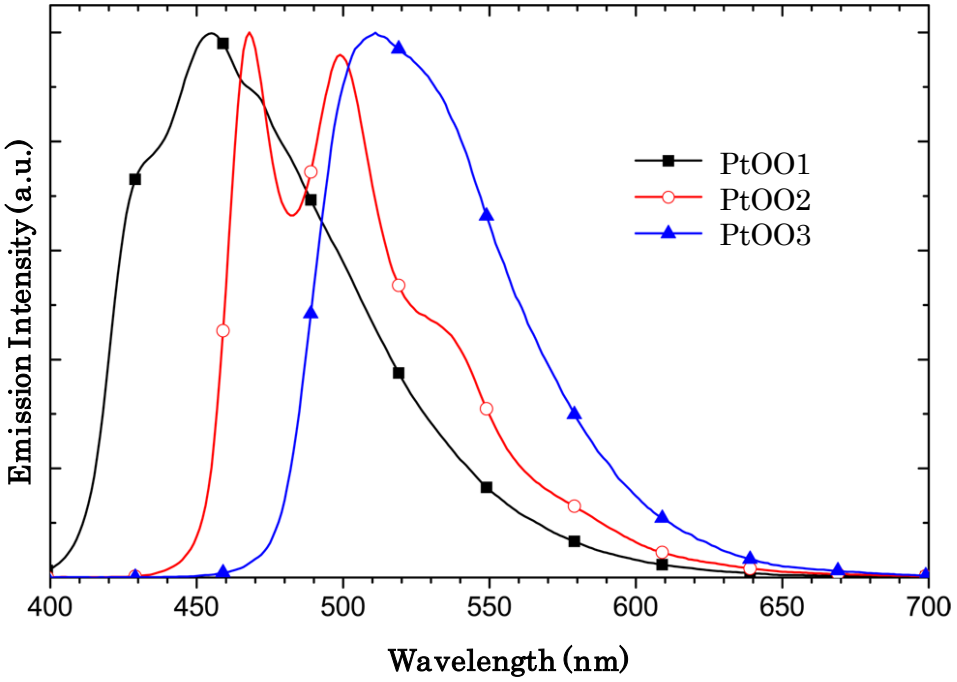

Figure 4.6 Room temperature emission spectra of PtOO1, PtOO2, and PtOO3 in 2-methyltatrahydrofuran.

4.6 Comparison with Analogs

The influence of the (popy) portion of the ligand on the photophysical properties of the tetradentate complexes can be understood by comparing similar complexes lacking the (popy) fragment. To this end, a series of ppy-based complexes were synthesized and characterized. This included the bidentate complex (ppy)Pt(acac), the tridentate complex Pt(dpyb)Cl (Pt-1, Chapter 3), where dpyb is dipyridylbenzene, and the triscyclometalated complex *fac*-Ir(ppy)$_3$ (Figure 4.7).

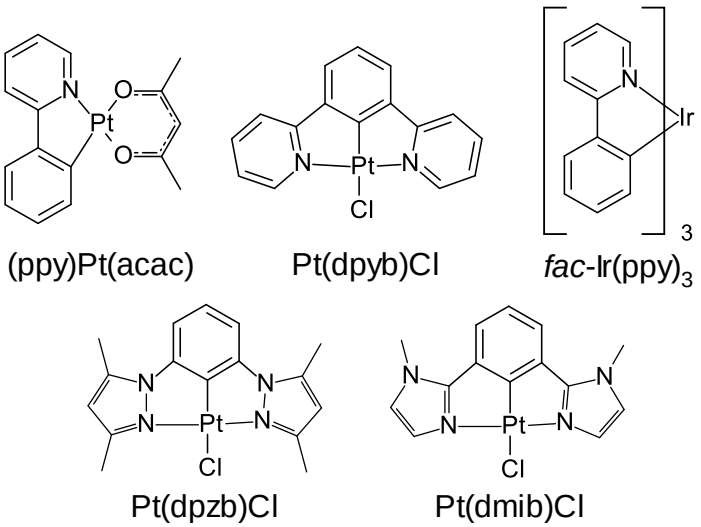

Figure 4.7 Structures of the synthesized ppy based comparative complexes (top) and the structures of literature reported ppz and pmi based comparative N^C^N tridentate complexes (bottom) discussed in this chapter.

The ppy based platinum complexes studied all show irreversible oxidation processes and quasi-reversible reduction processes. The reduction potential of Pt(dpyb)Cl is 300 mV less negative than PtOO3 or (ppy)Pt(acac), which have similar values. This trend was observed in the study conducted in the previous chapter, with the difference attributed to the extended conjugation present in the tridentate ligand.

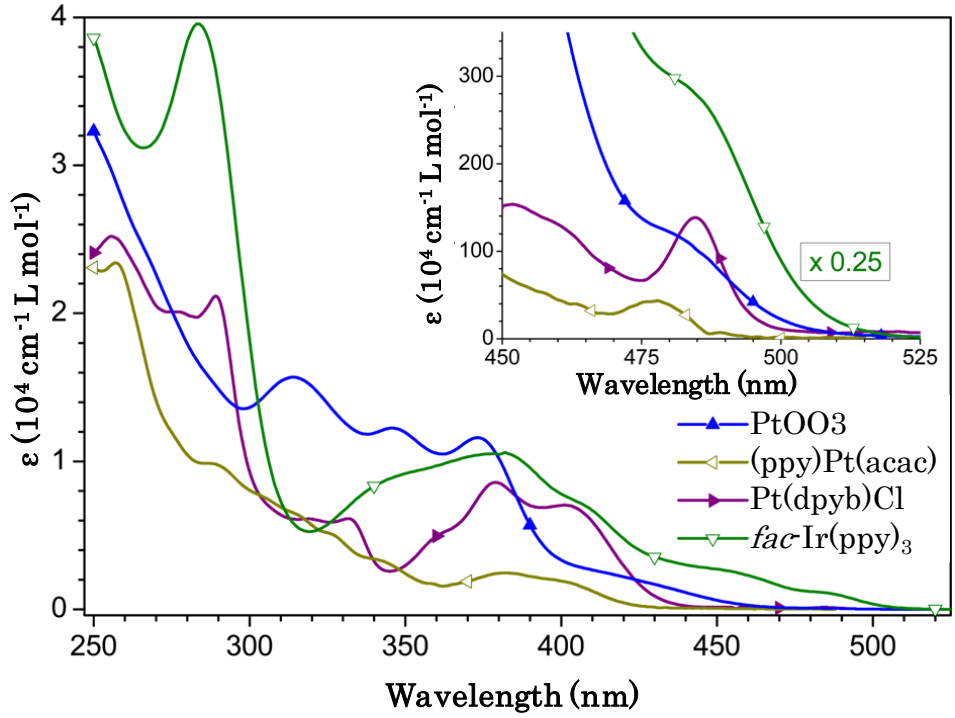

Figure 4.8 The comparison of the absorption spectra of PtOO3, Pt(dpyb)Cl, (ppy)Pt(acac) and *fac*-Ir(ppy)$_3$ complexes in dichloromethane at room temperature. The T_1 absorption transitions are shown in the inset.

The absorption features of the complexes were compared and appear in Figure 4.8. All show strong absorption bands below 300 nm, the result of $^1\pi-\pi^*$ ligand centered (LC) transitions. Less intense absorption bands appear between 300 and 420 nm, and can be attributed to metal-to-ligand charge transfer (MLCT) events. The weaker absorption bands that appear between 470 and 500 nm are identified as triplet transitions ($S_0 \rightarrow T_1$) due to their close proximity to the emission energy. Owing to their closely related structure, the absorption bands of the platinum complexes between 350 and 420 nm are similar. The triplet absorption of PtOO3 is higher (based on integration) that its platinum analogs, but remains significantly weaker than *fac*-Ir(ppy)$_3$.

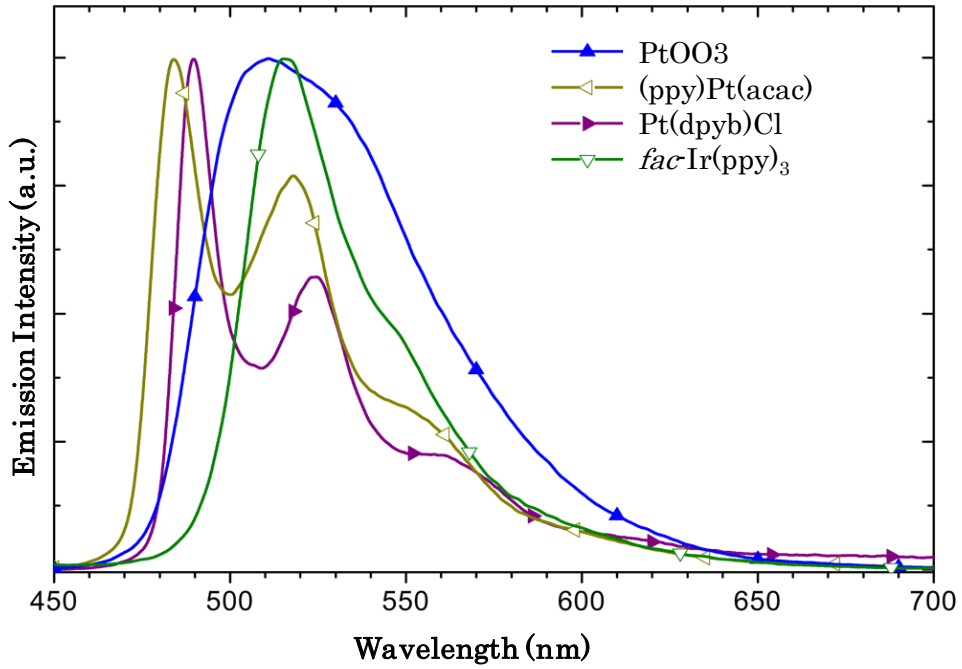

Figure 4.9 The emission spectra of PtOO3, Pt(dpyb)Cl, (ppy)Pt(acac) and *fac*-Ir(ppy)$_3$ complexes in dichloromethane at room temperature.

All of the synthesized comparative complexes are luminescent at room temperature, with quantum yields (Φ) ranging from 0.15 and 0.63 in solution and between 0.53 and 0.97 in a poly(methyl methacrylate) (PMMA) thin film. Luminescent lifetimes (τ) fall between 2 and 9 μs in solution and 4 and 10 μs when doped in a PMMA thin film.

The emission spectra of PtOO3, Pt(dpyb)Cl, (ppy)Pt(acac), and *fac*-Ir(ppy)$_3$ complexes are shown in Figure 4.9. The spectrum of PtOO3 is less resolved than either of its vibronic-dominated platinum based analogs, Pt(dpyb)Cl and (ppy)Pt(acac). It instead shares a broad, relatively featureless profile with *fac*-Ir(ppy)$_3$, suggesting more significant MLCT character in the excited states. Moreover, PtOO3 demonstrates a shorter luminescent lifetime (~2 μs), a higher quantum yield (0.63), and a larger rigidochromic shift between room temperature

and 77 K than either of its platinum analogs. When doped into a PMMA thin film, the quantum efficiency of PtOO3 approaches 100%. This compares favorably with tetradentate homoleptic bis-cyclometalated platinum complexes [1,1-bis(6-(4,6 difluorophenyl)-2-pyridyl-N,C2)-1-methoxyethane]-platinum(II)[125] (Φ = 0.54, τ = 0.38 μs) and the highly efficient [N,N-di(2-phenylpyrid-6-yl)aniline]-platinum(II)[124] (Φ = 0.74, τ = 7.6 μs) while possessing a shorter lifetime than the latter.

4.7 OLED Application

Devices were fabricated with PtOO3 and *fac*-Ir(ppy)$_3$ using the structure: ITO/PEDOT:PSS/20 nm TAPC[135]/25 nm 26mCPy[66]:emitters(8%)/10 nm PO15[136]/30 nm BmPyPB[137]/LiF/Al (Figure 4.10). Both PtOO3 and *fac*-Ir(ppy)$_3$ based devices have external quantum efficiencies (EQE) over 20%, peaking at 22.3% ph/el and 23.6% ph/el respectively. This is close to the theoretical limit of efficiency for a device on a planar glass substrate.

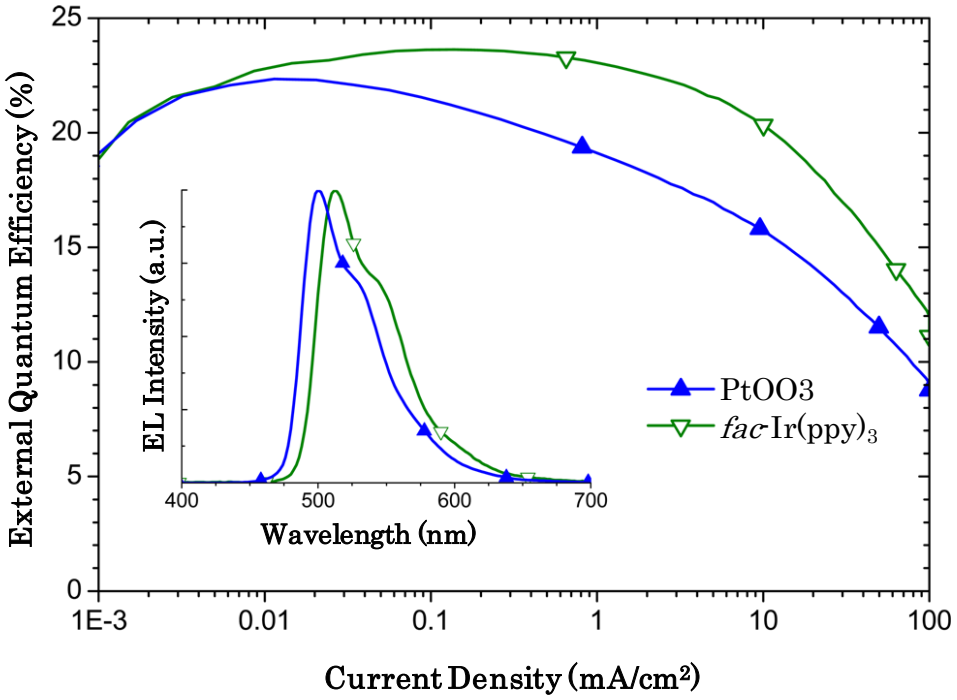

Figure 4.10 Quantum efficiency-current density characteristics of PtOO3 and *fac*-$Ir(ppy)_3$ devices with the structure of ITO/PEDOT:PSS/TAPC/26mCPy:emitters(8%)/PO15/BmPyPB/LiF/Al; Inset shows the EL spectra of the PtOO3 and *fac*-$Ir(ppy)_3$ devices.

The two OLEDs share similar current-voltage characteristics (Figure 4.11), but the EQE of the PtOO3 device shows more pronounce roll-off at higher currents. This may be the result of charge imbalance within the emissive layer. Despite this, devices based on PtOO3 demonstrated remarkably high quantum efficiencies of 20.6% ph/el at 100 cd/m^2 and 17.6% ph/el at 1000 cd/m^2.

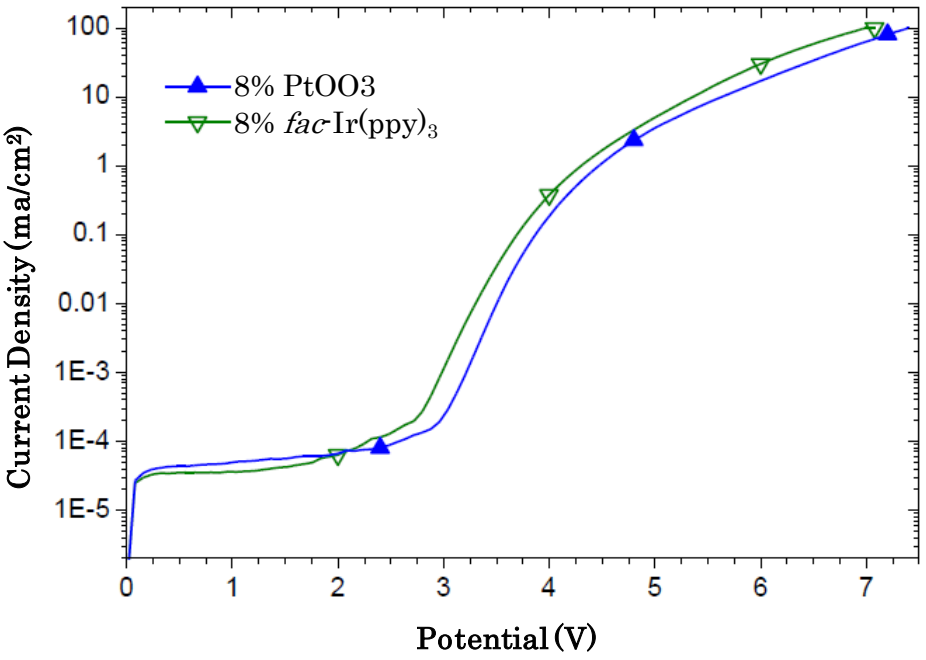

Figure 4.11 Current-voltage characteristics of PtOO3 and *fac*-Ir(ppy)$_3$ devices with the structure: ITO/PEDOT:PSS/TAPC/26mCPy:emitters(8%)/PO15/BmPyPB/LiF/Al.

4.8 Conclusion

The molecular engineering method employed yielded a series of efficient complexes of the type Pt[N^C−O−LL']. Of particular interest, the (ppy) variant, PtOO3 has an quantum yield in thin film that approaches unity. When employed as an emitter in an OLED device, it achieved approximately 100% electron-to-photon conversion efficiency. The method also produced PtOO1 and PtOO2, which demonstrated quantum efficiencies over 0.80, much higher than values reported for similar complexes (Table 4.3). The design strategy presented in this chapter served as a foundation for the development of emitters with the potential to span the visible spectrum. A natural progression of this study is to explore this class of ligand with different metal systems. Such complexes will yield valuable information as to the

dynamics of the photophysical system and aid in the further development of display and lighting technology.

CHAPTER 5

TETRADENTATE PALLADIUM COMPLEXES

5.1 Introduction

As discussed in previous chapters, most successful phosphorescent complexes have been based on iridium[42, 138, 139] or platinum metals.[80, 102, 103, 140-142] Other possibilities include osmium, ruthenium, gold, copper, rhodium, and palladium.[127, 129, 143] Regardless of the metal system employed, efficient emission relies on the radiative process of the complex out pacing competitive non-radiative decay processes. Optimization of efficiency can be achieved via modification of the ground and lowest excited states through a rational ligand design.

Owing to their utility, versatility of ligand modification, and rich photophysics, the luminescent properties of platinum complexes have been especially well studied.[144] Phosphorescent platinum complexes featuring several types of ligands have been reported. The structure of the coordinating ligand strongly affects the emission properties, and as such, photoluminescent quantum efficiencies vary greatly across ligand designs. While they are frequently emissive at room temperature, designs based on bidentate,[145-147] C^N^C terdentate,[140, 148, 149] and N^N^C terdentate[141, 150, 151] ligands typically offer lower efficiencies than those based on N^C^N[102, 103, 152] designs. Some recently reported tetradentate[121, 123, 126, 153-156] platinum complexes offer very high efficiency and the potential for improved stability in devices. In contrast to the success found in platinum complexes, when moving up within group ten to palladium the landscape becomes considerably dimmer.

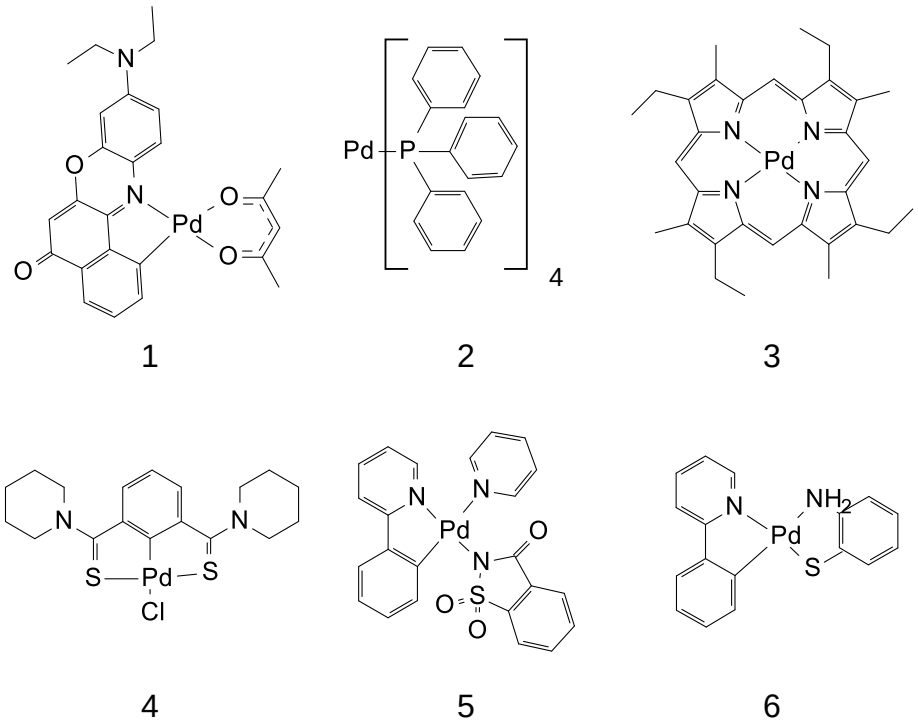

Figure 5.1 Phosphorescent cyclometalated palladium complexes reported in literature.[157]

In many cases, existing palladium emitters possess levels of spin-orbit-coupling that are insufficient to affect efficient intersystem crossing from the excited singlet to the triplet state. As a result, emission presents as metal perturbed fluorescence. Certain ligand designs (Figure 5.1, complexes: 1, 4, 5, 6) have increased levels of spin-orbit-coupling, and as a result, their intersystem crossing rates are more rapid. Complexes of this type can produce phosphorescent emission, but relatively sluggish radiative rates combined with high non-radiative rates inhibit efficient emission at room temperature (Table 5.1).

Table 5.1 Luminescence data for literature reported palladium complexes[157]

	room temperature, solution			77k, glass matrix		
	Φ	τ (μs)	λ_{max}(nm)	Φ	τ (μs)	λ_{max} (nm)
1	0.23	0.0046	660	nr	nr	nr
2	0.38	0.0032	667	nr	nr	nr
3	nr	nr	nr	0.5	1900	660
4	ne	ne	ne	0.12	89	575
5	0.004	8.08	430	nr	nr	nr
6	0.0125	1	430, 459	nr	nr	459

"ne", not emissive. "nr" not reported

Another interesting class results when an excited singlet state is thermally accessible from the triplet state (Figure 5.1, complex 2). This results in transfer from the triplet to singlet state, producing delayed fluorescence. Palladium(II) complexes based on porphyrin structures have also been investigated (Figure 5.1, complex 3), but have only weak room temperature emission that is limited to the red region of the spectrum.

The difference in quality between analogous platinum and palladium emitters has two main causes. First, when compared to platinum complexes, palladium based emitters tend to have much faster non-radiative decay rates. These non-radiative modes out compete the radiative decay path, resulting in greatly reduced efficiency.[158] A major culprit is thought to be lower lying metal centered excited states found in palladium complexes, which are thermally accessible from the lowest triplet state. Metal centered d-d excited states are anti-bonding in nature, and as a result, possess a repulsive potential energy surface. This results in large

geometric distortions in the excited state, which in turn provides an efficient route for non-radiative deactivation through direct coupling to the ground state.

In addition, palladium complexes have slower radiative decay rates when compared to those based on platinum. This is due to the inherently weaker heavy atom effect provided by palladium. If the success found in platinum complexes is to be replicated, careful ligand design is needed to overcome the inherent shortcomings of the lighter metal.

A suitable design for an efficient phosphorescent complex should minimize common radiationless pathways while simultaneously enhancing intersystem crossing to, and radiative decay from, the lowest triplet state. To reduce non-radiative decay rates, the d-d quenching state can be made less accessible through the use of a ligand that possesses strong σ donating character. Furthermore, if the ligand can be made more rigid, both "loose bolt" effects resulting from metal-ligand bond weakness generated in excited states, and coupling to low-frequency vibrations of the ground state can be reduced. To enhance radiative rates, additional low lying singlet states may be useful to mitigate the weaker heavy atom effect provided by palladium. A ligand design that contains a region that has sufficiently high triplet energy as to not directly participate in the emission process, but that is still relatively easy to reduce, may increase the amount of singlet character available for mixing into the lowest lying triplet state.

The ligands presented in Chapter 4 satisfy these design criteria and several examples were coordinated to palladium (Figure 5.2). By incorporating established emitting ligands, the color of the platinum complexes could be tuned from blue to red. In this work, we report the design, synthesis, photophysical study, and OLED

performance of this new class of ligands applied to palladium. This new series of cyclopalladated complexes have emission energies that span the visible spectrum and demonstrate room temperature phosphorescence with quantum efficiencies far in excess of any reported for palladium complexes. When incorporated in to an OLED, device performance is comparable to many existing platinum based emitters.

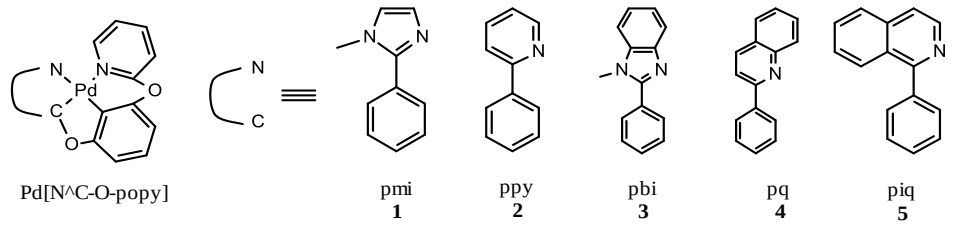

Figure 5.2 Structural formula and abbreviations used for the cyclopalladated complexes.

5.2 Synthesis and Characterization

Preparation of 3-(pyridin-2-yloxy)phenol. Williamson ether coupling was performed using a literature procedure[130] that was modified to cope with the poor solubility of resorcinol and the existence of a hydroxyl group on the intended product. A dry pressure vessel was charged with 2-bromopyridine (15.80 g, 100 mmol), resorcinol (16.51 g, 150 mmol), 1-methylimidazole (4.11g, 50 mmol), potassium carbonate (27.64g, 200 mmol), and a 1:1 mixture of pyridine and toluene (200mL). The vessel was flushed with nitrogen and the solution bubbled for 10 minutes. Copper(I) iodide (1.90 g, 10 mmol) was then added, the solution bubbled 10 minutes further, and the vessel sealed. The mixture was stirred for 2 days at 120˚ C, allowed to cool, diluted with toluene (200 mL), and added to stirring 5% acetic acid solution (300 mL). The organic phase and undisolved solids were collected and washed three times with water, ethanol was added until all solids were dissolved,

and the solution dried over magnesium sulfate. The solvent was removed under reduced pressure, and an off white powder was obtained (yield 35%) after recrystallization from hot toluene. ^{1}H NMR (400 MHz, $CDCl_3$): δ, ppm 8.20 (b, 1H), 7.70 (vt, 1H, *J* 8.0 Hz), 7.23 (vt, 1H, *J* 8.1 Hz), 6.94 (d, 1H, *J* 8.3 Hz),6.69-6.62 (m, 2H), 6.59 (s, 1H), 5.98 (s, 1H).

2-(3-(3-iodophenoxy)phenoxy)pyridine. Under a nitrogen atmosphere, a three neck flask was charged with 3-(pyridin-2-yloxy)phenol (3.74 g, 20 mmol), cesium carbonate (13.03 g, 40 mmol) and1-methyl-2-pyrrolidinone (30mL) and allowed to stir with nitrogen bubbling for 5 minutes. Next, 1,3-Diiodobenzene (9.90 g, 30 mmol), and 2,2,6,6-Tetramethylheptane-3,5-dione (0.37 g, 2 mmol) were added, followed by copper(I) iodide (1.90 g, 10 mmol). The mixture was bubbled 5 minutes further, fitted to a condenser, and heated to 120˚ C for 2 days. After cooling, dichloromethane was added, and the slurry was filtered, and the filter cake washed with dichloromethane. The filtrate treated with successive 100 mL washings of 2 N hydrochloric acid solution, 0.5 N hydrochloric acid solution, 2 M sodium hydroxide solution, and brine. The organic layer was dried over magnesium sulfate, and the solvent removed under reduced pressure. The crude brown oil was chromatographed on silica with dichloromethane as the mobile phase to give a colorless viscous oil in 55% yield ^{1}H NMR (400 MHz, $CDCl_3$): δ, ppm 8.22 (dd, 1H, *J* 5.0, 1.9 Hz), 7.70 (dd, 1H, *J*7.3, 2.0 Hz), 7.45-7.40 (m, 2H), 7.35 (vt, 1H, *J*8.2 Hz), 7.05 (vt, 1H, *J*8.2 Hz), 7.03-6.99 (m, 2H), 6.94-6.90 (m, 2H), 6.83 (dd, 1 H,*J* 4.2, 0.8 Hz), 6.80 (vt, 1H, *J*2.2 Hz).

2-(3-(3-(4,4,5,5-tetramethyl-1,3,2-dioxaborolan-2-yl)phenoxy)phenoxy)pyridine. A round bottom flask was charged with 2-(3-(3-

iodophenoxy)phenoxy)pyridine (1.95 g, 5 mmol), bis(pinacolato)diboron (1.40 g, 5.5 mmol), potassium acetate (1.47 g, 15 mmol), [1,1′-Bis(diphenylphosphino)ferrocene]dichloropalladium(II) (0.22 g, 0.15 mmol), and anhydrous dimethyl sulfoxide, and fitted to a condenser under a nitrogen atmosphere. The mixture was heated to 80° C and stirred for 24 hours. After cooling, the reaction mixture was diluted with dichloromethane, and washed three times with brine. The organic phase was dried over magnesium sulfate and the solvent removed under reduced pressure. The crude oil was chromatographed on silica with dichloromethane as the mobile phase to give a colorless, viscous oil that crystallized slowly in 55% yield. ^{1}H NMR (400 MHz, $CDCl_3$): δ, ppm 8.22 (dd, 1H, *J* 5.1, 1.9 Hz), 7.67 (dd, 1H, *J* 7.8, 2.0 Hz), 7.57 (d, 1H, *J* 7.6 Hz), 7.51 (d, 1H, *J* 2.5 Hz), 7.37-7.28 (m, 2H), 7.16 (ddd, 1H, *J* 8.1, 2.6, 0.9 Hz), 6.99 (dd, 1H, *J* 7.3, 5.0Hz), 6.90 (d, 1 H, *J* 8.3 Hz), 6.85 (dd, 1H, *J* 8.2, 1.7 Hz), 6.80 (dd, 1H, *J* 8.1, 2.1 Hz), (6.77 vt, 1H, *J* 2.2 Hz), 1.33 (s, 12H).

2-(3-(3-(1-methyl-1H-imidazol-2-yl)phenoxy)phenoxy)pyridine (LOO2). A microwave vessel was charged with 1-methylimidazole (0.31 g, 3.75mmol), 2-(3-(3-iodophenoxy)phenoxy)pyridine (0.97 g, 2.5mmol), triphenylphosphine (0.13 g, 0.50 mmol), and dimethylformamide(15 mL), flushed with nitrogen, and the solution subjected to nitrogen bubbling. Next, copper(I) iodide (0.95 g, 5 mmol) and palladium acetate (0.06 g, 0.25 mmol) were added, the vessel sealed, and subjected to microwave irradiation for 2 hours at 150 watts and 165°C. The resulting mixture was cooled, diluted with dichloromethane, and added to a stirring ammonium hydroxide solution and dichloromethane. The organic phase was collected, the aqueous rinsed with dichloromethane, and the organic phases combined, dried over

magnesium sulfate, and concentrated under reduced pressure yielding a red-brown viscous liquid. The crude product was chromatographed on basic aluminum oxide with dichloromethane and methanol(100:1) mobile phase to give a colorless amorphous solid in 75% yield. ^{1}H NMR (400 MHz, ($CDCl_3$): δ, ppm 8.19 (dd, 1H, *J* 4.7, 1.9 Hz), 7.68 (dd, 1H, *J* 7.2, 2.0 Hz), 7.45-7.39 (m, 2H), 7.34-7.30 (m, 2H), 7.13-7.08 (m, 2H), 7.00 (dd, 1H, *J* 5.0, 0.9 Hz), 6.96 (d, 1H, *J* 1.0 Hz), 6.93-6.82 (m, 4H), 3.26 (s, 3H).

2-(3-(3-(pyridin-2-yl)phenoxy)phenoxy)pyridine (LOO3). A vessel was charged with 2-(3-(3-iodophenoxy)phenoxy)pyridine (1.95 g, 5mmol), 2-(tributylstannyl)pyridine (4.42g, 12.5mmol), tetrakistriphenylphosphine palladium(0) (0.29g, 0.25 mmol), potassium fluoride (1.16g, 20 mmol), and anhydrous, degassed toluene (75 mL). The vessel was set to reflux under a nitrogen atmosphere for 3 days. The resulting solution was cooled, the solids filtered off, and poured into a stirring aqueous solution of potassium fluoride. The organic phase was collected, washed once more with aqueous potassium fluoride, and dried of magnesium sulfate. The solvent was removed under reduced pressure and the crude product was chromatographed over silica initially with hexane followed by dichloromethane to a yield viscous, colorless oil in 70% yield.^{1}H NMR (400 MHz, ($CDCl_3$): δ, ppm 8.68 (ddd, 1H, J 4.8, 1.5, 0.8 Hz), 8.19 (ddd, 1H, J 5.0, 2.1, 0.7 Hz), 7.78-7.64 (m, 5H), 7.44 (vt, 1H, J 7.9 Hz), 7.34 (vt, 1H, J 8.2 Hz), 7.24 (ddd, 1H, J 7.4, 4.8, 1.3 Hz), 7.11 (ddd, 1H, J 8.2, 2.5, 1.0 Hz), 6.99 (ddd, 1H, J 7.3, 5.0, 0.9 Hz), 6.93-6.83 (m, 4H).

1-methyl-2-(3-(3-(pyridin-2-yloxy)phenoxy)phenyl)benzoimidazole(LOO4). This ligand was synthesized via the same procedure used for L-1, yielding a white

solid in 45% yield.^{1}H NMR (400 MHz, ($CDCl_3$): δ, ppm 8.18 (ddd, 1H, J 5.0, 2.1, 0.6 Hz), 7.83-7.79 (m, 1H), 7.68 (d, 1H, J 6.8, 2.0 Hz), 7.53 (vt, ^{1}H, J 1.5), 7.50 (vt, 1H, J 7.7 Hz), 7.45 (vt, 1H, J 1.7 Hz), 7.41-7.35 (m, 2H), 7.34-7.30 (m, 2H), 7.20 (ddd, 1H, J 7.8, 2.4, 1.6 Hz), 7.00 (ddd, 1H, J 7.2, 4.9, 0.8 Hz), 6.94-6.86 (m, 3H, J 8.4), 6.86 (vt, 1H, J 2.2 Hz), 3.86 (s, 3H).

2-(3-(3-(pyridin-2-yloxy)phenoxy)phenyl)quinolone (LOO5). A flask was charged with 2-chloroquinoline (0.49 g, 3 mmol), 2-(3-(3-(4,4,5,5-tetramethyl-1,3,2-dioxaborolan-2-yl)phenoxy)phenoxy)pyridine (0.78 g, 2 mmol), palladium acetate (0.022g, 0.1mmol), triphenylphosphine (0.105 g, 0.4 mmol) and dimethoxyethane (20 mL). After the solids dissolved, 2M potassium bicarbonate in water (20 mL) was added, the flask fitted to a condenser under a nitrogen atmosphere, and set to reflux for 24 hours. The reaction mixture was cooled, concentrated, and separated between water and dichloromethane. The organic layer was collected, the aqueous layer rinsed with dichloromethane, and the organic layers combined, dried, and concentrated. The crude product was chromatographed over silica with a dichloromethane mobile phase to give glassy solid in 80% yield.1H NMR (400 MHz, (CDCl3): δ, ppm 8.29 (dd, 1H, J 8.0, 0.6 Hz), 8.22 (dvt, 1H, J 7.7, 1.0 Hz),7.96-7.92 (m, 2H), 7.84-7.81 (m, 1H), 7.72-7.66 (m, 2H), 7.64 (dd, 1H, J 8.0, 1.4 Hz), 7.58-7.50 (m, 6H), 7.43-7.40 (m, 1H), 7.37 (dd, 1H, J 6.4, 1.8 Hz), 7.34-7.30 (m, 2H).

2-(3-(3-(pyridin-2-yloxy)phenoxy)phenyl)quinoline 1-(3-(3-(pyridin-2-yloxy)phenoxy)phenyl)isoquinoline (LOO6). This ligand was synthesized via the same procedure used for LOO5, producing a glassy solid in 85% yield.^{1}H NMR (400 MHz, ($CDCl_3$): δ, ppm 8.59 (d, 1H, J 5.7 Hz), 8.22 (dvt, 1H, J 7.7, 1.0 Hz),8.09 (d, 1H, J 8.5 Hz), 7.88 (d, 1H, J 8.4 Hz), 7.72-7.64 (m, 3H), 7.56-7.43 (m, 3H), 7.40 (s, 1H),

7.34 (vt, 1H, J 8.9 Hz), 7.20 (dvt, 1H, J 7.9, 1.2 Hz), 6.98 (dd, 1H, J 7.1, 5.0 Hz), 6.92-6.85 (m, 4H).

A series of cyclometalated palladium complexes were prepared (Figure 5.2). The metallization procedure previously used to synthesize platinum-based analogs[98, 159] proved unsuitable for palladium. This may be due to the increased reactivity of palladium which resulted in rapid coordination in undesired C^N sites or the formation of palladium bridge oligimers.[160] Literature reported methods utilizing mercury intermediates[161, 162] were also unsuccessful due to the uncontrolled formation of mercury bridged [N^C-O-popy] oligimers. A slow ramping of reaction temperatures was used to provide conditions that promoted initial coordination at both nitrogen sites, followed by oxidation and coordination at the carbon sites (Scheme 5.1). The use of molecular sieves greatly increased yields. In spite of the cooler conditions, the solutions became noticeably emissive under ultraviolet illumination after 36 hours stirring at room temperature.

Scheme 5.1 Proposed cyclopalladation process for N^C-O-popy ligands[160]

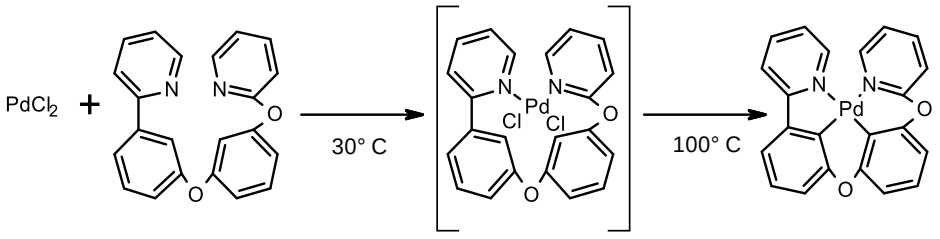

The respective ligand (1.1 mmol), palladium(II) chloride (1 mmol), and 4 Å molecular sieves (0.3 g) were stirred in degassed acetic acid under nitrogen at room temperature for 2 days, 70° C for 3 days, and then refluxed overnight. The mixture was cooled, diluted with dichloromethane, filtered, and the filtrate added to stirring

water (100 mL). The organic layer was collected, and the water rinsed once more with dichloromethane. The organic layers were combined, washed twice with water (200 mL), twice with a saturated sodium bicarbonate solution (200 mL), and twice more with water. The organic phase was dried over magnesium sulfate, and concentrated under reduced pressure. The resulting solid was flash chromatographed over aluminum oxide with dichloromethane as the eluent, and recrystallized through slow diffusion of ether into dichloromethane. Samples used for OLEDs were subjected to further purification by train sublimation.

Palladium(II)(2-(3'-(3''-(1-methyl-1H-imidazol-2'''-yl)phenoxy)phenoxy)pyridato-N,C2',C2'',N''') (PdOO2), yield 36% ^{1}H NMR (400 MHz, $(CD_3)_2SO$): δ, ppm 8.65 (dd, 1H, J 5.6, 1.7 Hz), 8.15 (dd, 1H, J 7.3, 1.8 Hz), 7.74 (d, 1H, J 8.4 Hz), 7.46 -7.41 (m, 3H),7.21 (vt, 1H, J 7.6 Hz), 7.14-7.09 (m, 2H), 7.01 (dd, 1H, J 8.1, 0.7 Hz),6.95 (dd, 1H, J 8.0, 1.1 Hz), 6.86 (dd, 1H, J 7.7, 1.1 Hz), 4.07 (s, 3H). Anal. Calcd for $C_{21}H_{15}N_3O_2Pd$: C, 56.33; H, 3.38; N, 9.38. Found: C, 56.21; H, 3.54; N, 9.13. MS: m/z calcd 497.04; Found 497.68.

Palladium(II) (2-(3'-(3''-(pyridin-2'''-yl)phenoxy)phenoxy)pyridato-N,C2',C2'',N''') (PdOO3), yield: 38%. ^{1}H NMR (400 MHz, $(CD_3)_2SO$): δ, ppm 8.64 (dd, 1H, J 5.7, 1.7 Hz), 8.40 (d, 1H, J 5.5 Hz), 8.25 (d, 1H, J 8.2 Hz), 8.18 (dd, 1H, J 7.0, 1.9 Hz),8.10 (dd, 1H, J 7.7, 1.4 Hz), 7.72 (d, 1H, J 7.4 Hz), 7.53 (d, 1H,J 8.3 Hz), 7.52-7.47 (m, 2H), 7.24 (vt, 1H, J 7.8 Hz), 7.14 (vt, 1H,J 7.9 Hz),7.09 (dd, 1H, J 7.9, 0.8 Hz), 6.99 (dd, 1H, J 8.1, 1.1 Hz), 6.90 (dd, 1H, J 7.7, 1.1 Hz).13C NMR (400 MHz, (CD3)2SO): δ, ppm 163.2, 159.5, 156.2, 152.7, 151.2, 148.6, 148.4, 147.9, 142.1, 139.1, 136.8, 125.7, 125.4, 123.6, 121.1, 119.9, 118.8, 116.6, 116.6, 115.5, 112.2,

110.8.Anal.Calcd for $C_{22}H_{14}N_2O_2Pd \cdot 0.5H_2O$: C, 58.23; H, 3.33; N, 6.17. Found: C, 58.45; H, 3.44; N, 6.20. MS: m/z calcd 444.01; Found 444.59.

Palladium(II) (2-(3'-(3''-(1-methyl-1H- benzo[d]imidazole -2'''-yl)phenoxy)phenoxy)pyridato-N,C2',C2'',N''') (PdOO4), yield 31%. ^{1}H NMR (400 MHz, $(CD_3)_2SO$): δ, ppm 8.81 (dd, 1H, J 5.6, 1.8 Hz), 8.22 (dd, 1H, J 7.4, 1.9 Hz), 7.86 (d, 1H, J 8.3 Hz), 7.83 (d, 1H, J 7.7 Hz),7.58 (d, 1H, J 8.4 Hz), 7.45 (dd, 1H, J 5.8, 0.9 Hz), 7.38 (dd, 1H, J 6.8, 1.3 Hz), 7.33 (vt, 1H, J 7.8 Hz), 7.29 - 7.21 (m, 2H), 7.17 (dd, 1H, J 8.1, 0.6 Hz),7.13 (vt, 1H,J 7.8 Hz), 6.97 (dd, 1H, J 8.0, 1.1 Hz), 6.92 (dd, 1H, J 7.7, 1.1 Hz), 4.28 (s, 3H). Anal. Calcd for $C_{25}H_{17}N_3O_2Pd \cdot 2H_2O$: C, 56.24; H, 3.96; N, 7.87. Found: C, 55.99; H, 3.84; N, 7.51. MS: m/z calcd447.02; Found 447.52.

Palladium(II) (2-(3'-(3''-(pyridin-2'''-yloxy)phenoxy)phenyl)quinolato-N,C2',C2'',N''') (PdOO5), yield: 13%. ^{1}H NMR (400 MHz, $(CD_3)_2SO$): δ, ppm 8.69 (d, 1H, J 8.8 Hz), 8.48 (d, 1H, J 8.9 Hz), 8.16-8.10 (m, 2H), 8.07 (dd, 1H, J 5.8, 1.6 Hz),7.97 (d, 1H, J 7.6 Hz), 7.67 (d, 1H, J 8.6 Hz), 7.63-7.56 (m, 2H), 7.48 (dd, 1H, J 6.8, 1.4 Hz), 7.33 (vt, 1H, J 7.6 Hz), 7.21-7.14 (m, 3H),7.02 (dd, 1H, J 8.0, 1.1 Hz), 6.98 (dd, 1H, J 7.6, 1.1 Hz). Anal.Calcd for $C_{26}H_{16}N_2O_2Pd \cdot 0.25H_2O$: C, 62.54; H, 3.33; N, 5.61. Found: C, 62.57; H, 3.66; N, 5.52. MS: m/z calcd 496.03; Found 496.69.

Palladium(II) (1-(3'-(3''-(pyridin-2'''-yloxy)phenoxy)phenyl)isoquinolato-N,C2',C2'',N''') (PdOO6), yield 32%. ^{1}H NMR (400 MHz, $(CD_3)_2SO$): δ, ppm 8.88-8.83 (m, 2H), 8.31 (d, 1H, J 6.1 Hz), 8.21 (dd, 1H, J 7.1, 1.8 Hz), 8.14 (d, 1H, J 8.1 Hz),7.96 (d, 1H, J 6.2 Hz), 7.95-7.90 (m, 2H), 7.85 (dd, 1H,J 6.8, 0.9 Hz), 7.59-7.53 (m, 2H), 7.36 (vt, 1H, J 7.7 Hz), 7.20 (d, 1H,J 7.9 Hz),7.14 (vt, 1H, J 7.7 Hz), 7.02 (dd, 1H, J 8.0, 1.0 Hz),6.92 (dd, 1H, J 7.7, 1.0 Hz). Anal. Calcd for $C_{26}H_{16}N_2O_2Pd \cdot H_2O$: C,

60.89; H, 3.54; N, 5.46. Found: C, 60.98; H, 3.54; N, 5.28. MS: m/z calcd 496.03; Found 496.67.

Density functional theory calculations were performed on the synthesized palladium complexes. The B3LYP functional was used with the LACV3P basis set for palladium, and the 6-311G* basis set for all other atoms.[103, 163] The orbital densities for the highest and second highest occupied molecular orbitals (HOMO, HOMO-1) and the lowest and second lowest unoccupied molecular orbitals (LUMO, LUMO+1) are shown in Figure 5.6. For all compounds, the HOMO-1 surfaces are a mixture of phenyl-π and oxygen-n orbitals located on the popy motif and palladium-d orbitals, while the HOMO surfaces are composed of π orbitals distributed over both phenyl rings and palladium-d orbitals.

The LUMO and LUMO+1 surfaces vary across the series. In the case of PdOO2, the LUMO surface is composed exclusively of pyridyl-π orbitals whereas the LUMO+1 surface is made up of imidazolyl and phenyl-π orbitals. PdOO3 and PdOO4 have lower energy acceptor groups, and as a result, the LUMO and LUMO+1 are a mixture of π orbitals distributed over the pyridyl ring of popy the phenyl-prydyl/imidazolyl portion of the ligand. In the case of PdOO5 and PdOO6, the acceptor group is further reduced in energy and the LUMO and LUMO+1 surfaces are the reverse of PdOO2. The LUMO surface is composed of π orbitals from the phenyl-quinoloyl rings and the LUMO+1 surface contains only π orbitals from the pyridyl ring of popy.

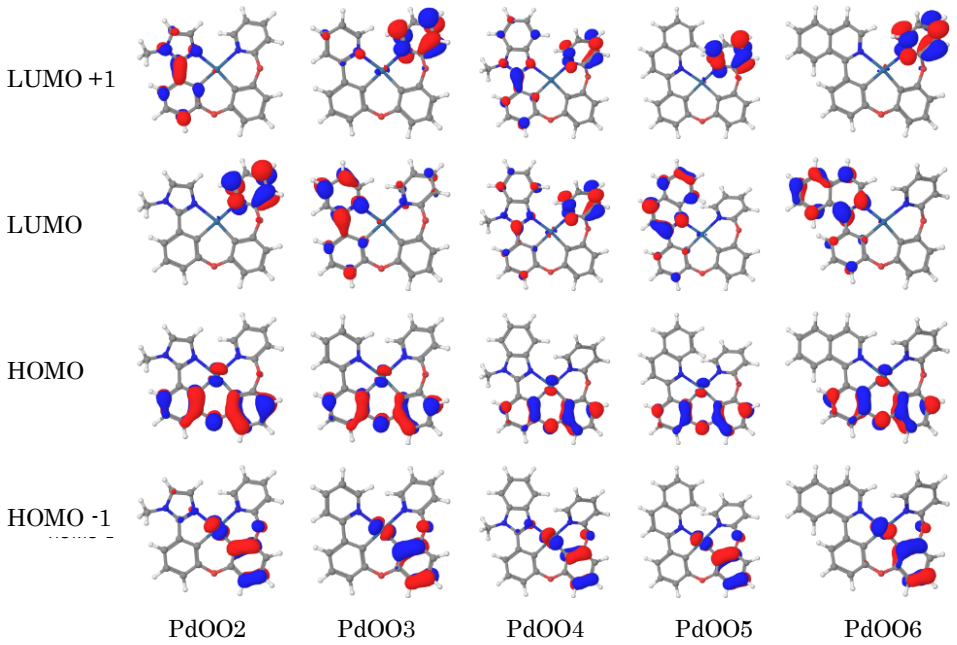

Figure 5.3 The HOMO-1, HOMO, LUMO, and LUMO+1 surfaces of palladium compounds from DFT calculations. HOMO and HOMO-1 consist of phenyl-π and Pd-d orbitals while LUMO and LUMO+1 consist of pyrdyl-π and (phenyl-heteroaryl)-π orbitals

5.3 Photophysical Properties

Table 5.2 Photophysical properties of Pd[N^C-O-popy] complexes

	room temperature									77 K	
	λ_{max} (nm)	τ (μs)		Φ_{PL}		k_r (10^5 s^{-1})		k_{nr} (10^5 s^{-1})		λ_{max} (nm)	τ (μs)
		sln	tf	sln	tf	sln	tf	sln	tf		
PdOO2	454	32	254	0.17	0.64	0.53	0.25	2.59	0.14	448	315
PdOO3	467	25	239	0.27	0.80	1.08	0.33	2.92	0.06	463	274
PdOO4	469	29	161	0.25	0.79	0.86	0.49	2.59	0.13	461	186
PdOO5	535	23	102	0.25	0.82	1.09	0.30	3.26	0.18	518	117
PdOO6	606	24	113	0.01	0.16	0.04	0.14	4.13	0.74	556	165

Room temperature emission spectra were measured in a solution of dichloromethane and in a doped PMMA film. 77 K emission spectra were measured in a solution of 2-MeTHF. Reference for quantum efficiency: Coumarin 47, PdOO2, PdOO3, PdOO4; Coumarin 6, PdOO5; Rhodamine B: PdOO6.

In addition to the d-d splitting provided by the ligand, efficient phosphorescence at room temperature requires sufficient spin-orbit coupling to mix the excited singlet and triplet states.[164-167] The absorption spectra (Figure 5.4) of the presented complexes show evidence of both ligand centered (π-π*) and metal to ligand charge transfer (d-π*) transitions. The ligand centered absorption bands fall in the UV region, with extinction coefficients in the range of 5,000 to 40,000 M^{-1} cm^{-1}. ^{1}MLCT bands fall in the range of 390-450nm with extinction coefficients ranging from 500 – 5000 M^{-1} cm^{-1}. ^{3}MLCT features are very diffuse, and more poorly resolved than in similar platinum and iridium compounds (Figure 3.3). Absorption energy decreases with increasing size of the pi system of the ligand.

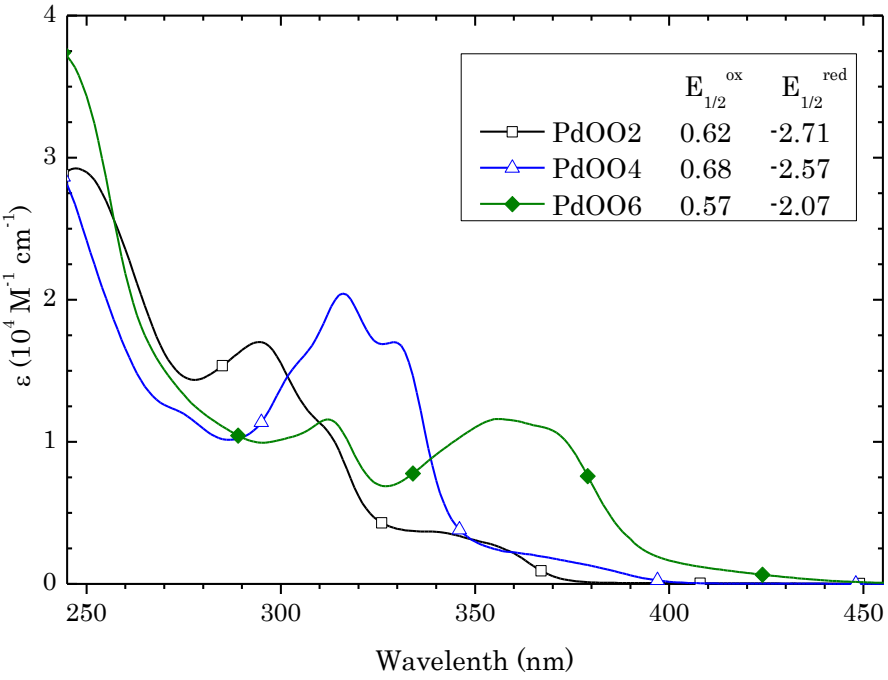

Figure 5.4 Absorption spectra of PdOO2, PdOO4, and PdOO6 in dichloromethane at room temperature. Redox values (V) are shown in the inset. Redox measurements were carried out in dry DMF solution. For all palladium complexes reported here, the oxidation process is irreversible

The room temperature and 77 K spectra of the synthesized palladium compounds are shown in Figure 5.5. The Pd[N^C-O-popy] complexes are luminescent in solution at room temperature (Φ=0.01-0.25) with lifetimes characteristic of phosphorescent emission (τ = 24-32 μs). When the complexes are doped into a thin film of PMMA, room temperature luminescent yields (Φ = 0.16-0.82) and luminescent lifetimes (τ = 102-254 μs) are both significantly larger. The emission energy is dependent on the size of the (C^N) portion of the ligand, with peak values ranging from 454-606 nm. The emission spectra are vibronic in nature, and show significant broadening at room temperature. Rigidochromic shifts increase monotonically with decreasing emission energy, and range in value from 6 nm in the case of PdOO2 to 50nm in the case of PdOO6.

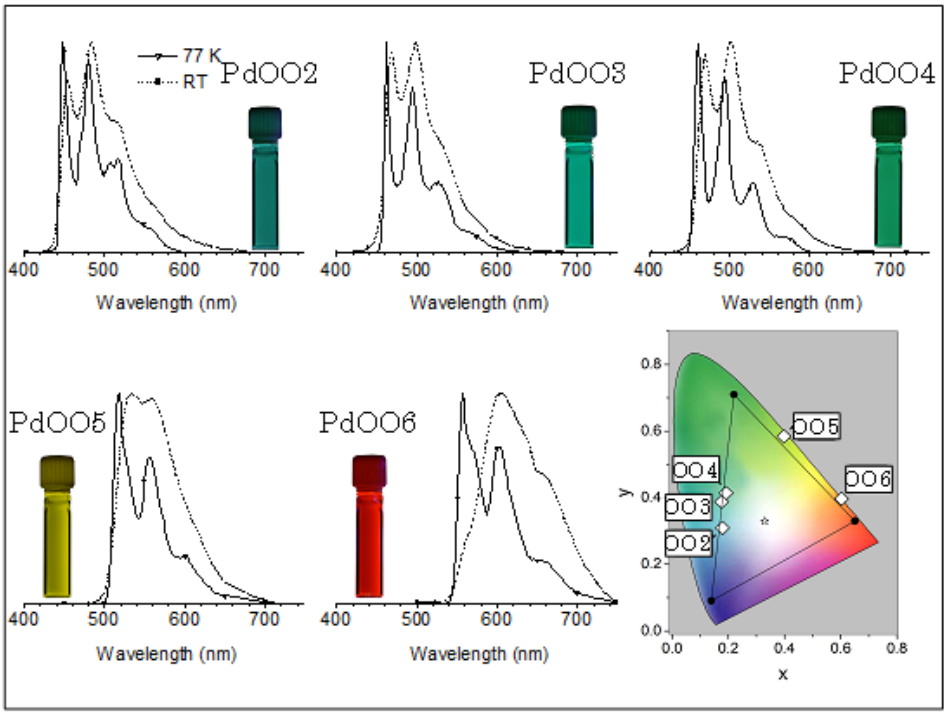

Figure 5.5 Emission spectra of Pd[N^C-O-popy] complexes at room temperature in DCM and at 77 K in 2-MeTHF. Photographs of dilute degassed dichloromethane solutions under ultraviolet illumination accompany the spectra. The Commission Internationale de L'Eclairage (CIE) coordinates of the complexes at room temperature is shown in the bottom right.

The performance of PdOO6 is notably lower than the other presented compounds. PdOO6 has the lowest emission energy and highest rate of non-radiative decay, which is indicative of energy gap law effects that result from pronounced vibronic coupling between the excited triplet state and the ground state. The highest energy emitter, PdOO2, does not suffer from significant transfer from the excited triplet state to the higher lying d-d quenching state,[157, 158] which is a fundamental cause of quenching in palladium complexes.

5.4 Comparison to Analogous Platinum Complex

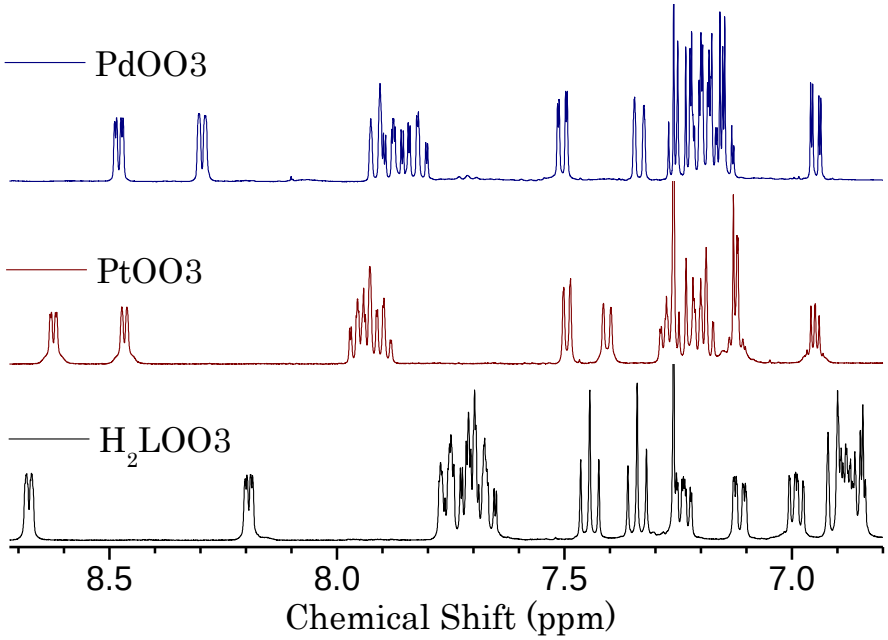

Figure 5.6 Proton NMR spectra of PdOO3, PtOO3, and free ligand in 2-methyltetrahydrofuran

Although similar, a comparison of the proton nuclear magnetic resonance spectra (Figure 5.6) of analogous platinum and palladium complexes do show distinct differences. As expected for spectra obtained at high magnetic field strengths,[168-170] the protons in close proximity to platinum in PtOO3 have diffuse satellite peaks resulting from ^{1}H-^{195}Pt coupling with broadening from chemical shift anisotropy (CSA). This effect is clearly visible in signal from the pyridyl protons in the 8.5 ppm region. Owing to the low sensitivity and fast relaxation times of ^{105}Pd, these satellites are absent in PdOO3. In PtOO3, the affected proton signals are shifted downfield in comparison to PdOO3, which is likely a result of electron density being pulled from the protons in close proximity to the more electronegative platinum core.

The nature of the metal plays a significant role in absorption properties (Figure 5.4) of the complex. When the LOO3 is complexed to platinum instead of palladium, the ^{1}LC absorption properties from 250 – 300 nm remain similar, but there is notably stronger ^{1}MLCT absorption from 350 - 450 nm, as well as additional peaks within the UV region (Figure 5.7). The area where ^{3}MLCT is expected is shown on the inset. The ^{3}MLCT transition in PdOO3 is not well resolved, whereas the ^{3}MLCT absorption of PtOO3 is well defined and an order of magnitude greater in intensity, owing to the larger amount of spin orbit coupling provided by the platinum metal.[171]

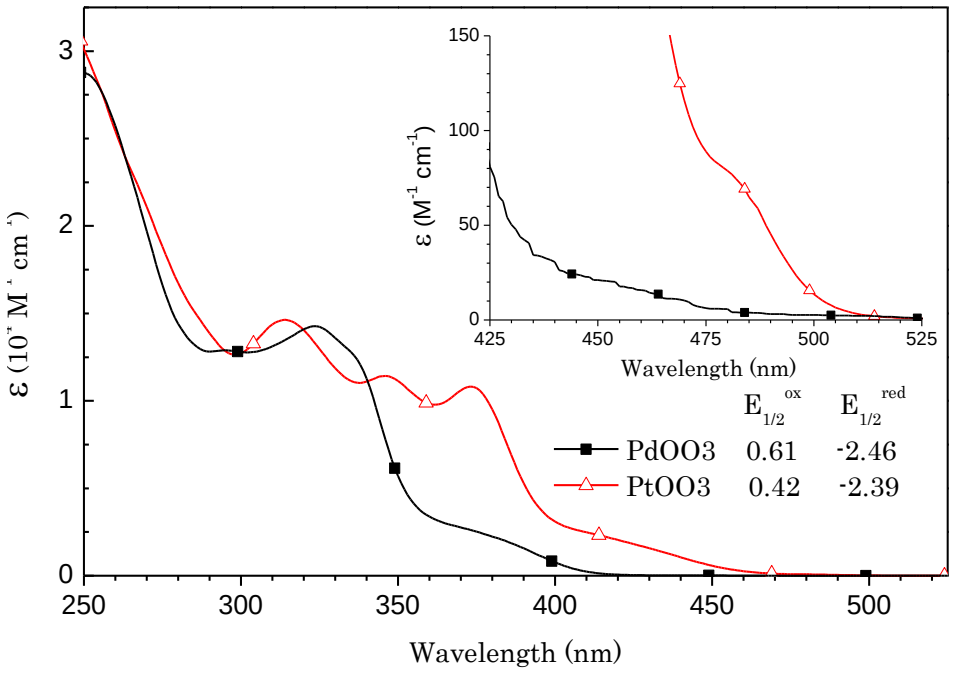

Figure 5.7 Absorption spectra of PdOO3 and PtOO3 in dichloromethane at room temperature. Redox values (V) and triplet absorption region appear in insets.

There is marked difference in the emission spectra (Figure 5.8) of analogous platinum and palladium complexes. Both PdOO3 and PtOO3 are emissive in

solution at room temperature. PdOO3 retains the vibronic structure at ambient temperature that is found at 77K, suggesting the emissive state is dominated by ligand centered transitions.[172, 173] When warmed to room temperature, the platinum compound adopts a more Gaussian appearance which suggests a greater contribution from MLCT states. This is supported by the absorption data presented in Figure 5.7. Another striking difference between the two compounds is the shift in emission maximum: from 487nm in PtOO3 to 462 nm in PdOO3.There is also a large difference in the phosphorescent lifetime between PtOO3 (2 μs at 77K) and PdOO3 (>200 μs at 77K).

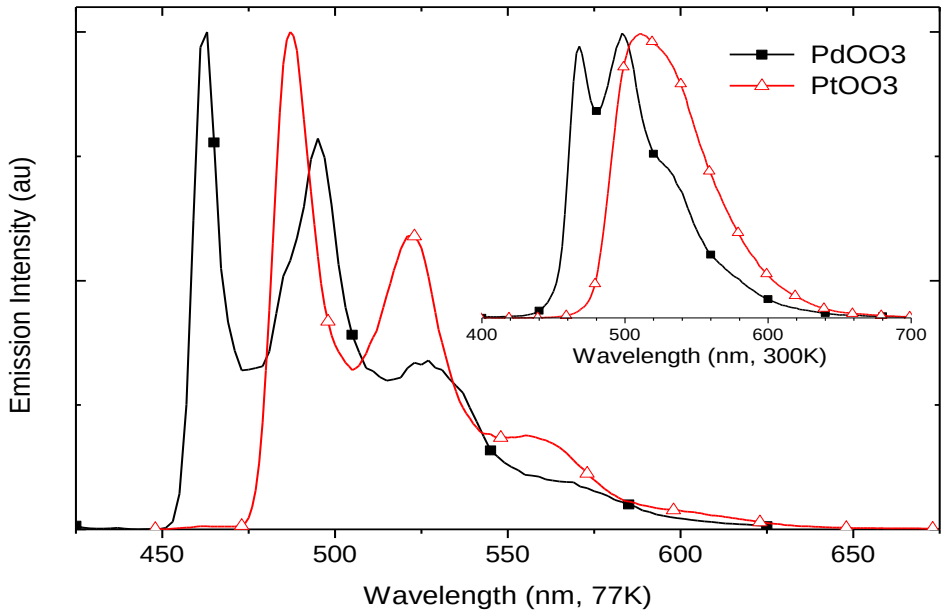

Figure 5.8 Emission spectra of PdOO3 and PtOO3 at 77K in 2-methytetrahydrofuran glass. Room temperature spectra in dichloromethane is shown on the inset.

5.5 OLEDs Prepared from MOO3 Complexes

Efficient OLEDs were be prepared using palladium and platinum metals coordinated to LOO3. The complexes were doped into the emissive layer at a concentration of 2%. Figure 5.9 shows the external quantum efficiency as a function of current density for PdOO3 and PtOO3 as dopants. PtOO3 achieves a maximum external quantum efficiency of 22.9% at a current density of 0.03 mA/cm^2, while PdOO3 has a maximum external quantum efficiency of 12.3% at a current density of 0.01 mA/cm^3. Both devices show a gradual roll off of external quantum efficiency (EQE) at increasing current density, with the roll off in PdOO3 occurring sooner, and with a steeper decent. This behavior is consistent with triplet-triplet annihilation, which is enhanced by the longer emissive lifetime of the palladium complex.[38]

The electroluminescence spectra of PdOO3 and PtOO3 are presented in Figure 5.9. Although the emission spectra are similar to that in dilute solution, both complexes have a more pronounced vibronic structure in the OLED. In addition, the intensity of the sideband in PdOO3 overtakes the $v_{0,0}$ peak. In PtOO3, the emission maximum is shifted 10 nm shift to higher energy in the device, while PdOO3 shows a 5 nm shift to lower energy. The performance of PtOO3 remains among the best reported for platinum compounds, while PdOO3 is the first reported phosphorescent palladium dopant used in an OLED.

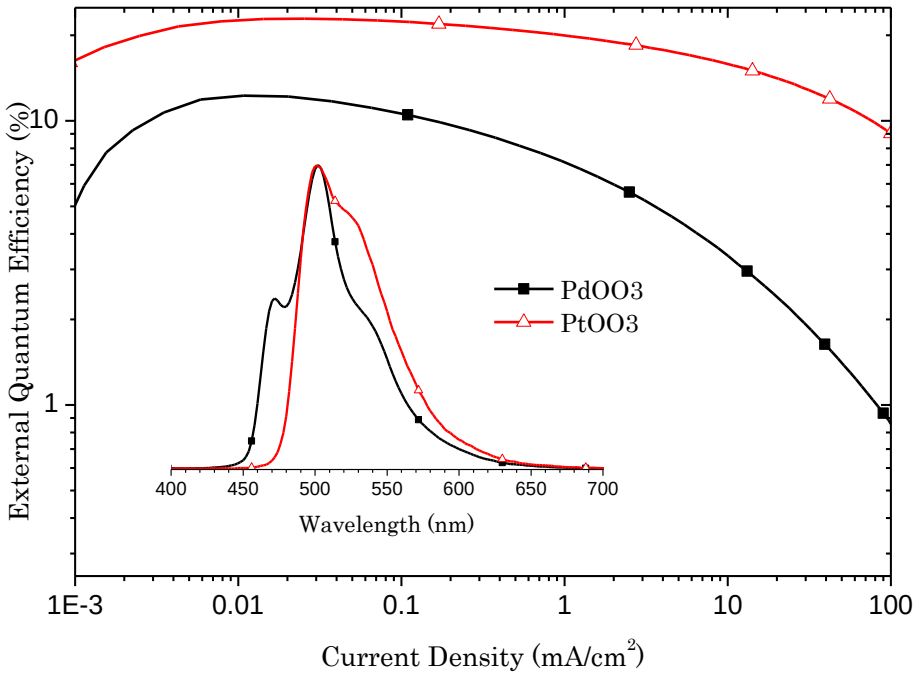

Figure 5.9 External quantum efficiencies of OLEDs using PdOO3 and PtOO3 as dopants. Electroluminescence spectra shown in inset.

5.6 Conclusion

The ligand design approached in this chapter allows for easy tuning across the visible spectrum. The reported palladium complexes retain the predominantly

^{3}LC character found the analogous platinum compounds, with lesser amounts of ^{1}MLCT admixture. This reduced mixture is a result of from weaker spin orbit coupling. As a result, palladium complexes have significantly longer lifetimes and lower photoluminescent efficiency. However, the presented complexes exhibit efficiencies and lifetimes far superior to any palladium compounds reported to date. When incorporated into a device, efficiency is notably good, and approaches values on a par with many previously reported platinum compounds.

CHAPTER 6

COMPLEXES CONTAINING CARBAZOLYL MOTIFS

6.1 Introduction

The transition to tetradentate ligands discussed in the previous chapters resulted in significant performance increases in both platinum and palladium complexes. These designs allowed tuning of emission color across the visible spectrum by modifying the N-aryl-phenyl portion of the ligand while leaving the common phenoxy-pyridinyl (popy) motif unchanged. A natural next step is to explore alternatives to this shared portion of the structure.

A particularly attractive candidate to replace popy are motifs built on carbazolyl functional groups. Carbozolyl complexes have been widely used as transport materials in OLEDs,[174] and more recently found use in emissive materials.[175, 176] The rigid, planar nature of the group has the potential to reduce non-radiative decay processes, reduce vibronic sidebands, provide reversible reduction sites, and enhance compatibility with existing host materials.[129, 143, 158]

6.2 Platinum Complexes with Narrow Emission

OLED displays produce a pixel of a specific color by individually varying the intensity of the sub-pixels (typically red, blue and green). To produce colors of high purity, emission from the sub-pixel must be restricted to a narrow range of energy. This may be accomplished by filtering out undesired regions, or preferably, by using materials that emit in a narrow region of the visible spectrum. The latter strategy

will simplify device design and improve efficiency, which is particularly important for mobile devices, which currently make up a sizable portion of the market.[5]

Several classes of materials currently exist that produce narrow-band emission. Two such classes, lanthanide complexes and porphyrin complexes were first studied during the dawn of OLED development (Chapter 1). The benefit provided by narrow emission are overshadowed by poor efficiency and lack of a clear path for color tuning. In contrast, materials based on quantum dots have progressed rapidly in recent years, producing narrow-band light across the visible spectrum.[177, 178] However, efficiency in the blue region remains poor, and compatibility with existing host materials remains a challenge.[179]

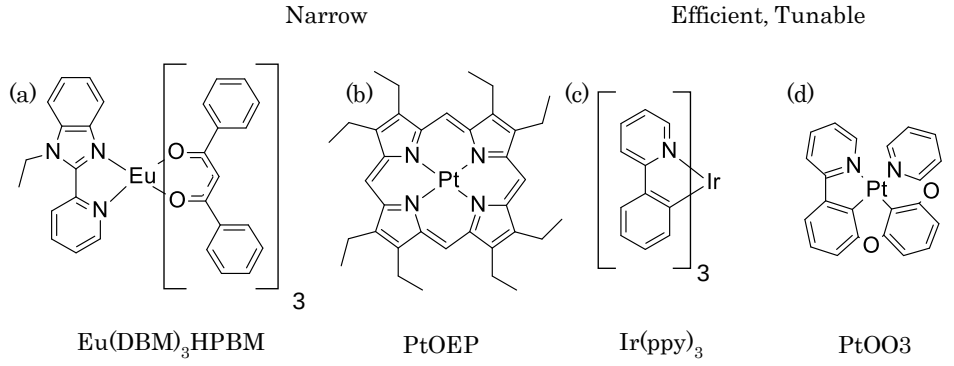

Figure 6.1 Examples of (a) lanthanide complex $Eu(DBM)_3HPBM$, (b) porphyrin PtOEP,(c) MLCT dominated cyclometalated complex $Ir(ppy)_3$, and (d) LC dominated cyclometalated complex PtOO3

Cyclometalated platinum and iridium complexes, have demonstrated tunability and high efficiency in OLED devices, but their emission is typically broad at room temperature. This a result of an excited state that is predominantly metal-to-ligand charge transfer (MLCT) in nature, or one that is predominantly ligand centered (LC) and has significant geometric distortions in comparison to the ground

state. The complexes presented in Chapter 4 and Chapter 5 belong to the latter. One route to decrease the full width half max (FWHM) of emission is to make the ligand more rigid, thereby reducing the distortion.[116] To do so, a series of platinum complexes were designed that coupled established emitting groups to a dual carbazolyl motif.

6.2.1 Synthesis

Scheme 6.1 Preparation of bis-carbazolyl platinum complexes.

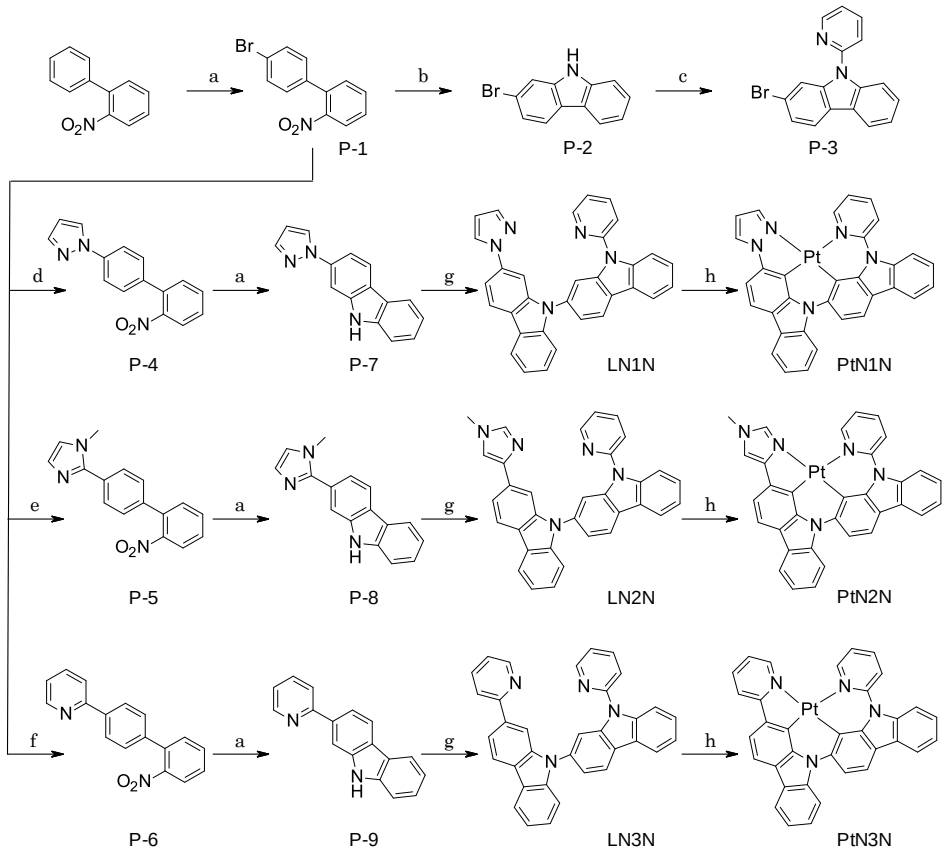

Reaction conditions: (a) 1 eq 2-nitrobyphenyl, bromine, 1.1 eq bromine, 10% iron trichloride, reflux, 24 hours. (b) 1 eq 4'-bromo-2-nitrobiphenyl, triethylphosphite, reflux, 24 hours. (c) 1 eq 2-bromo-9H-carbazole, 1 eq 2-bromopyridine, 10% copper(I) iodide, dimethyl sulfoxide, 90^0 C, 3 days. (d) 1 eq 4'-Iodo-2-nitrobiphenyl, 1.2 eq 1*H*-pyrazole, 2.5 eq potassium carbonate, 20% copper(I) iodide, 10 % trans-1,2-cyclohexanediamine, dioxane, 115^0 C, 3 days. (e) copper(I) iodide (2 equiv), palladium acetate (10%), 1-methylimidazole (1.5 equiv), dimethylformamide, microwave, 150 W, 160 °C. (f) tetrakis(triphenylphosphine)palladium(0) (5%), potassium fluoride (1.2 equiv), toluene, reflux (g) 1 eq P-3, 10% copper(I) iodide, dimethyl sulfoxide, 90^0 C, 3 days. (h) 0.9 eq potassium tetrachloroplatinate, acetic acid, reflux, 3 days.

Preparation of 4'-bromo-2-nitrobiphenyl (P-1). Under a nitrogen atmosphere, water 20mL was heated to 60˚ C and 2-nitrobyphenyl (125 mmol) was added and

stirred for 30 minutes before iron trichloride (6.3 mmol) was added and stirred for 30 minutes further. Bromine (140 mmol) was added drop wise over 40 minutes and allowed to stir overnight before setting to reflux for 4 hours. After cooling, residual bromine was removed by washing with a sodium bisulfate solution. The organic residue was then washed with concentrated sodium hydroxide, and then twice with water. The organic portion was separated and dissolved in dichloromethane before being dried with magnesium sulfate. The solution was concentrated under reduced pressure, subjected to flash column chromatography of silica with dichloromethane as the eluent, and concentrated again under reduced pressure. 4'-bromo-2-nitrobiphenyl was collected by recrystallization from methanol in 50% yield.

Preparation of 2-bromo-9H-carbazole (P-2). Under a nitrogen atmosphere, 100 mmol of 4'-bromo-2-nitrobiphenyl was set to reflux overnight in stirring triethylphosphite. After cooling, the triethylphosphite was distilled off and 2-bromo-9H-carbazole was isolated by recrystalization from methanol and further purified by train sublimation, resulting in a 65% yield.

Preparation of 2-bromo-9-(pyridin-2-yl)-9H-carbazole (P-3). Under a nitrogen atmosphere, 10 mmol of 2-bromo-9H-carbazole, 10 mmol of 2-bromopyridine, 1 mmol of copper(I) iodide, 25 mmol of potassium carbonate, and 2 mmol of L-proline were combined in stirring degassed dimethyl sulfoxide. The mixture was heated to 90° C for 3 days before being cooled and separated between dichloromethane and water. The water layer was washed twice with dichloromethane and the organics were combined and washed once with brine. The organic fraction was dried with magnesium sulfate and concentrated under reduced pressure and subjected to column chromatography of silica with dichloromethane as the eluent. After

concentrating under reduced pressure, 2-bromo-9-(pyridin-2-yl)-9H-carbazole was isolated in a 70% yield.

Preparation of 1-(2'-nitrobiphenyl-4-yl)-1*H*-pyrazole (P-4). 4'-Iodo-2-nitrobiphenyl (9.75 g, 30 mmol, 1.0 eq), 1H-pyrazole (2.45 g, 36 mmol, 1.2 eq) and potassium carbonate (8.71 g, 63 mmol, 3.1 eq) were added to a dry pressure tube equipped with a magnetic stir bar. Copper iodide (0.11 g, 0.6 mmol, 0.02 eq), trans-1,2-cyclohexanediamine (0.34 g, 3 mmol, 0.1 eq) and dioxane (30 mL) were added in a nitrogen filled glove box. The mixture was bubbled with nitrogen for 5 minutes. The mixture was stirred in an oil bath at a temperature of 115^0 C for 3 days. The mixture was cooled, diluted with ethyl acetate, filtered and washed with ethyl acetate. The filtrate was concentrated under reduced pressure and the residue was purified through column chromatography on silica gel using hexane and ethyl acetate (10:1-3:1) as eluent to obtain the desired product 1-(2'-nitrobiphenyl-4-yl)-1H-pyrazole 4 as an off-white solid 7.5 g in 94% yield. ^{1}H NMR (DMSO-d_6, 400 MHz): δ 6.57 (t, J = 2.0 Hz, 1H), 7.46 (d, J = 8.4 Hz, 2H), 7.59-7.65 (m, 2H), 7.75-7.79 (m, 2H), 7.92 (d, J = 8.4 Hz, 2H), 7.99-8.01 (m, 1H), 8.56 (d, J = 2.4 Hz, 1H). 13C NMR (DMSO-d_6, 100 MHz): δ 108.14, 118.56, 124.20, 127.88, 128.99, 129.06, 131.83, 133.01, 134.26, 134.62, 139.51, 141.33, 148.82.

Preparation of 2-(1*H*-pyrazol-1-yl)-9*H*-carbazole (P-7). To a three-necked flask equipped with a magnetic stir bar and a condenser, 1-(2'-nitrobiphenyl-4-yl)-1*H*-pyrazole (7.23 g, 27.26 mmol) was added. The flask was evacuated and backfilled with nitrogen 3 times. Triethyl phosphite (150 mL) was added and the mixture was stirred in an oil bath at a150^0C for 24 hours, cooled down and the excess triethyl

phosphite was removed by distillation under vacuum. The residue was recrystallized in ethyl acetate to get the desired product 3.60 g as a white solid. The filtrate was concentrated and the residue was purified through column chromatography on silica gel using hexane and ethyl acetate (10:1-5:1-3:1-2:1) as eluent to obtain the desired product 2-(1*H*-pyrazol-1-yl)-9*H*-carbazole **5** 1.30g in 77% total yield. ^{1}H NMR (DMSO-d$_6$, 400 MHz): δ 6.55-6056 (m, 1H), 7.17 (t, *J*= 7.6 Hz, 1H), 7.36-7.40 (m, 1H), 7.48-7.50 (m, 1H), 7.64 (dt, *J*= 8.0, 0.8 Hz, 1H), 7.76 (s, 1H), 7.90 (d, *J*= 2.0 Hz, 1H), 8.11 (d, *J*= 7.6 Hz, 1H), 8.18 (d, *J*= 8.8 Hz, 1H), 8.55 (d, *J*= 2.8 Hz, 1H), 11.40 (s, 1H). ^{13}C NMR (DMSO-*d*$_6$, 100 MHz): δ 100.97, 107.65, 109.96, 111.01, 118.94, 120.16, 120.74, 120.99, 122.11, 125.55, 127.96, 137.87, 140.11, 140.42, 140.71.

Preparation of 2-[4-(2-nitrophenyl)phenyl]pyridine (P-6). A vessel was charged with 5 mmol 4'-bromo-2-nitrobiphenyl, 12.5mmol 2-(tributylstannyl)pyridine, 0.25 mmol tetrakistriphenylphosphine palladium(0), 20 mmol potassium fluoride, and 75 mL anhydrous, degassed toluene. The vessel was set to reflux under a nitrogen atmosphere for 3 days. The resulting solution was cooled, the solids filtered off, and poured into a stirring aqueous solution of potassium fluoride. The organic phase was collected, washed once more with aqueous potassium fluoride, and dried of magnesium sulfate. The solvent was removed under reduced pressure and the crude product was chromatographed over silica initially with hexane followed by dichloromethane to yield a viscous, colorless oil in 60% yield.

2-(2-pyridyl)-9H-carbazole (P-9) Under a nitrogen atmosphere, 100 mmol of 2-[4-(2-nitrophenyl)phenyl]pyridine was set to reflux overnight in stirring tirethylphosphite. After cooling, the triethylphosphite was distilled off, the solids

dissolved in dichloromethane, and rinsed three times with water. The organic fraction was dried with magnesium sulfate and concentrated under reduced pressure and subjected to column chromatography of silica with dichloromethane as the eluent. After concentrating under reduced pressure, 2-(2-pyridyl)-9H-carbazole was isolated in a 60% yield.

2-(2-pyridyl)-9-[9-(2-pyridyl)carbazol-2-yl]carbazole (LN3N). Under a nitrogen atmosphere, 10 mmol of 2-(2-pyridyl)-9H-carbazole, 10 mmol of 2-bromo-9-(pyridin-2-yl)-9H-carbazole, 1 mmol of copper(I)iodide, 25 mmol of potassium carbonate, and 2 mmol of L-proline were combined in stirring degassed dimethyl sulfoxide. The mixture was heated to 90˚ C for 3 days before being cooled and separated between dichloromethane and water. The water layer was washed twice with dichloromethane and the organics were combined and washed once with brine. The organic fraction was dried with magnesium sulfate and concentrated under reduced pressure and subjected to column chromatography of silica with dichloromethane/ethyl acetate as the eluent. After concentrating under reduced pressure, the LN3N was isolated as a light yellow solid in 70% yield. ^{1}H NMR (400 MHz, DMSO-d_6, δ): 8.67-8.62 (m, 1 H), 8.61-8.55 (m, 2 H), 8.40 (d, J = 7.9 Hz, 1 H), 8.36 (d, J = 8.2 Hz, 1 H), 8.30 (d, J = 7.8 Hz, 1 H), 8.20-8.18 (m, 1 H), 8.09-7.98 (m, 4 H), 7.90 (s, 1 H), 7.87 (s, 1 H), 7.84 (td, J = 7.8, 1.9 Hz, 1 H), 7.61 (dd, J = 8.2, 2.0 Hz, 1 H), 7.59-7.52 (m, 1 H), 7.49-7.39 (m, 4 H), 7.35-7.27 (m, 2 H); ^{13}C NMR (101 MHz, DMSO-d_6, δ): 156.2, 150.4, 149.6, 149.5, 141.5, 141.3, 139.7, 139.65, 139.6, 137.2, 136.8, 134.8, 126.9, 126.7, 123.3, 123.1, 123.09, 122.4, 122.3, 122.2, 122.0, 121.5, 120.9, 120.8, 120.3, 120.2, 120.1, 119.2, 118.6, 111.3, 110.2, 109.8, 107.7; MS (MALDI-TOF) m/z: $[M]^+$ Calcd for $C_{34}H_{22}N_4$ 486.18, Found 486.40.

Preparation of PtN1N. Under a nitrogen atmosphere, 10 mmol of LOO1 and 9 mmol of potassium tetrachloroplatinate(II) were added to stirring acetic acid. The mixture was held at room temperature for 3 hours before being heated to reflux for 3 days. The solution was cooled, and poured into 100mL of stirring dichloromethane. The mixture was filtered, and the filtrate concentrated under reduced pressure. The solid was subjected to flash chromatography of alumina with dichloromethane as the eluent and isolate in 40% yield. ^{1}H NMR (DMSO-d6, 400 MHz): δ 6.86 (t, J = 2.0 Hz, 1H), 7.30 (t, , J = 7.6 Hz, 1H), 7.40-7.44 (m, 2H), 7.48-7.52 (m, 2H), 7.70 (d, J = 8.4 Hz, 1H), 7.95 (d, J = 8.0 Hz, 1H), 8.00 (d, J = 8.0 Hz, 1H), 8.07 (d, J = 8.0 Hz, 1H), 8.10 (d, J = 2.0 Hz, 1H), 8.14 (d, J = 8.0 Hz, 1H), 8.20-8.27 (m, 5H), 8.90 (d, J = 2.8 Hz, 1H), 9.20 (d, J = 5.6 Hz, 1H). 13C NMR (DMSO-d6, 100 MHz): δ 106.00, 107.65, 108.24, 11.58, 113.00, 113.54, 114.40, 115.31, 115.35, 116.47, 116.93, 118.27, 120.19, 120.45, 120.59, 120.91, 122.89, 125.09, 125.59, 126.09, 127.48, 128.87, 137.97, 138.21, 138.27, 139.28, 139.91, 140.23, 143.32, 143.35, 147.26, 151.84. Anal. Calcd. for $C_{32}H_{19}N_5Pt$: C, 57.48, H, 2.86, N, 10.47; Found: C, 57.29, H, 3.06, N, 10.39.

6.2.2 Photophysical Properties

The emission spectra of PtN1N and PtN3N at consist of a single dominant vibration transition, $v_{0,0,}$ at 491 nm and 542 nm respectively. The represents a significant shift to lower energy from the analogs presented in Chapter 4. Two additional, much weaker side bands occur in approximately 1400 cm^{-1} intervals. The first sideband, $v_{0,1}$ contributes between 25-45% of the total emission and the second sideband, $v_{0,2}$ contributes less than 10%. The Huang-Rhys factor increases with decreasing emission energy, as seen in the platinum complexes presented in Chapter

4. The full width half max values of the two complexes is extremely narrow, ranging between 18 and 21 nm. This compares favorably with reported emission width reported for quantum dot emitters, which range from 25 – 40 nm.[180, 181]

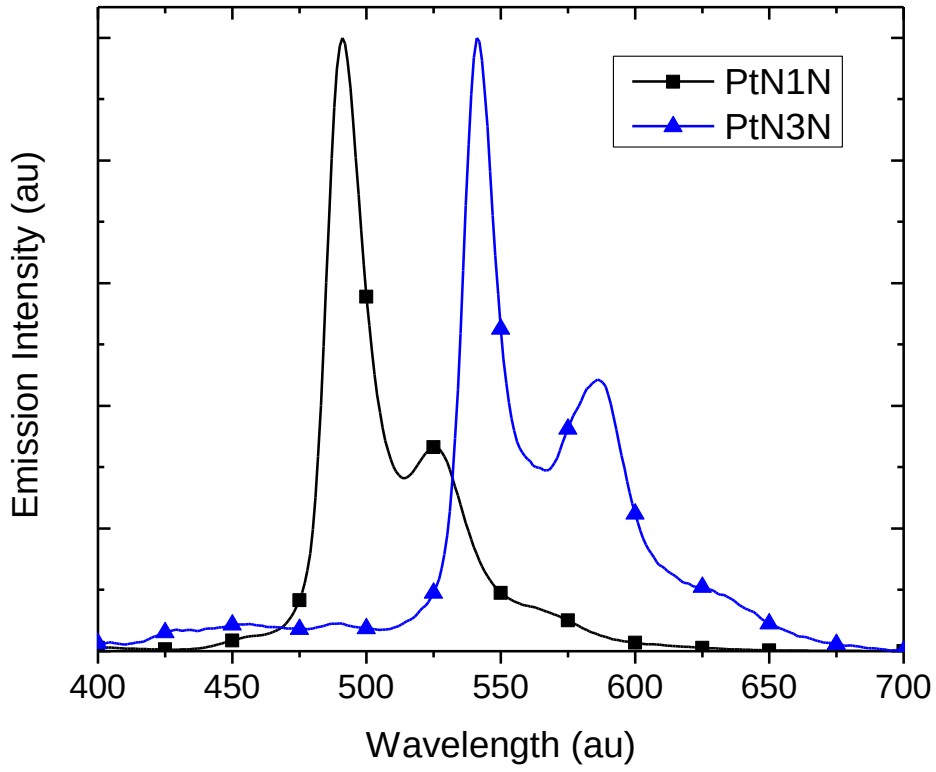

Figure 6.2 Room temperature emission spectra of PtN1N and PtN3N in dichloromethane.

This bis-carabazolyl arrangement can serve as foundation to which additional functionalization can be applied. Color tuning by adjusting the structure of the lumiphore as was undertaken in earlier chapters could easily be imagined. Furthermore, additional changes to the carbazoyl backbone may yield complexes with improved emission properties.

6.3 Palladium Complexes Exhibiting Dual Emission

As evidenced in Chapter 4 and Chapter 5, ligands that form efficient platinum complexes can produce interesting results when complexed to palladium. Furthermore, an anomalous emission peak higher in energy that the $v_{0,0}$ transition was observed in the tetradentate palladium complexes of Chapter 5. When a variable temperature study in a poly(methyl methacrylate) was undertaken, the high energy feature was shown to intensify at elevated temperatures (Figure 6.3). At the time, it was postulated that a delayed fluorescence mechanism[182-184] was involved and was slated for further study.

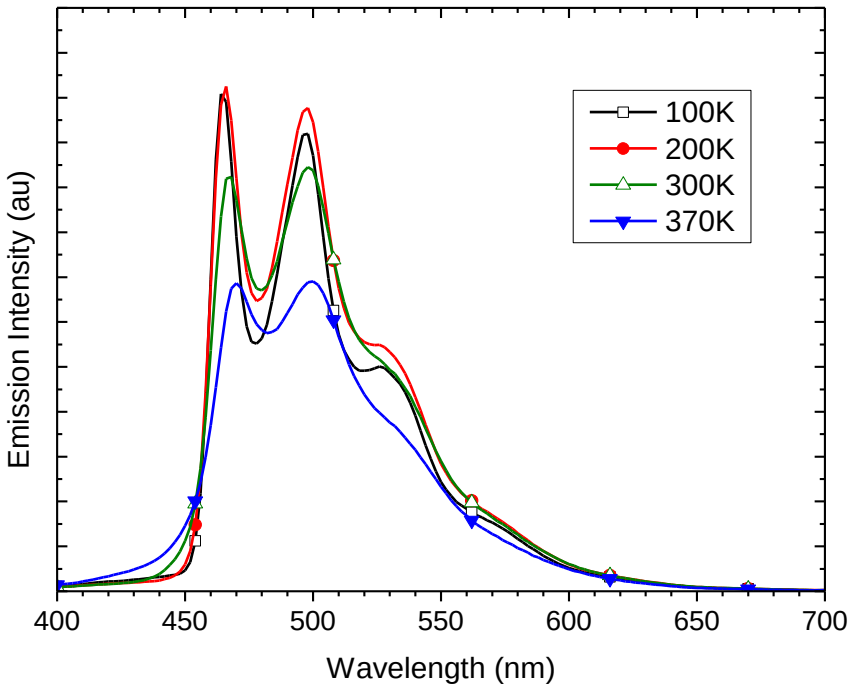

Figure 6.3 Variable temperature emission spectra of PdOO3 in a PMMA thin film. At elevated temperatures, emission below 450 nm appears.

Thermally activated delayed fluorescence (TADF) has found renewed interest in recent years as its potential as efficient emitters for OLEDS became

apparent. TADF occurs when an excited singlet state and the lowest triplet state are close enough in energy that the difference can be overcome with ambient thermal energy. Recent examples rely on well segregated HOMO and LUMO surfaces and a small (<100 meV) difference between the two states. Notably, the organic molecules do not emit efficiently from the triplet state, but instead rely on rapid rates of reverse intersystem crossing ($T_1 \rightarrow S_1$) and a fast radiative decay rate ($>10^6$ s^{-1}) from the excited singlet state.[175]

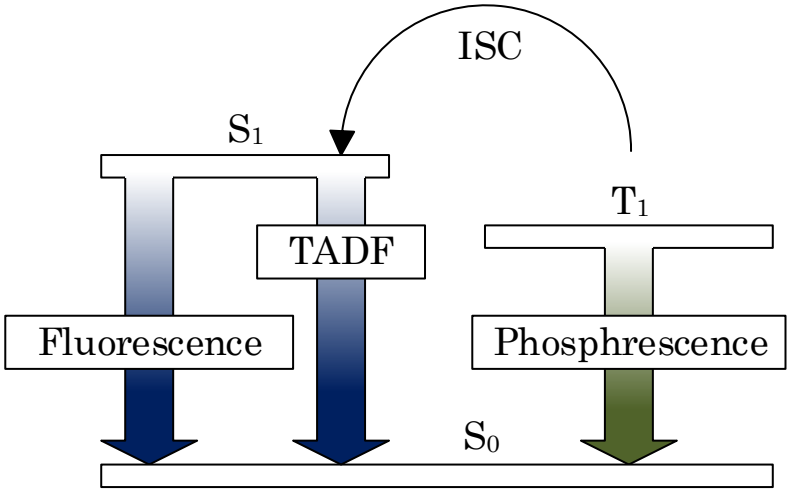

Figure 6.4 Schematic for the delayed fluorescence process. Significant phosphorescence is unique to metal assisted delayed fluorescence (MADF).

Conceivably, the presence of a heavy metal would significantly alter this paradigm. In a well designed system, rapid transitions between the excited singlet and triplet states would result in emission from both states. Furthermore, the requirement of extremely small energy spacing between the two states could be relaxed significantly, as the presence of the metal would increase intersystem crossing rates through spin orbit coupling.

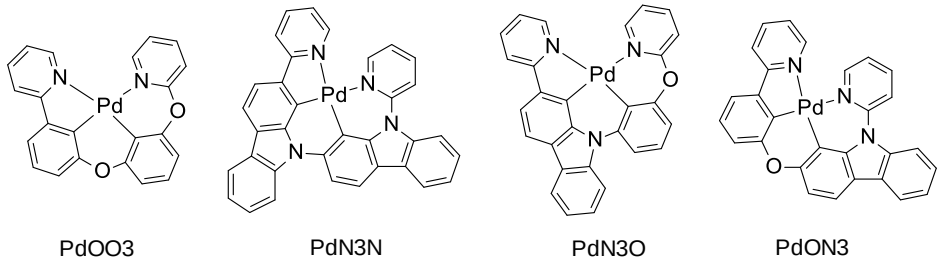

Figure 6.5 Molecular structures of the cyclopalladated pyridyl-carbazolyl palladium complexes synthesized for the delayed fluorescence study

To explore the possibility of metal assisted delayed fluorescence (MADF), four pyridyl based compounds (Figure 6.5) were synthesized. PdOO3 and PdON3 have a pyridyl-phenyl emitting motif, while PdN3N and PdN3O have a pyridyl-cabazolyl emitting motif. For the ancillary portion, PdOO3 and PdN3O use a popy fragment, while PdN3N and PdON3 have a pryidyl-carbazolyl fragment. This represents four unique combinations. Photoluminescence spectra were collected at temperatures ranging from 80 K to 370 K. The luminescent lifetimes across this range were studied to gain a better understanding of the nature of the thermally accessible singlet state.

6.3.1 Synthesis

Scheme 6.2 Synthetic strategy for PdN3O and PdON3

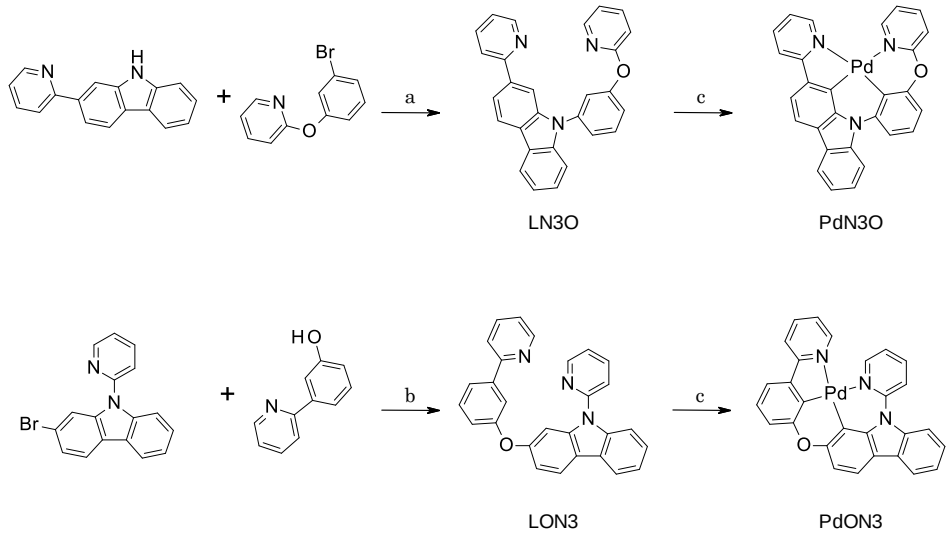

Reaction conditions: (a)1 eq 2-(pyridin-2-yl)-carbazole, 1 eq 2-(3-bromophenoxy)pyridine , 10% copper(I) iodide, 20% L-proline, 2.5 eq potassium carbonate, dimethyl sulfoxide, 90^0 C, 3 days. (b) 1 eq 3-(pyridin-2-yloxy)phenol, 1 eq 2-bromo-9-(2-pyridyl)carbazole), 50% 1-methylimidazole, 2 eq potassium carbonate, 20% copper(I) iodide, toluene, reflux, 2 days. (c) 1 eq ligand, 1.1 eq palladium acetate, acetic acid, slow ramp to refux, 4 days.

Preparation of LN3O. To a solution of 2-(pyridin-2-yl)-carbazole (244 mg, 1 mmol) in dioxane (5 mL, 0.2 M) were added 2-(3-bromophenoxy)pyridine (500 mg, 2 mmol), copper iodide (19 mg, 0.1 mmol), (±)-*trans*-1,2-diaminocyclohexane (24 µL, 0.2 mmol) and tripotassium phosphate (425 mg, 2 mmol). The reaction mixture was slowly heated to reflux for 4 days. The mixture was cooled to room temperature and filtered through a short pad of Celite. The filtrate was concentrated under reduced pressure. Purification by column chromatography (hexanes:ethyl acetate = 5:1 to 2:1) gave the N3O ligand (360 mg, 0.87 mmol, yield: 87%) as a light yellow solid. ^{1}H NMR (400 MHz, DMSO-d_6, δ): 8.67 (d, J = 4.6 Hz, 1 H), 8.32 (d, J = 8.2 Hz, 1 H), 8.27 (d, J = 7.8 Hz, 1 H), 8.24 (brs, 1 H), 8.23-8.20 (m, 1 H), 8.03-7.96 (m, 2 H), 7.91-7.83 (m, 2 H), 7.74 (t, J

= 8.1 Hz, 1 H), 7.57-7.43 (m, 4 H), 7.37-7.27 (m, 3 H), 7.19-7.11 (m, 2 H); ^{13}C NMR (101 MHz, DMSO-d_6, δ): 162.7, 156.3, 155.0, 149.5, 147.4, 140.8, 140.5, 140.4, 137.7, 137.2, 136.9, 131.2, 126.7, 123.5, 122.6, 122.5, 122.4, 120.9, 120.8, 120.4, 120.3, 119.7, 119.4, 118.9, 111.9, 109.8, 107.7; MS (MALDI-TOF) m/z: $[M]^+$ Calcd for $C_{28}H_{19}N_3O$ 413.15, Found 413.23.

Preparation of PdN3O. To a solution of N3O ligand (289 mg. 0.7 mmol) in acetic acid (35 mL, 0.02 M) were added palladium acetate (165 mg, 0.735 mmol) and *n*-tetra-n-butyl ammonium bromide (23 mg, 0.07 mmol). The mixture was heated to reflux for 2 days. The reaction mixture was cooled to room temperature and filtered through a short pad of silica gel. The filtrate was concentrated under reduced pressure. Purification by column chromatography (hexanes:dichloromethane = 1:1 to 1:2) gave the PdN3O (270 mg, 0.52 mmol, yield: 74%) as a light yellow solid. ^{1}H NMR (400 MHz, DMSO-d_6, δ): 8.62 (d, J = 5.1 Hz, 1 H), 8.30 (d, J = 5.1 Hz, 1 H), 8.26-8.12 (m, 4 H), 8.04 (t, J = 7.6 Hz, 1 H), 7.99-7.89 (m, 2 H), 7.81 (d, J = 8.2 Hz, 1 H), 7.57 (d, J = 8.2 Hz, 1 H), 7.53-7.44 (m, 2 H), 7.39 (t, J = 6.2 Hz, 1 H), 7.30 (d, J = 8.2 Hz, 1 H), 7.26 (d, J = 7.5 Hz, 1 H), 7.03 (d, J = 7.5 Hz, 1 H); ^{13}C NMR (101 MHz, DMSO-d_6, δ): 164.3, 159.0, 157.2, 149.1, 148.1, 143.7, 142.2, 139.9, 139.7, 139.3, 139.1, 138.6, 126.6, 126.35, 126.3, 125.6, 122.9, 121.3, 120.9, 120.3, 119.5, 117.6, 115.9, 115.3, 113.4, 113.1, 112.6; MS (MALDI-TOF) m/z: $[M]^+$ Calcd for $C_{28}H_{19}N_3OPd$ 517.04, Found 517.19.

Preparation of LON3. To an oven dried pressure vessel, 3-(pyridin-2-yloxy)phenol (0.94 g, 50 mmol), 2-bromo-9-(2-pyridyl)carbazole (1.6 g, 50 mmol), 1-methylimidazole (0.21 g, 25 mmol), potassium carbonate (1.38 g, 100 mmol) and toluene (20mL) were added. The solution was bubbled with nitrogen for 10 minutes. Copper(I) iodide (0.19 g, 10 mmol) was added, and the solution bubbled 10 minutes further. The vessel was

sealed under a nitrogen atmosphere, brought to reflux. The mixture was stirred for two days, cooled, and filtered. The filtrate was washed with water. The aqueous wash was then extracted with dichloromethane. The organic phases were combined, dried with anhydrous magnesium sulfate and filtered. The filtrate was evaporated to a thick oil which was flash chromatographed with silica and dichloromethane. The product was isolated in 45% yield.

Preparation of PdN3N. To a solution of N3N ligand (146 mg, 0.3 mmol) in acetic acid (15 mL, 0.02 M) were added palladium acetate (71 mg, 0.315 mmol) and *n*-Bu_4NBr (10 mg, 0.03 mmol). The mixture was heated to reflux for 2 days. The reaction mixture was cooled to rt and filtered through a short pad of silica gel. The filtrate was concentrated under reduced pressure. Purification by column chromatography (hexanes:dichloromethane = 1:1 to 1:2) gave the PdN3N (140 mg, 0.237 mmol, yield: 79%) as a yellow solid. ^{1}H NMR (400 MHz, DMSO-d_6, δ): 8.93 (d, J = 5.5 Hz, 1 H), 8.57 (d, J = 5.0 Hz, 1 H), 8.27-7.99 (m, 10 H), 7.97 (d, J = 8.0 Hz, 1 H), 7.84 (d, J = 8.0 Hz, 1 H), 7.55-7.43 (m, 4 H), 7.40 (t, J = 7.4 Hz, 1 H), 7.29 (t, J = 7.4 Hz, 1 H); ^{13}C NMR (101 MHz, DMSO-d_6, δ): 164.2, 150.2, 149.4, 148.7, 144.6, 143.6, 140.5, 140.1, 139.4, 139.1, 138.7, 138.5, 138.4, 127.6, 126.3, 126.2, 125.1, 123.0, 122.8, 122.7, 121.4, 121.1, 120.6, 120.2, 120.18, 119.5, 117.5, 117.2, 116.3, 116.0, 115.9, 114.4, 113.4, 112.7p; MS (MALDI-TOF) m/z: $[M]^+$ Calcd for $C_{34}H_{22}N_4Pd$ 590.07, Found 590.32.

6.3.2 Photophysical Properties

To study the luminescent properties, compounds were doped into a PMMA thin film and spin-coated onto glass slides. The glass slides were loaded into a cryostat and placed under vacuum (~10^{-3} Torr). The samples were cooled to cryogenic

temperatures and temperature was maintained with liquid nitrogen flow balanced with resistive heating. Emission spectra and luminescent lifetimes were recorded in 20 K increments up to 370 K. A sample of the emission spectra is presented in Figure 6.6.

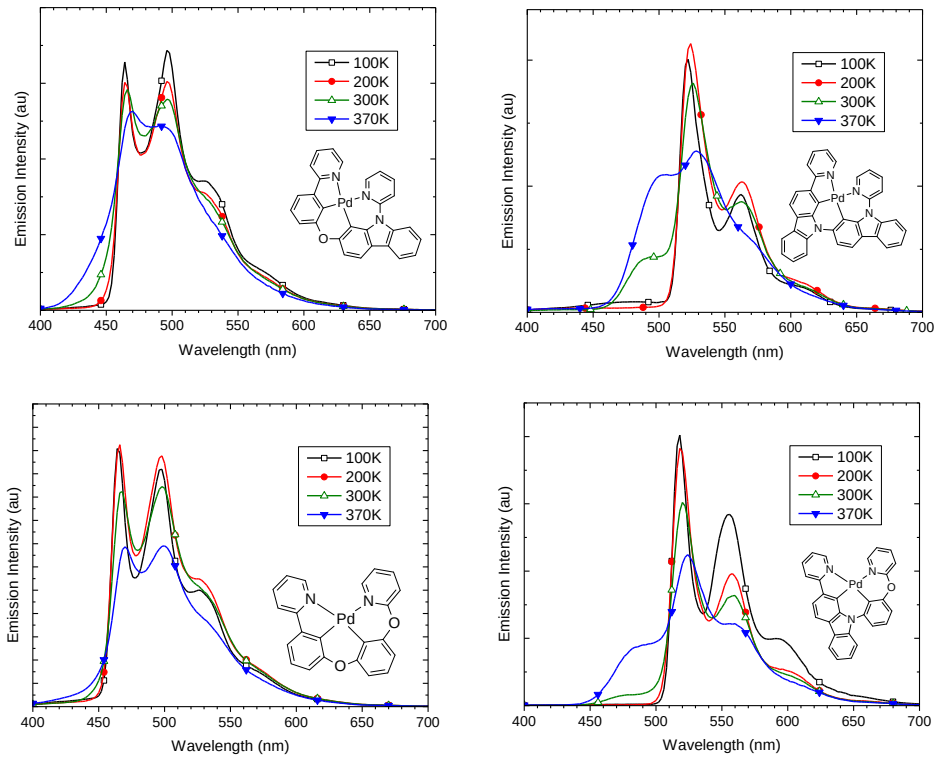

Figure 6.6 Variable temperature emission spectra of cyclopalladated complexes (clockwise, starting at upper left), PdON3, PdN3N, PdN3O, and PdOO3.

All complexes studied show a side band located at higher energy that the primary emission at 100K. The intensity of the band increases with temperature. The relative contributions from the delayed fluorescence and phosphorescence were modeled by fitting four Gaussian peaks to the spectra at 370 K. Delayed fluorescence was significantly more pronounced in the complexes with pyridyl-carbazolyl luminophores. PdN3O and PdN3N have delayed fluorescence contributions of 23%

and 26% respectively. The effect was much weaker in PdOO3 and PdON3, which had contributions of 2% and 8% respectively.

To date, there have been few examples dual emission from metal assisted delayed fluorescence, so the excited state properties of these properties remain relatively unexplored. However, methods developed to probe metal centered quenching states of phosphorescent complexes have been established for decades. These methods can be easily adapted to study a higher lying radiative state.[185, 186]

Changes in lifetime over large temperature ranges can be modeled by considering each thermally activated contribution to the decay process separately (Equation 6.1). 'A' represents the frequency factor and 'ΔE' represents the energy gap between the lowest exited state (triplet) and the thermally accessible excited state (singlet).

Equation 6.1 Equation modeling Arrhenius behavior for discrete thermally activated states

$$\frac{1}{\tau} = \sum_i A_i e^{\frac{-\Delta E_i}{RT}}$$

To accomplish this, a one exponential fit was applied to the plot of 1/τ vs. 1/T. If this proved unsatisfactory, a two exponential fit was used instead. From this fit, the frequency factor and energy gap could be readily determined (Table 6.1).

Table 6.1 Summary of fitted excited state Arrhenius terms

	k_0 (s^{-1} x 10^3)	A_1 s^{-1}	ΔE_1 cm^{-1}	A_2 s^{-1}	ΔE_2 cm^{-1}
PdN3O	4.70	4.90 x 10^9	3663	-	-
PdN3N	5.30	1.20 x 10^9	3307	-	-
PdOO3	3.66	3.00 x 10^3	486	2.50 x 10^{11}	4923
PdON3	3.57	5.19 x 10^3	358	3.17 x 10^{11}	4803

The PdN3O and PdN3N were fit will with one exponential term, while PdOO3 and PdON3 required two terms for an acceptable fit. The first term of the latter is less than 500 cm^{-1} above the triplet state and has a frequency factor on order of 10^3. This level appears frequently in platinum and palladium complexes, and is usually attributed to higher lying LC states of limited distortion. This state was not resolved in PdN3O and PdN3N. This state may exist, but be undetectable due to a sufficiently small energy gap and/or frequency factor.

The energy spacing between PdN3O (3663 cm^{-1}) and PdN3N (3307 cm^{-1}) is significantly lower than PdOO3 (4923 cm^{-1}) and PdON3 (4803 cm^{-1}). This difference in energy spacing is accompanied by a two order of magnitude higher frequency factor in the latter group. Furthermore, a study of the relative emission strength shows a downward trend with increasing temperatures in PdOO3 and PdON3 and a upward trend in PdN3O and PdN3N.

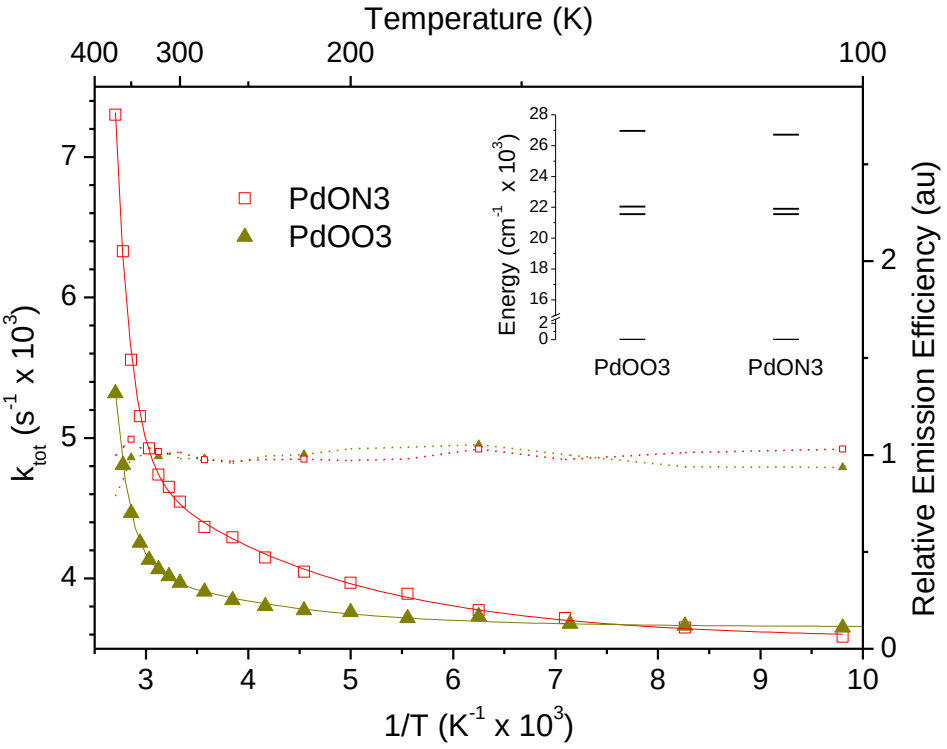

Figure 6.7 Plot of total decay rate (left axis) vs. inverse temperature and relative emission energy (right axis) vs. inverse temperature for the pyridyl-phenyl based complexes PdOO3 and PdON3.

This dissimilarity between the two groups of compounds suggests a different type of excited state is being accessed. The high frequency factor and weak delayed fluorescence sidebands in PdOO3 and PdON3 point to a ^{3}MC quenching state. The lower frequency factor and strong delayed fluorescence peaks in PdN3O and PdN3N suggests that an emissive singlet state was resolved in the experiment as opposed to the metal centered quenching state. It is worth noting that the ^{3}MC state lies at a higher level that reported values for the bis-thiopenyl-pyridyl palladium complex ($Pd(thpy)_2$, 2300 cm^{-1}) as well as its platinum analog ($Pt(thpy)_2$, 3700 cm^{-1}), [185] the result of a stronger ligand field in the presented compounds

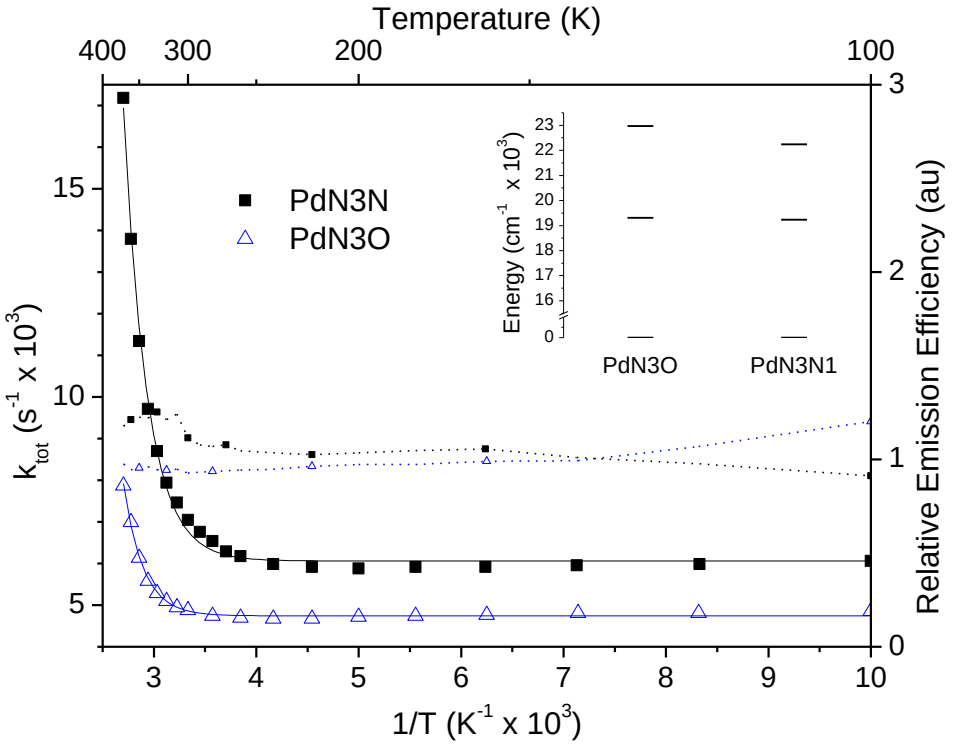

Figure 6.8 Plot of total decay rate (left axis) vs. inverse temperature and relative emission energy (right axis) vs. inverse temperature for the pyridyl-carbazolyl based complexes PdN3N and PdN3O.

6.4 Conclusion

The complexes presented in this chapter represent seminal compounds of two classes that are currently being researched further. Both platinum and palladium carbazolyl complexes demonstrated interesting, and potentially very useful emission properties. Complexes utilizing both metals were highly luminescent. The extremely narrow emission produced by the platinum complexes represents an exciting area for further development. Additional fine-tuning of the ligand structure may further reduce vibronic sidebands and enable precise color tuning.

The variable temperature experiments proved adept at resolving both metal centered quenching states and emissive singlet states. This versatile

characterization method will complement the photoluminescence and absorption techniques currently employed at the lab.

The metal assisted delayed fluorescence exhibited by the palladium complexes is a particularly fertile area for future development. The dual emission mechanism has the potential to provide emission wide enough for single doped white lighting. Additionally, if the excited state mechanics can be better understood, the fluorescent and phosphorescent contribution can be carefully tuned.

REFERENCES

1. Mertens, R. In The OLED Handbook; Metalgrass: Herzerlia, Israel, 2011; , pp 106.

2. Samsung Electronics Samsung Galaxy S5. http://www.samsung.com/global/microsite/galaxys5/ (accessed May 1, 2014).

3. LG Electronics Discover OLED. http://www.lg.com/us/oled-tv (accessed May 1, 2014).

4. Kalinowski, J. In Organic Light-Emitting Diodes: Principles, Characteristics, and Processes; Thompson, B., Ed.; Optical Engineering; Marcel Dekker: New York, New York, 2005; , pp 466.

5. BCC Research 2011, SMC069B, 1.

6. Bernanose, A.; Marquet, G. J. Chim. Phys. Phys. -Chim. Biol. 1954, 51, 255-259.

7. Pope, M. M. J. Chem. Phys. 1963, 38, 2042.

8. Sano, M. J. Chem. Phys. 1965, 43, 2920.

9. Helfrich, W. W. Phys. Rev. Lett. 1965, 14, 229-231.

10. Helfrich, W. W. J. Chem. Phys. 1966, 44, 2902.

11. Werner, T. J. Am. Chem. Soc. 1970, 92, 5560-5565.

12. Hwang, W. W. J. Chem. Phys. 1974, 60, 3845.

13. Geacintov, N. N. E. *Physical review.B, Solid state* **1975**, *12*, 4113-4134.

14. Kalinowski, J. *Chemical physics letters.* **1975**, *36*, 345.

15. Roberts, G. Journal of physics.C, Solid state physics **1978**, 11, 3847-3853.

16. Vincett, P. S. *Thin Solid Films* **1982**, *94*, 171.

17. Sinha, N. P. *Solid State Commun.* **1981**, *39*, 89.

18. Partridge, R. H. *Polymer* **1983**, *24*, 733.

19. Partridge, R. H. *Polymer* **1983**, *24*, 739.

20. Tang, C. C. W. *Appl. Phys. Lett.* **1987**, *51*, 913.

21. Burroughes, J. J. H. *Nature (London)* **1990**, *347*, 539-541.

22. Adachi, C. Japanese journal of applied physics 1988, 27, L269-L271.

23. Adachi, C. Japanese journal of applied physics 1988, 27, L713-L715.

24. Adachi, C. C. Appl. Phys. Lett. 1990, 56, 799.

25. Adachi, C. C. Appl. Phys. Lett. 1990, 57, 531.

26. Tang, C. C. W. J. Appl. Phys. 1989, 65, 3610.

27. Yersin, H., Ed.; In Highly Efficient OLEDs with Phosphorescent Materials; Wiley-VCH: Weinheim, Germany, 2008; , pp 438.

28. Brown, A. R. Chemical physics letters. 1993, 210, 61.

29. Baldo, M. A. Nature (London) 2000, 403, 750.

30. Hoshino, S. S. Appl. Phys. Lett. 1996, 69, 224.

31. Blumstengel, S. S. Japanese journal of applied physics 1999, 38, L403-L405.

32. Kido, J. J. Chem. Lett. 1990, 657-660.

33. Jabbour, G. G. Japanese journal of applied physics **1999**, 38, L1553-L1555.

34. Hong, Z. Z. R. Advanced materials (Weinheim) **2001**, 13, 1241.

35. Kido, J. J. *Chem. Rev.* **2002**, *102*, 2357-2368.

36. Forrest, S. M. A. *Nature (London)* **1998**, *395*, 151-154.

37. Ponterini, G. G. *J. Am. Chem. Soc.* **1983**, *105*, 4639-4645.

38. Baldo, M. M. A. Physical review.B, Condensed matter **2000**, 62, 10967-10977.

39. Adachi, C. C. *J. Appl. Phys.* **2001**, *90*, 5048.

40. Ikai, M. M. *Appl. Phys. Lett.* **2001**, *79*, 156.

41. Jean, Y.; Marsden, C. In *Molecular Orbitals of Transition Metal Complexes;* Oxford University Press: Oxford, , GBR, 2005; , pp 288.

42. Rausch, A. F. The journal of physical chemistry.A, Molecules, spectroscopy, kinetics, environment, & general theory **2009**, 113, 5927-5932.

43. Caspar, J. J. V. *J. Am. Chem. Soc.* **1984**, *106*, 3492-3500.

44. Colombo, M. *Inorg. Chem.* **1993**, *32*, 3081-3087.

45. Blessing, R. H. Acta Crystallogr. , Sect. A: Found. Crystallogr. **1995**, A51, 33-8.

46. Sheldrick, G. M. *Acta Cryst.* **2003***, A64*, 112-122.

47. Connelly, N. G.; Geiger, W. E. *Chem. Rev.* **1996***, 96*, 877-910.

48. Harris, D. C. In *Quantitative Chemical Analysis, Sixth Edition;* W. H. Freeman: New York, 2002; , pp 394-396.

49. Brooks, J.; Babayan, Y.; Lamansky, S.; Djurovich, P. I.; Tsyba, I.; Bau, R.; Thompson, M. E. *Inorg. Chem.* **2002***, 41*, 3055-3066.

50. Tamayo, A. B.; Alleyne, B. D.; Djurovich, P. I.; Lamansky, S.; Tsyba, I.; Ho, N. N.; Bau, R.; Thompson, M. E. *J. Am. Chem. Soc.* **2003***, 125*, 7377-7387.

51. Hay, P. J. *J Phys Chem A* **2002***, 106*, 1634-1641.

52. Jones, G., II; Jackson, W. R.; Choi, C. Y.; Bergmark, W. R. *J. Phys. Chem.* **1985***, 89*, 294-300.

53. Reynolds, G. A.; Drexhage, K. H. *Opt. Commun.* **1975***, 13*, 222-5.

54. Arbeloa, F. L. F. L. *J Lumin* **1989***, 44*, 105; 105-112; 112.

55. DePriest, J.; Zheng, G. Y.; Goswami, N.; Eichhorn, D. M.; Woods, C.; Rillema, D. P. *Inorg. Chem.* **2000***, 39*, 1955-1963.

56. Demas, J. N.; Harris, E. W.; Flynn, C. M.; Diemente, D. *J. Am. Chem. Soc.* **1975***, 97*, 3838-3839.

57. Wu, W.; Xu, X.; Yang, H.; Hua, J.; Zhang, X.; Zhang, L.; Long, Y.; Tian, H. *J. Mater. Chem.* **2011***, 21*, 10666-10671.

58. Gao, R.; Ho, D. G.; Hernandez, B.; Selke, M.; Murphy, D.; Djurovich, P. I.; Thompson, M. E. *J. Am. Chem. Soc.* **2002***, 124*, 14828-14829.

59. Zhang, D.; Wu, L.; Zhou, L.; Han, X.; Yang, Q.; Zhang, L.; Tung, C. *J. Am. Chem. Soc.* **2004***, 126*, 3440-3441.

60. Feng, K.; Zhang, R.; Wu, L.; Tu, B.; Peng, M.; Zhang, L.; Zhao, D.; Tung, C. *J. Am. Chem. Soc.* **2006***, 128*, 14685-14690.

61. Kunugi, Y.; Mann, K. R.; Miller, L. L.; Exstrom, C. L. *J. Am. Chem. Soc.* **1998***, 120*, 589-590.

62. Thomas, S. W., III; Venkatesan, K.; Mueller, P.; Swager, T. M. *J. Am. Chem. Soc.* **2006***, 128*, 16641-16648.

63. Siu, P. K. M.; Lai, S.; Lu, W.; Zhu, N.; Che, C. *Eur. J. Inorg. Chem.* **2003**, 2749-2752.

64. Baldo, M. A.; O'Brien, D. F.; You, Y.; Shoustikov, A.; Sibley, S.; Thompson, M. E.; Forrest, S. R. *Nature* **1998**, *395*, 151-154.

65. Baldo, M. A.; Lamansky, S.; Burrows, P. E.; Thompson, M. E.; Forrest, S. R. *Appl. Phys. Lett.* **1999**, *75*, 4-6.

66. Williams, E.; Haavisto, K.; Li, J.; Jabbour, G. *Adv Mater* **2007**, *19*, 197-202.

67. Yang, X.; Wang, Z.; Madakuni, S.; Li, J.; Jabbour, G. E. *Adv Mater* **2008**, *20*, 2405-2409.

68. Sotoyama, W.; Satoh, T.; Sawatari, N.; Inoue, H. *Appl. Phys. Lett.* **2005**, *86*, 153505.

69. Lu, W.; Chan, M. C. W.; Zhu, N.; Che, C.; Li, C.; Hui, Z. *J. Am. Chem. Soc.* **2004**, *126*, 7639-7651.

70. Sommer, J. R.; Farley, R. T.; Graham, K. R.; Yang, Y.; Reynolds, J. R.; Xue, J.; Schanze, K. S. *ACS Appl. Mater. Interfaces* **2009**, *1*, 274-278.

71. Adachi, C.; Baldo, M. A.; Thompson, M. E.; Forrest, S. R. *J. Appl. Phys.* **2001**, *90*, 5048-5051.

72. Kawamura, Y.; Goushi, K.; Brooks, J.; Brown, J. J.; Sasabe, H.; Adachi, C. *Appl. Phys. Lett.* **2005**, *86*, 071104.

73. Sajoto, T.; Djurovich, P. I.; Tamayo, A. B.; Oxgaard, J.; Goddard, W. A.; Thompson, M. E. *J. Am. Chem. Soc.* **2009**, *131*, 9813-9822.

74. Chassot, L.; Von Zelewsky, A. *Inorg. Chem.* **1987**, *26*, 2814-2818.

75. Williams, J. A. G.; Beeby, A.; Davies, E. S.; Weinstein, J. A.; Wilson, C. *Inorg. Chem.* **2003**, *42*, 8609-8611.

76. Wang, Z.; Turner, E.; Mahoney, V.; Madakuni, S.; Groy, T.; Li, J. *Inorg. Chem.* **2010**, *49*, 11276-11286.

77. Rausch, A. F.; Murphy, L.; Williams, J. A. G.; Yersin, H. *Inorg. Chem.* **2009**, *48*, 11407-11414.

78. Ravindranathan, D.; Vezzu, D. A. K.; Bartolotti, L.; Boyle, P. D.; Huo, S. *Inorg. Chem.* **2010**, *49*, 8922-8928.

79. Willison, S. A.; Krause, J. A.; Connick, W. B. *Inorg. Chem.* **2008**, *47*, 1258-1260.

80. Fleetham, T.; Wang, Z.; Li, J. *Org. Electron.* **2012**, *13*, 1430-1435.

81. Farley, S. J.; Rochester, D. L.; Thompson, A. L.; Howard, J. A. K.; Williams, J. A. G. *Inorg. Chem.* **2005**, *44*, 9690-9703.

82. Colombo, M. G.; Guedel, H. U. *Inorg. Chem.* **1993**, *32*, 3081-7.

83. Strouse, G. F.; Guedel, H. U.; Bertolasi, V.; Ferretti, V. *Inorg. Chem.* **1995**, *34*, 5578-87.

84. Wiedenhofer, H.; Schuetzenmeier, S.; von, Z., Alex; Yersin, H. *J. Phys. Chem.* **1995**, *99*, 13385-91.

85. Schmidt, J.; Wiedenhofer, H.; von, Z., A.; Yersin, H. *J. Phys. Chem.* **1995**, *99*, 226-9.

86. Yersin, H.; Donges, D. *Top. Curr. Chem.* **2001**, *214*, 81-186.

87. Rausch, A. F.; Murphy, L.; Williams, J. A. G.; Yersin, H. *Inorg. Chem. (Washington, DC, U. S.)* **2009**, *48*, 11407-11414.

88. Farley, S. J.; Rochester, D. L.; Thompson, A. L.; Howard, J. A. K.; Williams, J. A. G. *Inorg. Chem.* **2005**, *44*, 9690-9703.

89. Williams, J. A. G.; Beeby, A.; Davies, E. S.; Weinstein, J. A.; Wilson, C. *Inorg. Chem.* **2003**, *42*, 8609-8611.

90. Cardenas, D. J.; Echavarren, A. M.; Ramirez, d. A., M. Carmen. *Organometallics* **1999**, *18*, 3337-3341.

91. Ritter, K. *Synthesis* **1993**, 735-62.

92. Farina, V.; Roth, G. P. *Adv. Met. -Org. Chem.* **1996**, *5*, 1-53.

93. Ishiyama, T. T. *J. Org. Chem.* **1995**, *60*, 7508-7510.

94. Kappe, C. O. *Angew. Chem. , Int. Ed.* **2004**, *43*, 6250-6284.

95. Gibbs, R. A.; Krishnan, U.; Dolence, J. M.; Poulter, C. D. *J. Org. Chem.* **1995**, *60*, 7821-9.

96. Saito, K.; Matsusue, N.; Kanno, H.; Hamada, Y.; Takahashi, H.; Matsumura, T. *Jpn. J. Appl. Phys. , Part 1* **2004**, *43*, 2733-2734.

97. Konno, H.; Sasaki, Y. *Chem. Lett.* **2003**, *32*, 252-253.

98. Ryabov, A. *Chem. Rev.* **1990**, *90*, 403-424.

99. Jawad, J. K.; Puddephatt, R. J.; Stalteri, M. A. *Inorg. Chem.* **1982**, *21*, 332-7.

100. Kulikova, M. V.; Balashev, K. P.; Kvam, P. -.; Songstad, J. *Russ. J. Gen. Chem.* **2000**, *70*, 163-170.

101. Kvam, P.; Puzyk, M. V.; Balashev, K. P.; Songstad, J. *Acta Chem. Scand.* **1995**, *49*, 335-43.

102. Jude, H. *Inorg. Chem.* **2004**, *43*, 725-733.

103. Sotoyama, W.; Satoh, T.; Sato, H.; Matsuura, A.; Sawatari, N. *J Phys Chem A* **2005**, *109*, 9760-9766.

104. Caspar, J. V.; Westmoreland, T. D.; Allen, G. H.; Bradley, P. G.; Meyer, T. J.; Woodruff, W. H. *J. Am. Chem. Soc.* **1984**, *106*, 3492-500.

105. Damrauer, N. H.; Boussie, T. R.; Devenney, M.; McCusker, J. K. *J. Am. Chem. Soc.* **1997**, *119*, 8253-8268.

106. Rillema, D. P.; Blanton, C. B.; Shaver, R. J.; Jackman, D. C.; Boldaji, M.; Bundy, S.; Worl, L. A.; Meyer, T. J. *Inorg. Chem.* **1992**, *31*, 1600-6.

107. Allen, G. H.; White, R. P.; Rillema, D. P.; Meyer, T. J. *J. Am. Chem. Soc.* **1984**, *106*, 2613-20.

108. Balashev, K. P.; Puzyk, M. V.; Kotlyar, V. S.; Kulikova, M. V. *Coord. Chem. Rev.* **1997**, *159*, 109-120.

109. Constable, E. C.; Henney, R. P. G.; Leese, T. A.; Tocher, D. A. *J. Chem. Soc. , Chem. Commun.* **1990**, 513-15.

110. Lu, W.; Zhu, N.; Che, C. *Chem. Commun. (Cambridge, U. K.)* **2002**, 900-901.

111. Che, C.; Zhang, J.; Lin, L. *Chem. Commun. (Cambridge, U. K.)* **2002**, 2556-2557.

112. Che, C.; Fu, W.; Lai, S.; Hou, Y.; Liu, Y. *Chem. Commun. (Cambridge, U. K.)* **2003**, 118-119.

113. Yam, V. W.; Tang, R. P.; Wong, K. M.; Lu, X.; Cheung, K.; Zhu, N. *Chem. --Eur. J.* **2002**, *8*, 4066-4076.

114. Mdleleni, M. M.; Bridgewater, J. S.; Watts, R. J.; Ford, P. C. *Inorg. Chem.* **1995**, *34*, 2334-42.

115. Farley, S. S. J. *Inorg. Chem.* **2005**, *44*, 9690-9703.

116. Rausch, A.; Murphy, L.; Williams, J. A. G.; Yersin, H. *Inorg. Chem.* **2012**, *51*, 312-319.

117. So, F.; Kondakov, D. *Adv Mater* **2010**, *22*, 3762-3777.

118. Yersin, H.; Rausch, A.; Czerwieniec, R.; Hofbeck, T.; Fischer, T. *Coord. Chem. Rev.* **2011**, *255*, 2622-2652.

119. Yersin, H. Proc. SPIE-Int. Soc. Opt. Eng. **2004**, 5214, 124-132.

120. Williams, J. A. G.; Develay, S.; Rochester, D.; Murphy, L. *Coord. Chem. Rev.* **2008**, *252*, 2596-2611.

121. Kui, S.; Chow, P. K.; Tong, G. S. M.; Lai, S.; Cheng, G.; Kwok, C.; Low, K.; Ko, M. Y.; Che, C. *Chem. Eur. J.* **2013**, *19*, 69-73.

122. Che, C.; Kwok, C.; Lai, S.; Rausch, A.; Finkenzeller, W.; Zhu, N.; Yersin, H. *Chem. Eur. J.* **2010**, *16*, 233-247.

123. Lin, Y.; Chan, S.; Chan, M. C. W.; Hou, Y.; Zhu, N.; Che, C.; Liu, Y.; Wang, Y. *Chem. Eur. J.* **2003**, *9*, 1263-1272.

124. Vezzu, D. A. K.; Deaton, J. C.; Jones, J. S.; Bartolotti, L.; Harris, C. F.; Marchetti, A. P.; Kondakova, M.; Pike, R. D.; Huo, S. *Inorg. Chem.* **2010**, *49*, 5107-5119.

125. Feng, K.; Zuniga, C.; Zhang, Y.; Kim, D.; Barlow, S.; Marder, S. R.; Brédas, J. L.; Weck, M. *Macromolecules* **2009**, *42*, 6855-6864.

126. Huo, S.; Harris, C. F.; Vezzu, D. A. K.; Gagnier, J. P.; Smith, M. E.; Pike, R. D.; Li, Y. *Polyhedron* **2012**, *DOI:10.1016/j.poly.2012.06.078*.

127. Evans, R. C.; Douglas, P.; Winscom, C. J. *Coord. Chem. Rev.* **2006**, *250*, 2093-2126.

128. Li, J.; Djurovich, P. I.; Alleyne, B. D.; Yousufuddin, M.; Ho, N. N.; Thomas, J. C.; Peters, J. C.; Bau, R.; Thompson, M. E. *Inorg. Chem.* **2005**, *44*, 1713-1727.

129. Chou, P. T.; Chi, Y.; Chung, M. W.; Lin, C. C. *Coord. Chem. Rev.* **2011**, *255*, 2653-2665.

130. Schareina, T.; Zapf, A.; Cotté, A.; Müller, N.; Beller, M. *Tetrahedron Lett.* **2008**, *49*, 1851-1855.

131. Wang, Z.; Bao, W.; Jiang, Y. *Chem. Commun.* **2005**, *0*, 2849-2851.

132. Bellina, F.; Cauteruccio, S.; Rossi, R. *Chem. Eur. J.* **2006**, *2006*, 1379-1382.

133. Littke, A. F.; Schwarz, L.; Fu, G. C. *J. Am. Chem. Soc.* **2002**, *124*, 6343-6348.

134. Develay, S.; Blackburn, O.; Thompson, A. L.; Williams, J. G. *Inorg. Chem.* **2008**, *47*, 11129-11142.

135. Sasabe, H.; Gonmori, E.; Chiba, T.; Li, Y.; Tanaka, D.; Su, S.; Takeda, T.; Pu, Y.; Nakayama, K.; Kido, J. *Chem. Mater.* **2008**, *20*, 5951-5953.

136. Cai, X.; Padmaperuma, A. B.; Sapochak, L. S.; Vecchi, P. A.; Burrows, P. E. *Appl. Phys. Lett.* **2008**, *92*, 083308-083308-3.

137. Su, S.; Gonmori, E.; Sasabe, H.; Kido, J. *Adv Mater* **2008**, *20*, 4189-4194.

138. Lamansky, S. S. *J. Am. Chem. Soc.* **2001**, *123*, 4304-4312.

139. Li, J. *Polyhedron* **2004**, *23*, 419.

140. Yam, V. Chemistry : a European journal **2002**, 8, 4066-4076.

141. Lai, S. *Inorg. Chem.* **1999**, *38*, 4046-4055.

142. Wang, Z. Z. *Inorg. Chem.* **2010**, *49*, 11276-11286.

143. Yam, V. W.; Wong, K. M. *Chem. Commun.* **2011**, *47*, 11579-11592.

144. Kalinowski, J. J. *Coord. Chem. Rev.* **2011**, *255*, 2401-2425.

145. Brooks, J. J. *Inorg. Chem.* **2002**, *41*, 3055-3066.

146. Chassot, L. L. *Inorg. Chem.* **1984**, *23*, 4249-4253.

147. Díez, A. A. *Organometallics* **2009**, *28*, 1705-1718.

148. Cave, G. W. V. *Organometallics* **1999**, *18*, 1801-1803.

149. Lu, W. *Organometallics* **2001**, *20*, 2477-2486.

150. Che, C. Chemical communications (Cambridge, England) **2003**, 118-119.

151. Constable, E. Journal of the Chemical Society.Chemical communications **1990**, 513.

152. Cárdenas, D. *Organometallics* **1999**, *18*, 3337-3341.

153. Turner, E. E. *Inorg. Chem.* **2013**, *52*, 7344; 7344-7351; 7351.

154. Che, C. C. M. Chemistry : a European journal **2010**, 16, 233-247.

155. Li, K.; Guan, X.; Ma, C.; Lu, W.; Chen, Y.; Che, C. *Chem. Commun.* **2011**, *47*, 9075-9077.

156. Vezzu, D. A. K. D. A. K. *Inorg. Chem.* **2010**, *49*, 5107-5119.

157. Neve, F. F. In Photophysical Properties of Cyclopalladated Compounds; Palladacycles; 2008; pp 285-305.

158. Forster, L. S. *Coord. Chem. Rev.* **2002**, *227*, 59-92.

159. Sotoyama, W. W. *Appl. Phys. Lett.* **2005**, *86*, 153505.

160. Gómez, M.; Granell, J.; Martinez, M. *European Journal of Inorganic Chemistry* **2000**, *2000*, 217-224.

161. Neve, F. *Organometallics* **2002**, *21*, 3511-3518.

162. Santana, M. M. D. Dalton transactions (Cambridge, England : 2003) **2011**, 40, 3537.

163. Zhao, Y. *Acc. Chem. Res.* **2008**, *41*, 157-167.

164. Matsushita, T. T. The journal of physical chemistry.A, Molecules, spectroscopy, kinetics, environment, & general theory **2006**, 110, 13295-13302.

165. Rausch, A. *Inorg. Chem.* **2009**, *48*, 11407-11414.

166. Yersin, H. H. In Low-Lying Electronic States and Photophysical Properties of Organometallic Pd(II) and Pt(II) Compounds. Modern Research Trends Presented in Detailed Case Studies; Transition Metals and Rare Earth Compounds: Excited States, Transitions, Interactions II; 2001; Vol. 214, pp 81-186.

167. Yersin, H. *Top. Curr. Chem.* **2004**, *241*, 1-26.

168. Albinati, A. *Inorg. Chem.* **1987**, *26*, 503-508.

169. Berners-Price, S. J.; Ronconi, L.; Sadler, P. J. *Prog Nucl Magn Reson Spectrosc* **2006**, *49*, 65-98.

170. Ismail, I. M. *Polyhedron* **1982**, *1*, 57.

171. Rausch, A. F.; Homeier, H. H. H.; Yersin, H. *Top. Organomet. Chem.* **2010**, *29*, 193-235.

172. Strouse, G. G. F. *Inorg. Chem.* **1995**, *34*, 5578-5587.

173. Wiedenhofer, H. Journal of physical chemistry (1952) **1995**, 99, 13385-13391.

174. Strohriegl, P. P. *Advanced materials (Weinheim)* **2002**, *14*, 1439-1452.

175. Uoyama, H. H. *Nature (London)* **2012**, *492*, 234; 234-238; 238.

176. Serevičius, T. T. Physical chemistry chemical physics : PCCP **2013**, 15, 15850.

177. Mashford, B. B. S. *Nature photonics* **2013**, *7*, 407; 407-412; 412.

178. Qian, L. L. *Nature photonics* **2011**, *5*, 543; 543-548; 548.

179. Lee, K.; Lee, J.; Kang, H.; Park, B.; Kwon, Y.; Ko, H.; Lee, C.; Lee, J.; Yang, H. *ACS nano* **2014**.

180. Poznyak, S. K.; Talapin, D. V.; Shevchenko, E. V.; Weller, H. *Nano Letters* **2004**, *4*, 693-698.

181. Weisbuch, C.; Benisty, H.; Houdré, R. *J Lumin* **2000**, *85*, 271-293.

182. Kozhevnikov, D. *Inorg. Chem.* **2011**, *50*, 3804-3815.

183. Tsubomura, T. T. *Inorg. Chem.* **2008**, *47*, 481-486.

184. Callis, J. B. *J. Mol. Spectrosc.* **1971**, *39*, 410-420.

185. Barigelletti, F.; Juris, A.; Balzani, V.; Belser, P.; Von Zelewsky, A. *J. Phys. Chem.* **1987**, *91*, 1095-1098.

186. Sajoto, T. T. *J. Am. Chem. Soc.* **2009**, *131*, 9813-9822.